PFC/RR-79-10

FUSION REACTOR BLANKET HEAT REMOVAL USING HELIUM AND FLIBE

T.McManamy
B.Mikic
N.Todreas

FUSION TECHNOLOGY PROGRAM

Massachusetts Institute of Technology
Cambridge, MA 02139

February 1979

FUSION REACTOR BLANKET HEAT REMOVAL USING HELIUM AND FLIBE

T. McManamy
B. Mikic
N. Todreas

ABSTRACT

The use of helium and the molten salt flibe (Li_2BeF_4) is examined for a fusion reactor blanket. Two structural materials, 316 Stainless Steel and TZM (a molybdenum alloy) are considered. The first wall and interior blanket regions are analyzed separately because of their different constraints and operating conditions.

A stagnant lithium pool is employed for tritium breeding in the interior blanket. Heat removal is by tubes arranged in either of two distributions. The first has coolant tubes located throughout the blanket such that the heat removal per unit length is the same for all tubes. A second configuration was proposed in which the tubes are located at only a few discrete radial locations forming shells. The first gives the smallest number of tubes and lower peak thermal stresses. The second has improved neutronics and greater redundancy. For the first configuration with helium coolant, analytic expressions relating the neutron wall loading to the major design parameters of interest were found. The expressions should be quite useful in parametric studies since detailed design configurations and analysis are not required. Comparisons with several designs in the literature were made and the agreement between the analytical expressions and the detailed designs was good. In addition, for both

helium and flibe a design window methodology was developed and several examples given. An example of the second concept is given by the HFCTR conceptual design.

A tubular radiation shield for the first wall was examined. Copper cladding on 316SS was proposed and found to significantly reduce the peak thermal stress.

A second first wall configuration employing a thick sacrificial TZM block with cooling tubes on the side away from the plasma was also considered. A checkerboard pattern of grooves is used for stress relief. The large thermal mass of the block will protect the tubes and for short pulse operation it can reduce fatigue damage by reducing the altermating component of thermal stress.

ACKNOWLEDGEMENT

It is a pleasure to acknowledge the advice and comments of Larry Lidsky and John Meyers of the M.I.T. Nuclear Engineering Department, Dan Cohn of the HFCTR design group, Jason Chao, and Steve Herring. We also wish to thank Sandy McManamy for typing this report.

This work was supported in part by the U.S. Department of Energy and in part through a General Electric Fellowship.

TABLE OF CONTENTS

PAGE

PAGE

LIST OF FIGURES

LIST OF TABLES

NOMENCLATURE

B	Magnetic Field (T)
b	Exponential decay constant for heat generation (m^{-1})
C_p	Heat capacity (J/kg)
D	Coolant tube diameter (m)
E	Youngs modulus (Pa)
H	Heat transfer coefficient (W/m^2)
Ha	Hartmann number
K	pumping power to heat removal ratio
k	Thermal conductivity (W/m-°C)
L	Coolant tube length (m)
N	Number of shells in Shell concept
n	Number of coolant tubes
P	Coolant Pressure (Pa)
ΔP	Coolant pressure drop (Pa)
P_r	Prandtl number
P_W	First wall neutron loading (W/m^2)
q"'	Local volumetric energy generation rate (W/m^3)
<q"'>	Average blanket energy generation rate (W/m^3)
q"	Surface heat flux from plasma (W/m^2)
R	Gas constant (J/kg-°K)
$\bar{T}$	Average coolant temperature (°C)

ΔT	Bulk coolant temperature rise (°C)
ΔT_F	Film temperature drop (°C)
ΔT_W	Wall temperature drop (°C)
T_F	Bulk fluid temperature (°C)
ΔT_{Li}	Temperature rise in lithium pool (°C)
T_{LMax}	Maximum lithium pool temperature
t	tube thickness (m)
U	Radial displacement for stress analysis (m)
V_m	Induced voltage (volts)
v	Coolant velocity
W_s	Surface heat flux on interior blanket tube (W/m^2-°C)
Z	Blanket thickness (m)
α	Energy multiplication factor
α	coefficient of thermal expansion (Chapter 5)
β	Ratio of q"' minimum/ q"'
ϵ	Mechanical strain
μ	Viscosity of coolant (kg/m·sec)
ρ	Coolant density (kg/m^3)
ρ_t	Coolant tube density (m^{-3})
σ	Hoop stress (Pa)
$\sigma_{r,\theta,z}$	Thermal stresses (Pa)
η	Resistivity Ω.m
η_s	Fraction of structural material
η_v	Void fraction
ν	Poisson's ratio

ψ Friction factor

INTRODUCTION

Fusion power offers a promise of a virtually limitless energy supply for the future of mankind.[1] For the last twenty years, science has pursued this promise, at first underestimating the difficulties, but through a world-wide effort, an understanding of the behavior of this fourth state of matter is beginning to emerge. Recent experimental progress has been especially encouraging. The Alcator tokamak at M.I.T. has achieved values of $n\tau$ (the product of density and confinement time) which are on the order of 3×10^{13} cm^{-3}. sec are in the the range needed for two-component reactor configurations, but at relatively low temperatures. At Princeton, the required temperatures for ignition have been reached in PLT but at a low $n\tau$ product.[2] If the next generation of experimental machines such as TFTR perform as expected, the scientific feasibility of controlled thermonuclear power will be demonstrated.

For fusion power to make a meaningful contribution to electrical energy generation however, feasibility is not enough. It must be economically competitive with the alternatives available at the time. The scientific feasibility of fission power was proven by 1945, but it was 20 years before it began to be economically competitive.

Because of the dwindling and uncertain extent of oil and natural gas reserves along with real or perceived problems with other alternatives, the development of fusion power as a possibility has a certain sense of urgency. Engineering studies of conceptual power reactors have therefore, been done and will continue in the attempt to predict as early as possible whether a given approach would yield a desirable power plant. Hopefully, these engineering studies will provide feedback so that the regimes of plasma physics studies are those leading to desirable reactors.

This work represents part of a blanket technology study. The objective was to evaluate the relative thermo-hydraulic and neutronic characteristics of three coolants - helium, flibe and lithium for a

liquid lithium fusion reactor blanket. In this thesis, the use of helium and flibe will be examined for cooling the interior blanket and several first wall cooling options proposed. The use of lithium and neutronic calculations are incorporated in J. Chao's thesis.[3]

I. HELIUM COOLING OF A STAGNANT LITHIUM POOL

1.1 Objective and Physical Model

The objective of this section is to develop a methodology which will permit the rapid estimation of the thermal hydraulic requirements for removing the heat from a stagnant lithium pool using a distributed set of cooling tubes with helium coolant.

The model used assumes that the heat removed per unit length of coolant tube is the same for all tubes. In addition, the blanket surface heat flux from bremsstrahlung and charged particle flux is to be removed by a separate radiation shield which will be analyzed later. It is further assumed that an initial neutronic study will give an approximate thickness of lithium required for breeding tritium and the energy per fusion event deposited in the region. The plasma engineering gives the first wall shape and major radius so that the volume of the breeding zone and energy per fusion event to be removed is known.

The following quantities are used to describe the thermal hydraulic system.

1. $\bar{T}$ (°C): The average bulk coolant temperature
2. ΔT (°C): The bulk coolant temperature rise
3. P (Pa): The average coolant pressure
4. ρ (kg/m^3): the average coolant density
5. v (m/sec): Average coolant velocity
6. ΔP (Pa): Coolant pressure drop; inlet to exit

7. ψ: Friction Factor
8. K: Pumping power to heat removal ratio
9. h (w/m^2-°C): Heat transfer coefficient
10. η_s: The average volume ratio of structural material in the coolant tubes to lithium.
11. η_v: The average volume ratio of void to lithium zone volume (i.e. void fraction)
12. σ (Pa): Coolant tube hoop stress due to pressure.
13. D(m): Coolant tube diameter
14. L(m): Coolant tube length
15. t(m): Coolant tube thickness
16. $P_w(W/m^2)$: First wall loading(neutron)
17. $\langle q''' \rangle$ (W/m^3): Average energy generation rate in the lithium
18. W_s (W/m^2): Surface heat flux on all coolant tubes.
19. ΔT_F: Coolant tube film temperature drop.
20. ΔT_W: Coolant tube wall temperature drop.
21. ρ_t (m^{-3}): Average tube density; number of tubes divided by lithium zone volume.

These quantities are not all independent. What will be developed is the functional relations between them.

Another possible parameter of interest which is not explicitly included is the peak temperature in the lithium pool. This can vary greatly depending on the shape of the area of lithium being cooled by a single tube which depends on the exact coolant tube layout. Presumably in a point design, the design philosophy concerning maintenance

and accessability will determine the module shape. The analysis to be given here will give a reasonable choice for the number of coolant tubes, their diameter, thickness and length. These would then be arranged as most suitable for a given module and subsequently the peak lithium temperatures and wall temperatures check by a detailed analysis.

The quantity η_s is included as a separate parameter because it affects the breeding of tritium and there will be some upper limit on the total fraction of structure material which also includes that required for mechanical design.

The number of coolant tubes is included as a separate quantity of interest because the reliability of the system is inversely proportional to the number of tube to header joints.[4]

1.2 Governing Relations

The system being considered has the 21 unknowns listed previously. In this section it will be shown that there are 13 applicable relations This means there are eight degrees of freedom. In the design window methodology to be developed, a rational will be given for fixing six quantities so that on a diameter versus length plot all points are determined.

From conservation of energy the following holds

$$\frac{\pi D^2}{4} \rho v C_p \Delta T = \pi D L W_s \qquad (1.1)$$

$$\rho_t \pi D L W_s = \langle q''' \rangle \qquad (1.2)$$

By definition:

$$\alpha \equiv \frac{\langle q''' \rangle Z}{P_W} = \frac{Z\, A_{fw}}{(1-\eta_v) V_T} \cdot \frac{E_f(\text{Mev})}{14.06} \qquad (1.3)$$

where Z is the blanket thickness, V_T the total blanket volume, A_{fw} the first wall surface area and E_F the total energy deposited in the blanket region per fusion neutron as determined from neutronic calculations.

$$H\, \Delta T_F = W_S \qquad (1.4)$$

$$K = \Delta P/\rho C_p \Delta T \qquad (1.5)$$

For thin tubes and small void fractions the following averages can be found

$$\eta_s = \rho_t\, \pi D t L \qquad (1.6)$$

$$\eta_v = \rho_t \frac{\pi D^2 L}{4} \qquad (1.7)$$

Where ρ_t = number of tubes/lithium volume. For thin tubes the hoop stress due to pressure can be approximated by:

$$\sigma = PD/2t \qquad (1.8)$$

The pressure drop in the tube is approximated by

$$\Delta P = 1/2\ \rho v^2\ \Psi\ L/D \qquad (1.9)$$

Where for smooth tubes the turbulent factor is approximated by:

$$\Psi = .184\ (\rho v D/\mu)^{-0.2} \qquad (1.10)$$

A relation between the friction factor and the heat transfer coefficient can be obtained from the Colburn analogy. This gives

$$h = P_r^{-0.6}\ \rho v\ C_p\ \Psi/8 \qquad (1.11)$$

An ideal gas law approximation gives

$$\rho \approx \frac{P}{RT} \qquad (1.12)$$

Finally the wall temperature drop is given by

$$\Delta T_W = (D W_g/2k)\ \ln\ (1+2t/D) \qquad (1.13)$$

Since the thermal stresses are proportional to ΔT_W a limit on this is equivalent to a limit on thermal stress.

1.3 Design Window Development

The parameters a designer has the most control over are the number of coolant tubes, their geometry and the wall loading. To help make an initial choice for these parameters a graphical presentation is introduced to show the allowable range of tube diameter, length and number of tubes as a function of wall loading given a set of fixed parameters and constraints. In addition, analytic relations will be developed which should be very useful in parametric studies. For a given design window, the following six quantities were considered as fixed parameters:

a) $\overline{T}$

b) ΔT

c) σ

d) K

e) ηs

f) P

The choice for $\overline{T}$ and ΔT would depend on the structural material temperature limits, desired steam cycle and possibly thermal shock considerations. The hoop stress would be based on the allowed creep rate with a suitable safety factor. A maximum allowed pumping power to heat removal ratio would probably be approximately 2%. This could vary depending on the allowed recirculating power fraction for a given design concept. The allowed fraction of structural material in the tubes would be limited by a minimum desired breeding ratio. It will be shown the void fraction is proportional to ηs and increasing either

will decrease the breeding ratio for a given thickness of lithium. Finally the pressure choice is a compromise between decreasing the pumping power for a given rate of heat removal and increasing the thermal stress due to thicker walls.

With the six fixed parameters, a point on a D versus L plane gives eight known quantities which together with the 13 relations form a closed determined set of equations in our 21 parameters. The algebraic manipulations to follow have the objective of obtaining expressions for D versus L as a function of the six (or fewer) fixed parameters and one additional quantity of interest at a time. Lines of constant P_W, T_F, T_W, and $_T$ are obtained in this manner.

1.3.1 Derivation of Analytic Relations

Equations 1.9, 1.11, 1.5, 1.4 and 1.1 can be combined as shown in Reference 5 to give

$$\Delta T_F = \frac{16}{P_r^{-.6} C_P^3} \frac{W_s^2 L^2}{K \Delta T^2 D^2 \rho^2} \tag{1.14}$$

From (2) and (6) it can be seen

$$W_s = \frac{t}{\eta_s} \langle q''' \rangle \tag{1.15}$$

Substituting (1.15) in (1.14) and using (1.8) and (1.2) gives

$$\Delta T_F = \frac{4R^2}{P_r^{-.6} C_P^3} \frac{1}{K} \left[\frac{\bar{T} \langle q''' \rangle L}{\eta_s \sigma \Delta T} \right]^2 \tag{1.16}$$

Equations (1.11), 1.4), (1.1) and (1.10) can be combined to give

$$\frac{\pi D^2}{4} \rho v C_p \Delta T = \frac{\Delta T_F P_r^{-.6} \rho v C_P}{\pi D L} \frac{1}{8} (.184 Re^{-.2}) \tag{1.17}$$

$$\text{or } D = \frac{T_F}{\Delta T} L P_r^{-.6} (.092) Re^{-.2}$$

but from (1.1)

$$Re \equiv \frac{\rho V D}{\mu} = \frac{4 W_s L}{\mu C_p \Delta T} \tag{1.18}$$

Substituting (1.18) in (1.17) gives

$$D = .069723 P_r^{-.6} (\mu C_p)^{.2} \left(\frac{L}{\Delta T}\right)^{.8} \frac{\Delta T_F}{W_s^{.2}} \tag{1.19}$$

Substituting in (1.19) for ΔT_F from (1.14) and using the relation

$$W_s = \frac{PD}{2\sigma\eta s} \langle q''' \rangle$$

and simplifying gives

$$D = \frac{.3873 \mu^{1/6} R^{5/3}}{C_p^{7/3}} \quad \frac{\bar{T}^{5/3} \langle q''' \rangle^{3/2} L^{7/3}}{(\sigma\eta_s)^{3/2} K^{5/6} P^{1/6} \Delta T^{7/3}} \tag{1.20}$$

This is the equation which permits lines of constant wall loading, P_W, to be determined since $\langle q'' \rangle = \alpha P w / Z$.

From equation (1.2) allowing for a finite void fraction

$$n\pi DL W_s = (V_T - \frac{n\pi D^2}{4} L) \langle q'' \rangle$$

Simplifying yields

$$D = \frac{1}{\sqrt{1 + \frac{\sigma\eta s}{2P}}} \sqrt{\frac{2 \sigma\eta s V_T}{\pi n PL}} \tag{1.21}$$

Which for $\sigma\eta s/2P \ll 1$, which is true for small ηv ($\lesssim 5\%$), using the definition of ρ_t yields

$$D = \frac{2 \sigma \eta_s}{\pi P \rho_t L} \tag{1.22}$$

This gives the lines of constant ρ_T.

For a given ΔT_W a relation for D versus L can also be found.

Substituting for Ws and t/D in equation (1.13) gives

$$D^2 = \frac{4k\,\eta s\,\sigma\Delta T_W}{P\,\ln\,(1+P/\sigma)\langle q'''\rangle}\,\frac{1}{}$$

Substituting for $\langle q'''\rangle$ from (1.20) gives after simplifying

$$D = .7889\left[\frac{4k\Delta T_W}{\ln\,(1+P/\sigma)}\right]^{3/8}\frac{\mu^{1/24}}{K^{5/24}}\left(\frac{R\bar{T}}{P}\right)^{5/12}\left(\frac{L}{C_P\Delta T}\right)^{7/12} \qquad (1.23)$$

If ΔT_F is fixed, then substituting for $\langle q'''\rangle$ in equation (1.16) and solving for D gives

$$D = .1345\,\frac{Pr^{-.45}\,\mu^{1/6}\,R^{1/6}}{C_P^{1/12}}\,\frac{\bar{T}^{1/6}\Delta T_F^{3/4}\,L^{5/6}}{K^{1/12}\,\Delta T^{5/6}\,P^{1/6}} \qquad (1.24)$$

This is the last of the desired expressions for diameter versus length in terms of the six fixed parameters and an additional quantity of interest. Summarizing, the applicable expressions are:

Constant Quantity	Equation for D vs L
P_W	1.20
ρ_T	1.22
ΔT_W	1.23
ΔT_F	1.24

1.3.2 Void Fraction Estimate

A simplified approach can be used to estimate the required void fraction given σ, η_s and P.

For a given tube

$$\eta_v(r_t) = \frac{\pi D^2/4}{\pi D^2/4 + A\ (r_t)} \simeq \frac{1}{1 + \frac{4W_s}{D\ q'''(r_t)}} \qquad (1.25)$$

where $A\ (r_t)$ is the cross sectional area of lithium being cooled by the tube at r_t. For a rough averaging consider r_t as a continuous variable (Z) and a flat plane geometry with thickness L.

$$\langle \eta_v(Z) \rangle = \eta_v \simeq \frac{1}{L} \int_0^L \frac{1}{\frac{4W_s}{Dq'''(Z)} + 1}\, dz \qquad (1.26)$$

Assume $q'''(Z) = q_o''' e^{-bx}$ and let $C = 4W_s/Dq_o'''$

$$\eta_v \simeq \frac{1}{L} \int_0^L \frac{1}{1 + Ce^{bz}}\, dz \qquad (1.27)$$

$$\text{or } \eta_v \simeq 1 - \frac{1}{bL} \ln \left[\frac{1 + Ce^{bL}}{1+C}\right] \qquad (1.28)$$

An approximation can also be made for $\langle q''' \rangle$ as

$$\langle q''' \rangle \simeq \frac{1}{L} \int_0^L q_o''' e^{-bZ}\, dz \qquad (1.29)$$

$$\text{or } q_o''' = \frac{bL}{(1-e^{-bL})} \langle q''' \rangle$$

Using the approximation $W_s = PD\langle q''' \rangle / 2\sigma\eta_s$ and substituting for C in equation 1.28 gives

$$\eta_v \simeq 1 - \frac{1}{bL} \ln \left[\frac{1 + \frac{2P}{\sigma\eta_s}\left(\frac{e^{bL} - 1}{bL}\right)}{1 + \frac{2P}{\sigma\eta_s}\left(\frac{1-e^{-bL}}{bL}\right)}\right] \qquad (1.30$$

for $bL \gtrsim 2.5$

$$\eta_v \simeq \frac{1}{bL} \ln \left[1 + bL \frac{\sigma \eta_s}{2P} \right]$$

for $bL \frac{\sigma \eta_s}{2P} \ll 1$

$$\eta_v \simeq \frac{\sigma \eta_s}{2P} - \frac{bL}{2} \left(\frac{\sigma \eta_s}{2P} \right)^2 \tag{1.31}$$

Further, for typical lithium systems b is on the order of $4m^{-1}$ and L on the order of .5m so to a fair approximation.

$$\eta_v \simeq \frac{\sigma \eta_s}{2P} - \left[\frac{\sigma \eta_s}{2P} \right]^2 \tag{1.32}$$

This simple expression allows a rapid estimate of the void fraction for a given choice of σ, η_s and P. A comparison with several published designs gives good agreement as will be shown later.

1.4 316 - He Design Window

The allowable design window or region in the D versus L plane is determined by the constraints imposed. For the helium - 316SS design the following constraints were imposed.

1. $\Delta T_F \leq T_{F\ Max}$
2. $\rho_t \leq \rho_{T\ Max}$
3. $\Delta T_w \leq T_{wMax}$
4. $P_w \geq P_{w\ Min}$

The values chosen for the constraints and parameters depend on the structural material, overall reactor design and an evaluation of radiation damage. Part of the reason for expressing the blanket

design in terms of these parameters is that it should permit easy iteration in order to find an overall reactor design with a given heat exchange type which gives a desirable compromise between efficiency, cost and reliability.

The following table gives a set of parameters and constraints for a 316SS system that illustrate the methodology and are believed to be conservatively chosen.

TABLE 1.1 316-He DESIGN WINDOW EXAMPLE

PARAMETERS			CONSTRAINTS		
$\bar{T}$	=	573°K	ΔT_F	$\leq$	83°C
ΔT	=	200°C	ΔT_W	$\leq$	17°C
P	=	3.8 MPa	# tubes	$\leq$	1.5×10^4
η_s	=	.02			
σ_H	=	48.3 MPa			
K	=	.02			
First Wall Radius	=	2.25m	E_f	=	15.2 Mev/neutron
Major Radius	=	6.0m	Z	=	60 cm

CONSTRAINT SECTION

The sum of the coolant exit temperature, ΔT_F and ΔT_W were chosen to give a peak tube structural temperature of 500°C. The coolant tubes could be arranged in several passes so that the portion of the tubes near the first wall would be below 500°C. Available irradiation test data indicates that these temperatures should be acceptable.[6] At higher temperatures at anticipated damage rates the ductility would be excessively reduced.

The limit chosen for ΔT_W gives a thermal stress of 34 MPa (5000 Psi). This provides a large margin of safety against fatigue failure. Irradiated fatigue data is not presently available but the loss of ductility would indicate a decrease in the fatigue limits. The ASME code 1592 allows a strain range of .175% for 10^6 cycles at 800°F.[7] This would correspond to a peak stress of 273 MPa (39.6 ksi).

The constraint of 1.5×10^4 for the total number of tubes was chosen arbitrarily. If testing can give reliability data then the blanket can be engineered for a given reliability level. Fraas gives a rough estimate for the mean time between leaks as [4]

$$\text{MTBF (hr)} = \frac{10^9}{(\#\text{tube joint} + \#\text{ ft. weld})} \cdot \frac{A}{B}$$

Where A = (coolant temp rise/50). $\frac{E\alpha}{E\alpha ss}$

B = nominal pressure stress/allowable stress

For $A = 4$, $B = 2$ and 1.5×10^4 tubes, the above relation would give a mean time between failures (ignoring the feet of weld) as

$$\text{MTBF} = \frac{10^9}{(2)\ (1.5 \times 10^4)} \cdot \frac{2}{4} = 1.67 \times 10^4 \text{ hours (1.9 years)}$$

PARAMETER SECTION

The reactor size picked corresponds to a small reactor comparable to a design such as the HFCTR[29] or NUMAK.[33] The 60 cm thickness of the lithium zone should insure sufficient breeding. Previous neutron studies[3] indicate that approximately 15.2 MeV will be deposited in the blanket region for each fusion neutron.

The average temperature and ΔT were chosen to give the 500°C maximum structural temperature limit for reasonable values of ΔT_F and ΔT_W. Lower inlet temperatures would be possible but the effect on the heat exchanger design would have to be evaluated.

The pressure of 3.8 MPa (550 Psi) was selected arbitrarily. Higher pressures give lower allowed wall loadings with the assumed limit of 17 °C on ΔT_W and the design value of 48.3 MPa (7000 Psi) for hoop stress.

The fraction of structural material selected was well within what would be allowed for tritium breeding and gave a void fraction of 12%.

The hoop stress of 48.3 MPa is also conservatively chosen. For 316SS at 550°C the stress limit for 0.2% creep in 100,000 hours is 100 MPa in unirradiated steel.[8]

The pumping power to heat removal ratio was set at 2% which is the maximum recommended by Fraas in his comparative survey.[4]

RESULTS

The program listed in Appendix 1 was used to evaluate the analytic expressions derived previously. The result is shown in Figure 1. From equation (1.20) lines of constant neutron wall loading of 1, 2, 3, 4, 5, 6 and 7 MW/m^2 are shown. The film temperature drop line for 83°C is graphed using equation 24. Also shown are four lines for a constant number of tubes using the values of 5×10^3, 10^4, 1.5×10^4 and 2×10^4 tubes in equation (1.21). Finally, the

DESIGN WINDOW DEVELOPMENT

HELIUM - 316 SS SYSTEM

Coolant Tube Diameter vs. Length

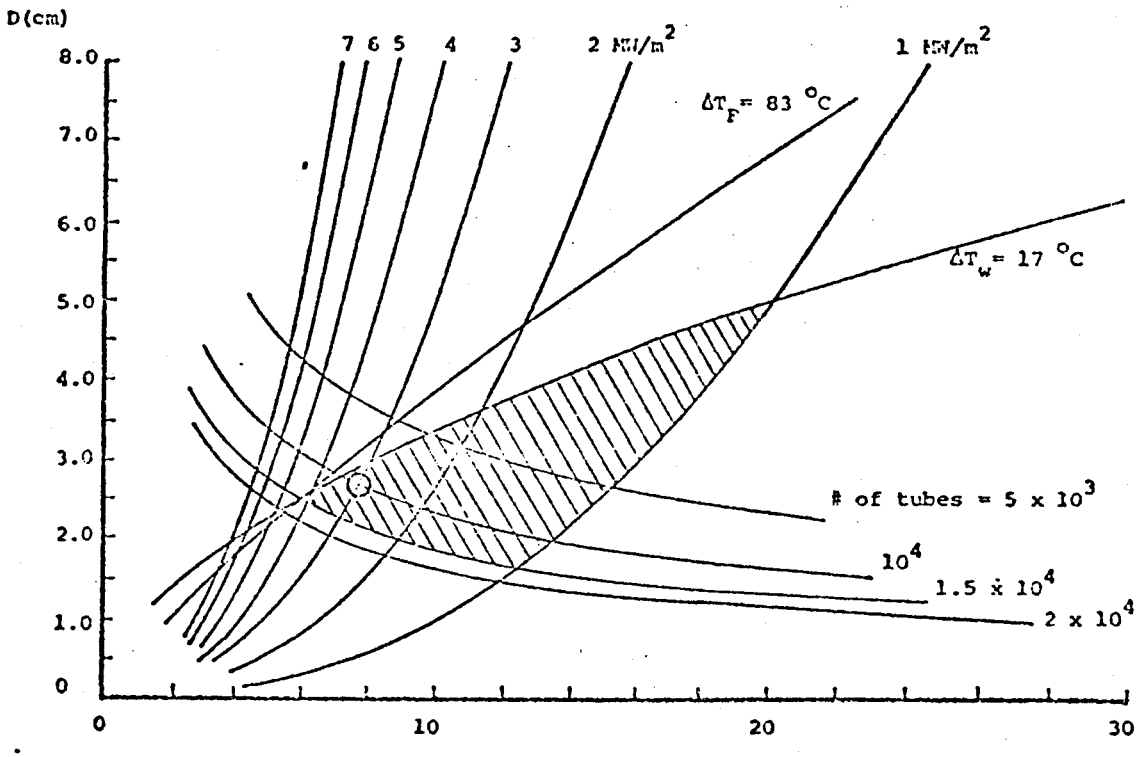

FIXED PARAMETERS		CONSTRAINTS	
$T_{out} - T_{in}$	= 200 K	ΔT_w	$\leq$ 17 °C
$\bar{T}$	= 573 K	# OF TUBES	$\leq 1.5 \times 10^4$
P	= 3.8 MPa	T_{film}	$\leq$ 83°C
η_s	= .02	P_w	$\geq$ 1 MW/m²
σ_H	= 48.3 MPa		
K	= .02		
Z	= .60 m		
r_w	= 2.25		
R	= 6.0 m		

FIGURE 1. HELIUM - 316SS DESIGN WINDOW

(Case 1)

line for a constant wall temperature drop of 17°C is shown as calculated from equation (1.23). For the constraints listed above and a minimum wall loading of 1.0 MW/m^2 the design window is the shaded region shown. The maximum possible wall loading with the given parameters and constraints is 4 MW/m^2 and occurs at the simultaneous intersection of the 15,000 tubes line with the ΔT_W = 17°C and ΔT_F = 83°C lines. This peak wall loading capacity occurs for a diameter of 2.4 cm and a length of 6.0 meters.

If the fraction of tube structural material in the blanket is reduced from 2% to 1% with all other parameters and constraints kept constant, the design window changes as shown in figure 2. In this case, the peak allowed wall loading is only approximately 2.7 MW/m^2 and the optimum geometry changes as shown.

It would be desirable to be able to predict the maximum possible wall loading for a given set of parameters and constraints. This will be done in the following section.

1.5 Analytic Expressions for Maximum Wall Loading

For a given number of coolant tubes in the reactor, the maximum

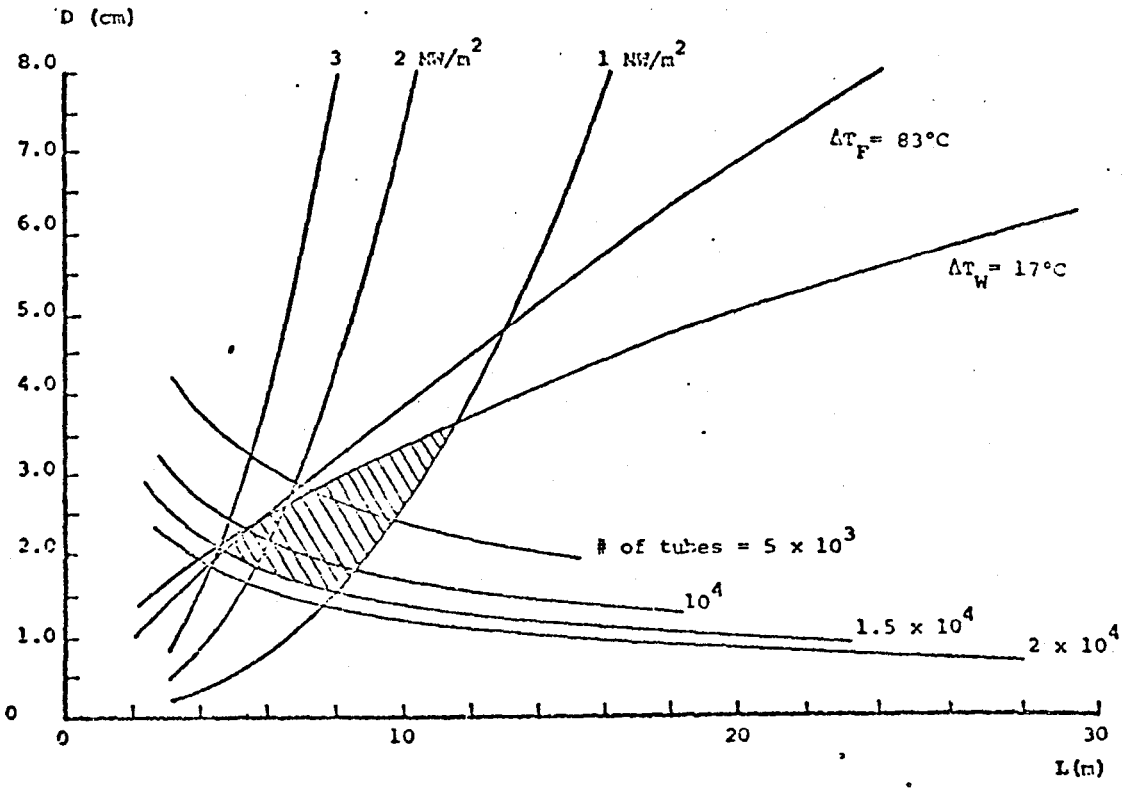

Constraints and parameters same as Figure 1 except

$\eta_s = .01$

FIGURE 2. HELIUM - 316SS DESIGN WINDOW

(Case 2)

wall loading occurs at the intersection of this line with either the ΔT_W or ΔT_F line, whichever gives the lower wall loading. The wall loading at these points can be expressed as a function of the parameters and constraints, independently of geometry.

For $\eta_v \ll 1$ equations (1.21), (1.24) and (1.19) can be expressed respectively as:

$$D = C_1 L^{-1/2} \tag{1.33}$$

$$D = C_2 L^{5/6} \tag{1.34}$$

$$D = C_3 P_W^{3/2} L^{7/3} \tag{1.35}$$

Solving for P_W gives

$$P_W = \frac{C_2^{17/12}}{C_1^{3/4} C_3^{2/3}} \tag{1.36}$$

Substituting for C_1, C_2, and C_3 gives

$$P_W = F_1 \frac{Z}{\alpha} \frac{P^{.25} (\sigma n_s)^{.625} K^{.4375} (\rho_T \Delta T)^{.375} \Delta T_F^{17/16}}{\bar{T}^{.875}} \tag{1.37}$$

where

$$F_1 = .1333 \frac{P_r^{-.6375} \mu^{.125} Cp^{1.4375}}{R^{.875}}$$

For helium at 300°C, $F_1 = 12.3$. The dependence of F_1 on $\bar{T}$ is weak.

For a given ΔT_W the wall loading can also be found. Equation (1.23) can be expressed as

$$D = B_2 L^{7/12} \tag{1.38}$$

Equations (1.33), (1.35) and (1.38) can then be solved for Pw to give

(1.39)

$$P_W = \left[\frac{C_1}{C_3} \right]^{2/3} \frac{1}{\left[\left[\frac{C_1}{B_2} \right]^{12/13} \right]^{17/9}} = \frac{B_2^{1.7436}}{C_1^{1.077} C_3^{2/3}}$$

Substituting and simplifying gives

(1.40)

$$P_W = F_2 \frac{Z}{\alpha} \left[\frac{k\Delta T_W}{\ln(1+P/\sigma)} \right]^{.6538} \frac{(\sigma\eta_s)^{.4615} K^{.1923} (\rho_t \Delta T)^{.5385}}{\bar{T}^{.3846} P^{.07689}}$$

Where

$$F_2 = 3.929 \frac{C_P^{.53855}}{\mu^{.03846}_R}$$

For helium at 300°C $F_2 = 31.1$

Equations (1.37) and (1.40) should be very useful to show the relative effectiveness of changing one parameter or constraint versus another. For example, from the first design window the maximum wall loading was 4 MW/m^2 at 2% structure. Equation (1.37) predicts that for the same film temperature, number of tubes and given parameters of Table 1.1 the maximum wall loading with 1% structure should be

$$P_W\ (1\%) = P_W(2\%) \left(\frac{1}{2} \right)^{.625} = 2.6\ MW/m^2$$

which agrees with figure 2.

Equations (1.37) and (1.40) were in fact, used for Table 1.1 to estimate the ΔT which would give the maximum wall loading for the assumed $\bar{T}$ and a maximum tube temperature of 500°C. This is shown in Figure 3 where the wall loadings limits set by the two equations are shown for the given parameters. The lowest curve is the most limiting

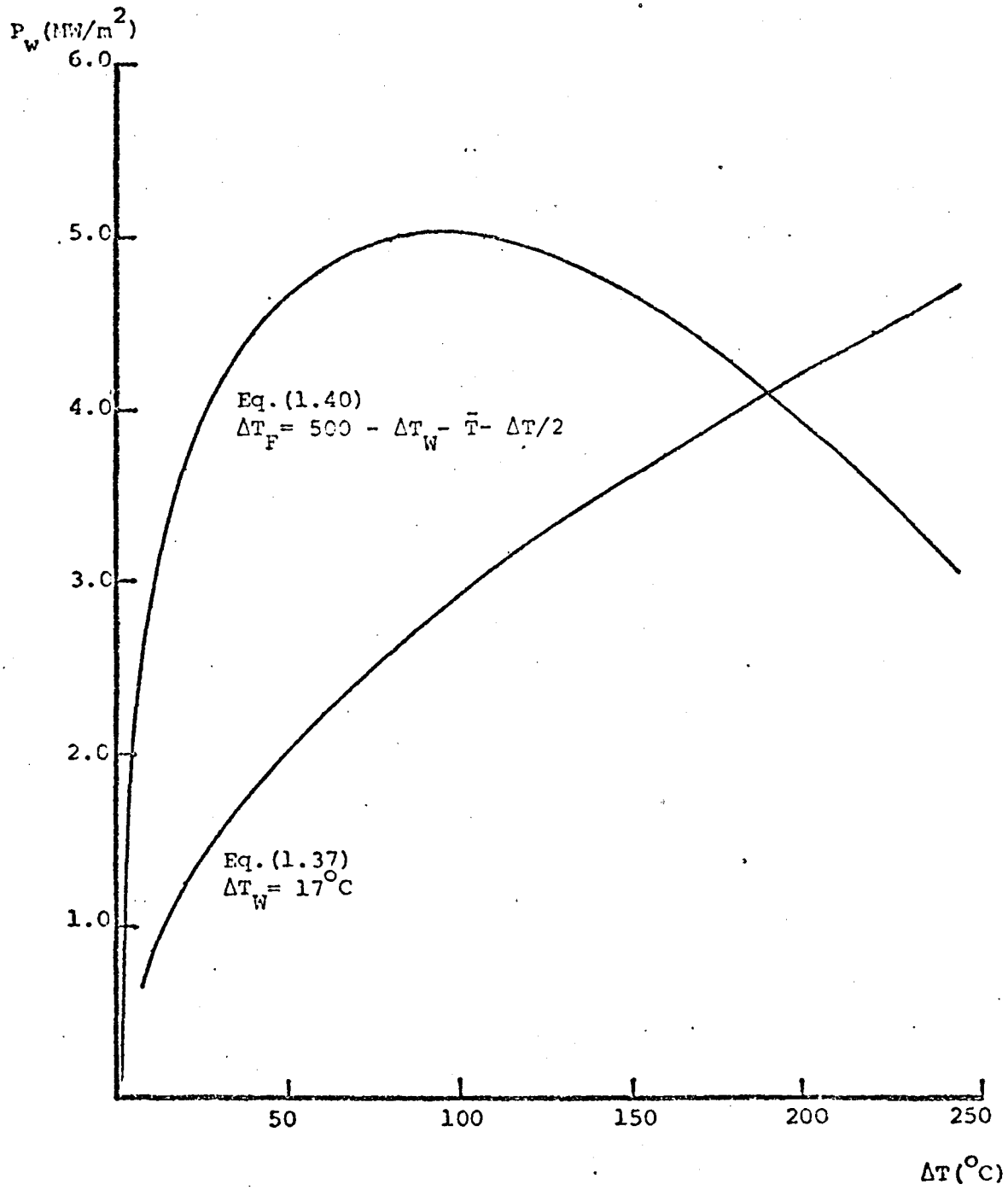

FIXED PARAMETERS

$\bar{T}$ = 573 K
P = 3.8 MPa
η_s = .02
σ_H^s = 48.3 MPa
K = .02
z = .60 m
r_w = 2.25 m
R = 6.0 m

FIGURE 3. MAXIMUM WALL LOADING VS. ΔT

and the maximum occurs at their intersection.

1.6 TZM-He DESIGN WINDOW

1.6.1 General Considerations

The use of TZM as an alternative advanced structural material was also studied. Such a refractory material offers the advantage of higher thermal efficiency through the use of higher temperatures. Other refractory materials such as niobium or vanadium were not analyzed because present data indicates a strong possibility of excessive corrosion caused by trace impurities in the helium at temperatures above 600°C.

Irradiated material data on TZM is presently limited. Data taken by Wiffen[11], however, does indicate that irradiation at or below 450°C to the damage levels expected in a fusion reactor will cause the Ductile to Brittle Transition (DBT) temperature to rise to that temperature or higher. There consequently appears to be a lower limit on the allowable temperature range, although the precise value is not presently known. For this reason inlet coolant temperatures of at least 600°C were imposed for this study. The upper temperature limit is set by the loss of mechanical strength. 1000°C was set as a design limit in the UWMAK III study[12] and will be used here also. Because of the higher temperatures used in the TZM designs, the importance of the peak lithium pool temperature increases compared to the 316SS designs. The vapor pressure of lithium

at 1070°C is 0.1 atm. and at 1300°C it is 1 atm. The pressure in a module strongly effects the structural design and should be above the vapor pressure if boiling is not desired. For the TZM designs a rough estimate will be made for the peak lithium pool temperature in the next section.

1.6.2 Peak Lithium Temperature Estimate

A rough estimate of the peak temperature in the lithium pool will be made by assuming a cylindrical lithium region with an adiabatic boundary on the outside surrounding a single coolant tube. It will also be assumed that within a given region the volumetric energy generation rate is a constant and that the heat conduction is only radial. With these assumptions, the solution of the 1-D conduction equation for the lithium pool temperature rise can be shown to be (see appendix 1.2)

$$\Delta T_{Li} = \left[\frac{q'''D^2}{16\,k_L} + \frac{DW_S}{4k_L}\right] \ln\left(1 + \frac{4W_S}{q'''D}\right) - \frac{DW_S}{4k_L} \qquad (1.41)$$

Where it has been assumed that the diameter of the lithium cell (D_C) is such that

$$\pi DW_S = \frac{\pi}{4}\,(D_C^2 - D^2)\,q''' \qquad (1.42)$$

Let $q''' = \beta\ \langle q''' \rangle$

$$W_S = \frac{PD}{2\sigma\eta_s}\langle q''' \rangle$$

Substituting and simplifying gives

$$\Delta T_{Li} = \langle q''' \rangle \frac{D^2}{8k_L} \left[\left[\frac{\beta^2}{2} + \frac{P}{\sigma\eta_s} \right] \ln \left(\frac{1+2P}{\beta\sigma\eta_s} \right) - \frac{P}{\sigma\eta_s} \right] \tag{1.43}$$

For normal exponential decrease in q''' this expression will have a maximum where q''' or β is a minimum because of the large conduction length required. By introducing the value for $\beta = q'''_{min}/\langle q''' \rangle$, lines for a given maximum lithium pool temperature can be introduced into the D versus L plane. Start with the following definition for T_{LMax}

$$T_{LMax} = \bar{T} + \Delta T/_{Z-} + \Delta T_W + \Delta T_F + \Delta T_{L_i} \tag{1.44}$$

From (1.23) $\Delta T_W = \dfrac{D^{8/3}}{L^{1.555} F_1^{8/3}}$

where $F_1 = .7889 \left[\dfrac{4k}{\ln \frac{(1+P/\sigma)}{}} \right]^{3/8} \mu^{1/24}$

From (1.24) $\Delta T_F = \dfrac{D^{4/3}}{F_2^{4/3} L^{10/9}}$

were $F_2 = .1369 \dfrac{P_r^{-.45} \mu^{1/6} R^{1/6}}{C_P^{1/}} \dfrac{\bar{T}^{1/6}}{K^{1/12} \Delta T^{5/6} P^{1/6}}$

From (1.43 and 1.20)

$$\Delta T_{Li} = \frac{F_3}{F_4^{2/3}} \frac{D^{8/3}}{L^{19/9}}$$

where $F_3 = \dfrac{1}{8k_L} \left[\left[\dfrac{\beta}{2} + \dfrac{P}{\sigma\eta_s} \right] \ln \left(\dfrac{1+2P}{\beta\sigma\eta_s} \right) - \dfrac{P}{\sigma\eta_s} \right]$

$$F_4 = .3873 \frac{\mu^{1/6} R^{5/3}}{C_P^{7/3}} \frac{\bar{T}^{5/3}}{(\sigma\eta_s)^{3/2} K^{5/6} P^{1/6} \Delta T^{7/3}}$$

Let $C = T_{LMax} - \bar{T} - \Delta T/2$

Substituting in (1.44) gives a quadratic equation for $D^{3/4}$ or

$$D = \left[\frac{\sqrt{B^2 + 4AC} - B}{2A} \right]^{4/3} \qquad (1.45)$$

where $B = 1/(F_2^{4/3} L^{10/9})$

$$A = \left[\frac{1}{F_1^{8/3}} + \frac{F_3}{F_4^{2/3}} \right] \frac{1}{L^{14/9}}$$

Equation (1.45) gives the relation between D and L for a constant maximum pool temperature under the given assumptions.

1.6.3 Numerical Results

The 316SS design had two constraints on the peak structural temperature and the allowable thermal stress. With TZM however, the thermal stresses are generally not very large because for a given tube thickness and surface heat flux $q''L^2T$ is approximately 1/10 that for 316SS. In addition, if the pool temperature is limited to approximately 1000°C then the peak tube temperature will always be below this. It is not clear what the peak pool temperature limit would have to be, but limiting it to 1000°C would allow structural members to be placed anywhere.

Figure 4 shows a design window for a TZM design with parameters similar to the previous 316SS design. For this system a higher pressure was chosen (6.9 MPa) because it reduces the pumping power required for a given rate of heat removal. Compared to the 316SS-He system, the temperature and pressure are both higher resulting in a gas density slightly higher (3.41 vs. 3.19 kg/m^3). The higher pressure was not used for the stainless steel design because it would

HELIUM - TZM SYSTEM
Coolant Tube Diameter vs. Length

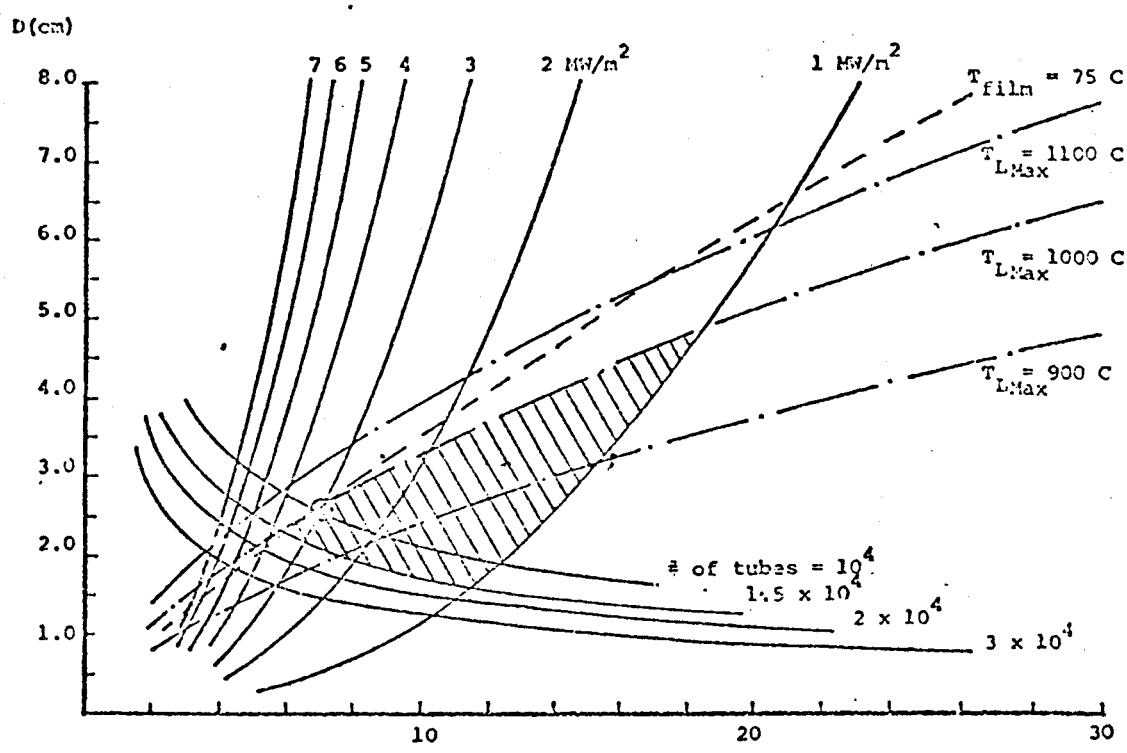

FIXED PARAMETERS		CONSTRAINTS	
$T_{out}-T_{in}$	= 200 K	$T_{Lithium}$	$\leq$ 1000 C
$\bar{T}$	= 973 K	# OF TUBES	$\leq 1.5 \times 10^4$
P	= 6.9 MPa	ΔT_w	$\leq$ 27 C
η_s	= .03	P_w	$\geq$ 1 MW/m^2
σ_H	= 48.3 MPa		
K	= .02		
Z	= .60 m		
r_w	= 2.25 m		
R	= 6.0 m		

FIGURE 4. HELIUM - TZM DESIGN WINDOW

have shifted the constant wall temperature drop line to the right (see figure 1) limiting the design to lower wall loadings. For TZM, however, the wall temperature drop is not limiting. A higher fraction of structural material was also used since this gave a void fraction of 9.4%, which was close to the 11% void in the 316SS. The breeding ratio for the two designs should be close.

In figure 4, three peak lithium pool temperature lines are shown for 900°C, 1000°C and 1100°C. The ratio of q'''min/<q'''>was estimated from neutronic studies done by J. Chao[3] to be≈ 0.4. With a 1000°C constraint and 1.5×10^4 tubes, the maximum wall loading is nearly the same as for the 316SS-He design ($3.9 MW/m^2$ vs $4 MW/m^2$). The principal advantage would be the higher thermal efficiency. If 1100°C is allowable, however, up to $5 MW/m^2$ could be tolerated.

1.7 Comparison With Published Designs

The expressions developed in this chapter were compared with several published designs as shown in Table 1.2.

The first column is based on a Nb-He design presented by Fraas in reference 14. The predicted average energy generation rate (<q'''>) based on the nominal film drop and number of tubes using Equation (1.37) comes within approximately 6% of the design value. The predicted diameter is larger and tube length shorter than the published results. It appears the discrepency is due to an error in the calculated pumping power in the reference. The following parameters are given in the reference.

Heat loading of coolant tube 6100 Btu/ft/hr ($5.86/10^{3}$ w/m)

I.D.	.8 in	2.032×10^{-2} m
L	70 feet	21.3m
Coolant temperature rise	727°F	404 K
Pressure	494 Psi	3.4 MPa

Application of the standard correlations of section 1.2 gives a pumping power to heat removal ratio of 5.5% not the 1.5% listed. The film temperature drop also turns out to be 35.3°C not 55.5°C. Substitution of the higher pumping power and lower ΔT_F then gives a design with nearly the same $\langle q''' \rangle$ and the 2.0 cm diameter and 21 m length.

The next comparison is with the design presented by Mitchell and Booth[5]. Here equation (1.37) is approximately 10% low. The difference is probably due to error in the estimate for the tube density. The diameter and lengths cannot be compared directly because in the reference roughened tubes were assumed. The estimate for the void fraction agrees quite well for a pressure of 6 MPa.

The third comparison is with a design published by G. Melesse-d' Hospital and G. Hopkins[15]. It is taken from table 1 of that reference for L = 3m and P = 30 atm. The predicted q''' is about 16% below the design value, but the predicted tube diameter, length and void fraction agree well.

Another comparison was made for the UWMAK III inner graphite

blanket. As can be seen the agreement between predicted and design values is good.

The last comparison is shown in figure 5 for a published E.B.T. tubular design.[13] In this case the tubes were not designed to a constant W_s so the expressions for ΔT_F and ΔT_W are not applicable. The wall loading line, however intersects the number of tubes = $2x10^4$ line at a diameter and length which agree very well with the design values of D = 1.75 cm and L = 33.5m and n = 20,000 tubes.

TABLE 1.2

COMPARSION OF PUBLISHED DESIGNS WITH ANALYTIC EXPRESSIONS

PARAMETER	Ref. 14	Ref. 5	Ref. 15	Ref. 12 (ISSEC)
P (MPa)	3.35	11.2	3.04	6.89
σ (MPa)	13.4*	35	20.3*	62*
η_s	.02*	.049*	.017*	.028*
K	.015	.012	.0224	.0247*
$\rho_t (m^{-3})$	5.54	148*	109*	39.9*
ΔT (°K)	404	350	500	382
ΔT_F (°K)	55.5*	46	200*	48.6*
$\overline{T}$ °K	998	750	1023	952
	DESIGN (PREDICTED)			
$<q'''>$ (MW/m^3)	.685*(642)	10.1*(9.1)	13.7*(11.8)	6.85*(6.03)
η_v (%)	3.6(3.8)	12**(12)	5.1*(5.3)	11*(11)
D (cm)	2.03(2.44)	***	1.44(1.4)	1.8(1.8)
L (m)	21(14.8)	***	3(3)	11(12.6)

* Calculated based on data given in respective reference

** Calculated based on data in reference 3 for P = 6 MPa

*** Not directly comparable because the tubes were assumed to be roughened.

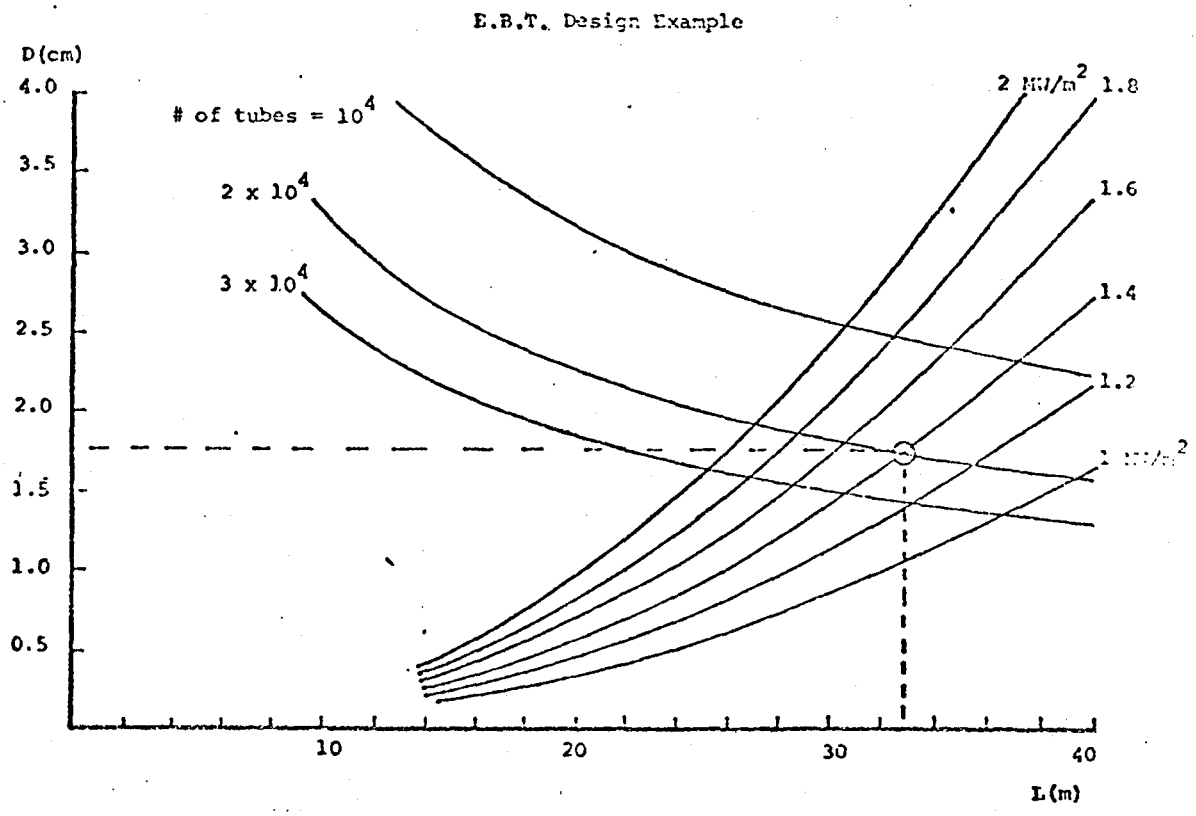

FIXED PARAMETERS

$T_{out} - T_{in}$	= 415 K
$\tilde{T}$	= 546.5 K
P	= 6.9 MPa
η_s	= .0144
σ_H	= 75.4 MPa
K	= .05
z	= .60 m
r_w	= 1.2 m
R	= 60 m

FIGURE 5. E.B.T. DESIGN EXAMPLE

CHAPTER II.

FLIBE COOLING

2.1 INTRODUCTION

The coolant known as flibe (Li_2BeF_4) has been proposed by a number of investigators as a potential coolant for a fusion reactor.[17,18,19] The eutectic mixture of LiF and BeF_2 melts at 459°C and has been used in the Molten Salt Reactor experiment.[20] A summary of its physical properties are given in table 2.1.

Table 2.1 PHYSICAL PROPERTIES FOR FLIBE[21]

(66 mole % LiF; 34 mole % BeF_2)

Liquidus Temperature	458 ± 1°C
Viscosity (T(°K)) Centipoise	$\eta = 0.116 \exp (3755/T)$ ± 15%
Thermal Conductivity (W/cm°C)	k = 0.01 ± 10%
Electrical Conductivity (ohm-cm)$^{-1}$	$K = 1.54+6\times10^{-3}(t(°C)-500)$ ± 10%
Heat Capacity (cal g^{-1}°C)	$C_p = .57$
Heat of Fusion (cal g^{-1})	$\Delta H_{fusion} = 107$
Density T(°C) (g/cm^3)	$\rho = 2.214-4.2\times10^{-4}T$ ± 2%

PRANDTL NUMBER:

T(C°)	P_r
500	35.6
600	20.4
700	13.1

These physical properties make possible a number of advantages

compared to a helium coolant design but also pose certain drawbacks. The principal differences are that much lower coolant pressures can be used with flibe but that MHD effects due to the finite electrical conductivity must be taken into account.

The physical model for the flibe systems is taken to be nearly the same as for the helium design. The tubes are assumed to be in a static lithium pool and distributed so that each tube removes the same amount of heat per unit length. In addition, the tubes are assumed to run primarily in the torroidal direction to minimize MHD effects although multiple passes are allowed. An entry and exit length perpendicular to the torroidal field is also assumed. As in the helium design, the surface heat flux is removed by a separate radiation shield.

2.2 MHD EFFECTS

The strong magnetic field can have three primary effects on the performance:

1) Decreased chemical stability[18]

2) Increased pressure drop[22]

3) Delay in the transition from laminar to turbulent[22] flow.

1. The maximum induced voltage caused by flow perpendicular to a magnetic field B is given by[17]

$$V_m = BvD \qquad (2.1)$$

Potential differences on the order of several volts will destabilize the LiF and BeF_2 releasing flourine and making these compounds very

corrosive toward metallic tube walls.[18] The maximum allowed voltage will most likely have to be determined experimentally. It will probably be a function of wall material and thickness. Grimes and Cantor[18] suggest that voltages on the order of 0.2 volts should be acceptable.

The magnetic field will also increase the pressure drop. The calculation of this effect is complicated by a lack of experimental data for turbulent flow of a weakly conducting fluid in a strong transverse field with conducting channel walls. For an order of magnitude estimate of the pressure drop, the correlation for circular tubes suggested by Hoffman and Carlson[22], was used with the substitution of a turbulent friction factor ($\Psi = .184\ Re^{-.2}$) in place of the laminar term ($\Psi = 64/Re$) in the equation. For a uniform B field over an entry and exit length of $L_\perp$ and a total tube length of L the pressure drop is approximately

$$\Delta P \simeq \frac{1}{2}\rho V^2 \Psi \frac{L}{D} + 1.3 \frac{L_\perp \mu V}{(D/2)^2}\left[\frac{Ha^2 \tanh Ha - 3 + Ha^2 C}{Ha - \tanh Ha \quad 1 + C}\right] \qquad (2.2)$$

where Ha is the Hartmann number and is given by

$$Ha = \frac{BD}{2(\eta\mu)^{1/2}} \qquad (2.3)$$

and $C = \frac{2T\eta_F}{D\eta_W} >> 1$ for flibe and metal walls.

This poloidal field is generally small enough to neglect in these calculations.

Hoffman and Carlson[22] suggest the following formula for predicting the transition Reynolds number for flow in a transverse magnetic field.

$$R_T = 500 \text{ Ha} \qquad (2.4)$$

The heat removal for the model chosen is accomplished primarily by tubes in the torroidal direction. For these tubes the transverse field component would be on the order of 1T or less. At 600°C the tube diameter would have to be greater then 5cm before R_T increased above 2100. This effect can, therefore, be neglected.

2.3 DESIGN WINDOW DEVELOPMENT

The unknowns for the system are the same 21 listed for the helium design, plus the Hartmann number and the maximum induced voltage V_m. This gives a total of 23 unknowns. The available relations are also quite similar to the helium case. Equations (1.1) through (1.8) still hold. Equation (1.9) for ΔP is replaced by Equations (2.2) and (2.3) from this chapter. The same correlations (1.10) and (1.11) are used for the friction factor and heat transfer coefficient. If the film temperature drop is large an improvement could be made by the use of the Sieder - Tate correlation which accounts for the difference in viscosity in the film region.[23] Equation (1.12) for the density is replaced by the correlation given in table 2.1. Equation (1.13) for ΔT_W still holds. This gives a total of 14 relations. In addition, Equation(2.1) for V_m from this section is applicable. Finally, it appears reasonable to assume that the inlet pressure is given by

$$P = \Delta P + 1 \text{ atm.} \qquad (2.5)$$

This gives a total of 16 relations. For every point on a tube diameter versus length plot to be determined,5 other quantities must

be specified.

The five chosen quantities for a given design window are:

a.) $\bar{T}$

b.) ΔT

c.) t

d.) η_s

e.) V_m

The average coolant temperature and ΔT are chosen as before based on material properties, desired thermodynamic cycle and also a minimum inlet temperature of approximately 500°C because of the 459°C melting point. The tube thickness is specified in this case instead of the stress because low coolant pressures are possible and a minimum practical thickness set by fabricability is greater than the thickness required for acceptable hoop stresses. Similar to the helium design a fraction of structural material is chosen based on a breeding ratio consideration. The last fixed parameter is the induced voltage. For a given B and $\bar{T}$ this also fixes the Reynolds and Nussult numbers.

2.4 ANALYTIC RELATION

From equation (1) an energy balance gives

$$\frac{\rho V D}{4} C_p \Delta T = L W_s \qquad (2.6)$$

Substituting $W_s = \frac{t}{\eta_s} \frac{\alpha P_w}{Z}$ and $V_m = BVD$

gives

$$P_W = \frac{z}{\alpha} \frac{\rho C_p}{4} \frac{V_m}{B} \frac{\eta_s}{t} \frac{\Delta T}{L} \tag{2.7}$$

Therefore, lines of constant neutron wall loading are inversely proportional to L and are independent of D.

To obtain an expression for a constant ρ_T start with eq. (1.2)

$$\rho_T \pi D\ L\ W_S = \langle q''' \rangle$$

Substituting for W_S gives

$$D = \frac{\eta_s}{\pi t \rho_t L} \tag{2.8}$$

From (2.1) the Reynolds and Nussult numbers are given by

$$Re = \frac{\rho}{\mu} \frac{V_m}{B}$$

$$Nu = .023 Re^{.8} Pr^{.4} = hD/k_f$$

The film temperature drop can be found to be expressed by

$$\Delta T_F = \frac{k_f \rho C_p \Delta T V_m D}{4B\ Nu\ L} \tag{2.9}$$

From equation (1.43) the temperature rise in the lithium pool is approximated by

$$\Delta T_L = \langle q''' \rangle \left[\frac{D^2}{8k} \left(\frac{\beta}{2} + \frac{2t}{D\eta_s} \right) \ln \frac{(1+4t)}{\beta \eta_s D} - \frac{2t}{D\eta_s} \right] \tag{2.10.1}$$

where for the flibe system from Equation (2.7)

$$\langle q''' \rangle = \frac{\rho C_p}{4} \frac{V_m}{B} \frac{\eta_s}{t} \frac{\Delta T}{L} \tag{2.10.2}$$

For structural materials with a high thermal conductivity and thin tube walls the wall temperature drop will be small. For this case the maximum lithium pool temperature can be approximated by

$$T_{L\,Max} = \bar{T} + \frac{\Delta T}{2} + \Delta T_F + \Delta T_{Li} \tag{2.11}$$

Substituting equations 2.9, 2.10 into 2.11 and simplifying gives the following relation between D and L for a constant maximum pool temperature

$$L = \frac{\Delta T}{\left[T_{LMax} - \bar{T} - \frac{\Delta T}{2}\right]} \frac{\rho C_p V_m D}{16\ B\ k_L} \left[\frac{4k_L}{Nu} - 1 + \frac{\beta D \eta_s}{4t} \ln\left(1 + \frac{4t}{\beta \eta_s D}\right)\right] \tag{2.12}$$

In a manner directly analogous to the helium and void fraction, the coolant fraction is approximated by

$$\eta_C = \frac{\eta_s D}{4t} - \left[\frac{\eta_s D}{4t}\right]^2 \tag{2.13}$$

Flibe will breed tritium itself, but not as well as pure lithium. It will probably be necessary to limit the fraction of flibe to attain a desired breeding ratio with a given structural material fraction. The neutronic evaluation of this has not been done however. Calculations with 12% flibe however, do indicate adequate breeding.[3] If a limit is placed on η_C this can be represented on the D vs L graph as an additional constraint line, limiting the maximum tube diameter.

2.5 CHOICE OF STRUCTURAL MATERIAL

When flibe was used in the MSR experiment, the structural material was Hastalloy, a nickel alloy. It performed well and there was little corrosion. Unfortunately, the nickel-based alloys are not compatible with the liquid lithium, ruling out their use in the interior blanket.

Stainless steel exhibits relatively low corrosion rates with flibe[24] and if this were the only problem it could probably be used. The irradiation data on 316SS however indicates that at above 500°C to 550°C at the expected damage rates, the ductility is reduced excessively so that the uniform elongation at failure is less then 1/2%.[25] Due to the high melting point of flibe, structural temperatures of at least 600°C are required so that 316SS and flibe do not appear compatible. If a stainless steel alloy could be developed that would allow operation at 600°C then an attractive design could be proposed.

The structural material that appears most compatible with flibe is molybdenum or TZM, a molybdenum alloy.[26] Further material research is required before it can be used however, in order to determine the effects of irradiation and develop fabrication techniques.

2.6 TZM - FLIBE DESIGN WINDOW

To facilitate a comparison with the helium coolant, a design window will be developed here for a system similar to the He-TZM design. The reactor size is the same and it is assumed that the total energy

deposited per fusion in the blanket is the same 15.2 MeV. The choice for fixed parameters is

$\bar{T}$ = 700°C

ΔT = 200°C

t = 1 mm

η_s = .02

V_m = 0.25 volts

The coolant inlet and exit temperatures are the same as for the helium case. The thickness appears as a reasonable minimum for fabrication. Smaller thicknesses might even be possible since the clad for fission reactor fuel pins which are on the order of several meters long and 1.15cm in diameter have been fabricated with thickness between 1/2 mm and 1 mm.[27] The fraction of structural material (2%) is well within what could be used and still breed and is close to that used for the helium designs. Finally, the induced voltage was fixed at 1/4 volt. In addition, to the above parameters it was assumed that the maximum B field was 10T and the longest sum of entry and exit path lengths was 10m.

The following constraints were imposed

$T_{Li\ Max} \leq$ 1000°C

tubes $\leq$ 15,000

$\Delta P \leq$ .69 MP

The $T_{Li\ Max}$ limit allows structure to be placed anywhere. The number of tubes corresponds to what was considered for the helium design. Finally, a maximum pressure drop limit was imposed. This corresponds to

the design requirement in the proposed Molten Salt Breeder Reactor to keep the pressure drop in a single leg to below 150 feet of head of salt so that single stage pumps could be used.[28]

The design window was constructed using the program in Appendix 2 to evaluate the analytical expressions developed here. The result is shown in figure 6. Vertical lines of constant neutron wall loading are shown for 3MW/m^2 through 10 MW/m^2. Three lines for 5,000, 7,000 and 15,000 tubes are shown. Lithium pool peak temperature (for β=0.4) are shown for 900°C, 1000°C and 1100°C. Finally the maximum pressure drop line completes the diagram. For the given constraints, the maximum wall loading is 7.8MW/m^2 and the corresponding geometry is D=1.25cm and L=10.5m.

The allowable window is shaded for $L \leq 30m$. At the maximum wall loading the pumping power to heat removal ratio is only approximately 0.07%. The hoop stress is only 4.3 MPa and the thermal stress (from a thin plate approximation) only 6.6 MPa. The steady state performance thus is much better then for helium.

Because of the ln term in the expression for the maximum pool temperature (eq. 2.10.1) it was not possible to obtain simple algebraic expressions for the wall loading in terms of the fixed parameters and constraints. To give some idea of the sensitivity of the design window to the parameters some additional design windows are shown in figures 7 through 10 for the same basic reactor.

Figure 7 shows the effect of reducing η_s to 1%. In this case the

FLIBE - TZM SYSTEM

Coolant Tube Diameter vs. Length

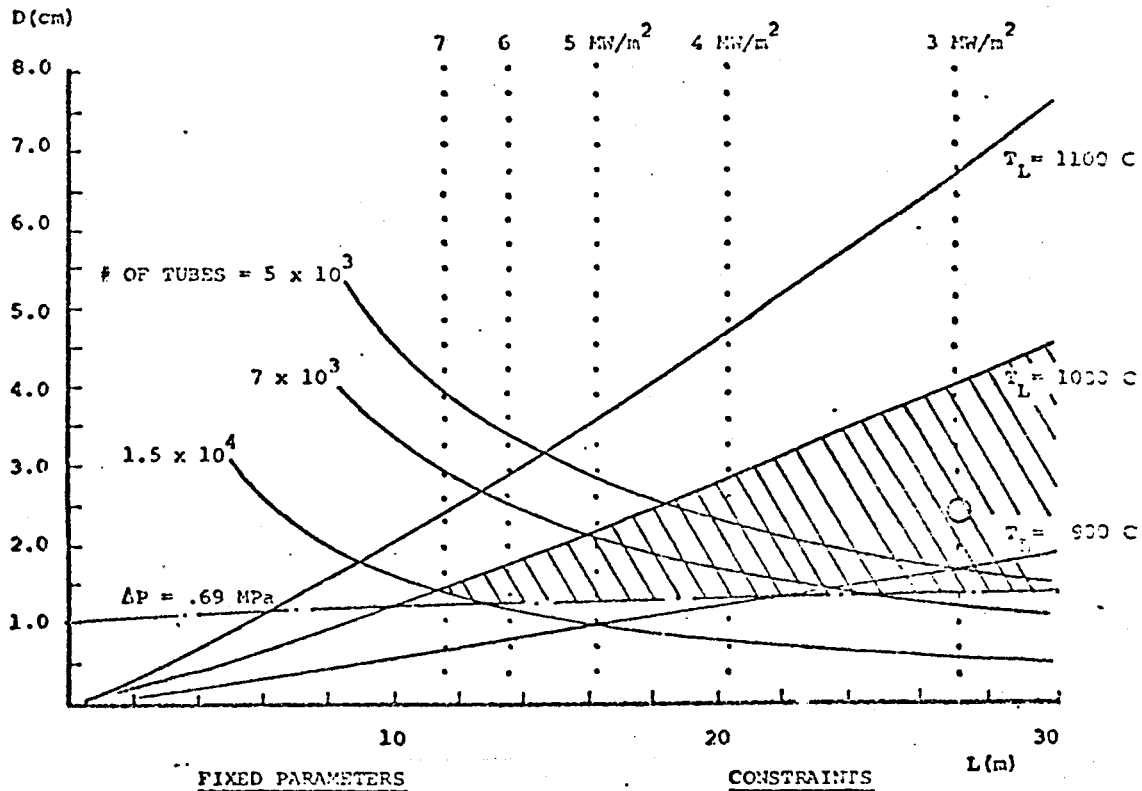

FIXED PARAMETERS

T_{in} = 600 C

T_{out} = 800 C

B = 10 T

BvD = 0.25 volts

η_s = .02

L entry & exit = 10 m

Reynolds # = 10^4

Z = 0.6 m

r_w = 2.25 m

R = 6.0 m

CONSTRAINTS

$T_{Lithium} \leq$ 1000 C

$\Delta P \leq$ .69 MPa

OF TUBES $\leq 1.5 \times 10^4$

FIGURE 6. FLIBE - TZM DESIGN WINDOW

(Case 1)

maximum wall loading is 4 MW/m^2 and is constrained by $T_{Li\ Max}$ and ΔP_{Max}. As shown in the figure the maximum number of tubes is limited to approximately 10^4.

If η_s is increased to 3% as shown in figure 8 up to 10 MW/m^2 is allowed by the given constraints with 1.5×10^4 tubes. This is most likely higher then material damage considerations would allow but indicates the high heat removal capacity.

In figure 9 the effect of reducing the allowed induced voltage to 0.15 volts is shown. In this case, the Reynolds number is only 6000 which is most likely a borderline case between laminar and turbulent flow. For the assumed 10T field this is about as low an induced voltage as is possible. If the flow were to become laminar the film temperature drops would increase greatly. Assuming turbulent flow, the wall loading limit for this case is 5.4 MW/m^2.

Figure 10 shows the effect of increasing the inlet temperature to 700°C with the same exit temperature of 800°C. The wall loading limit for this case is 5.7 MW/m^2.

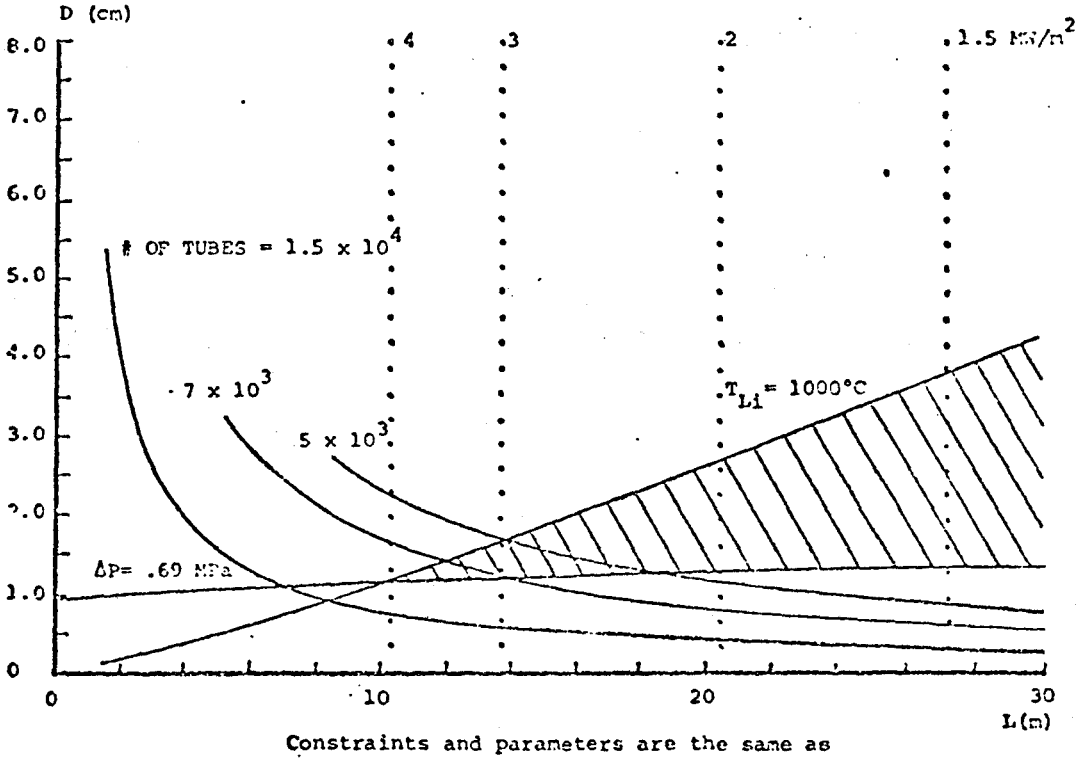

Constraints and parameters are the same as in Figure 6 except η_s = .01

FIGURE 7. FLIBE - TZM DESIGN WINDOW

(Case 2)

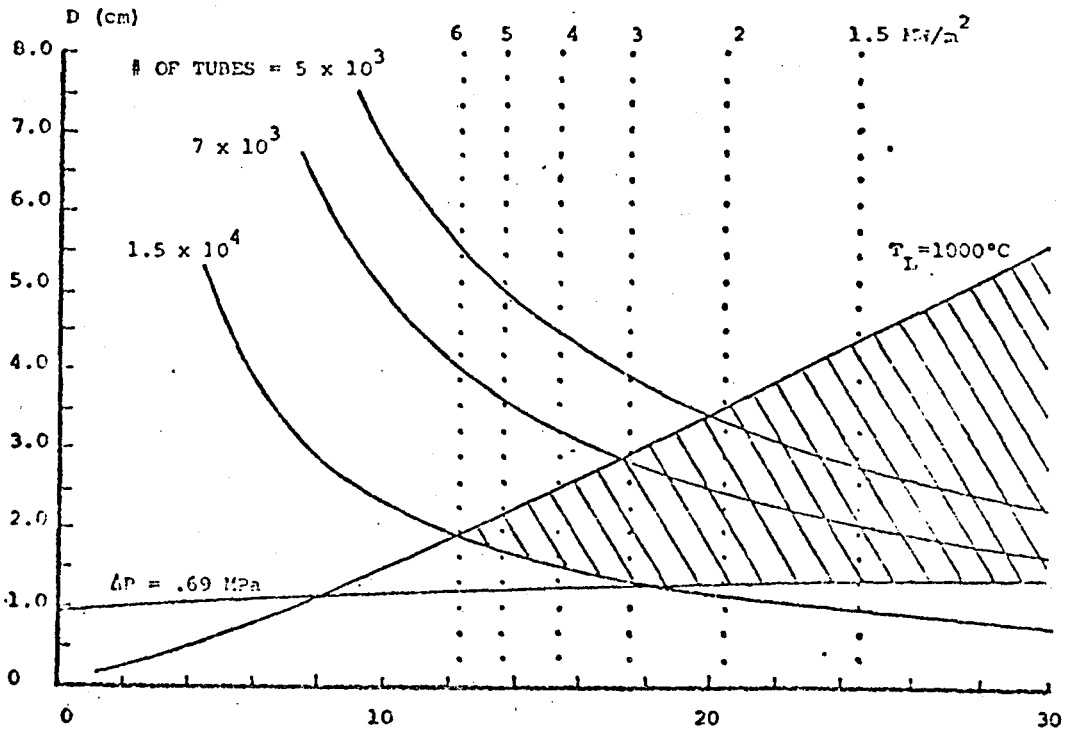

Constraints and parameters are the same as in Figure 6 except $\eta_s = .03$

FIGURE 8. FLIBE-TZM DESIGN WINDOW

(Case 3)

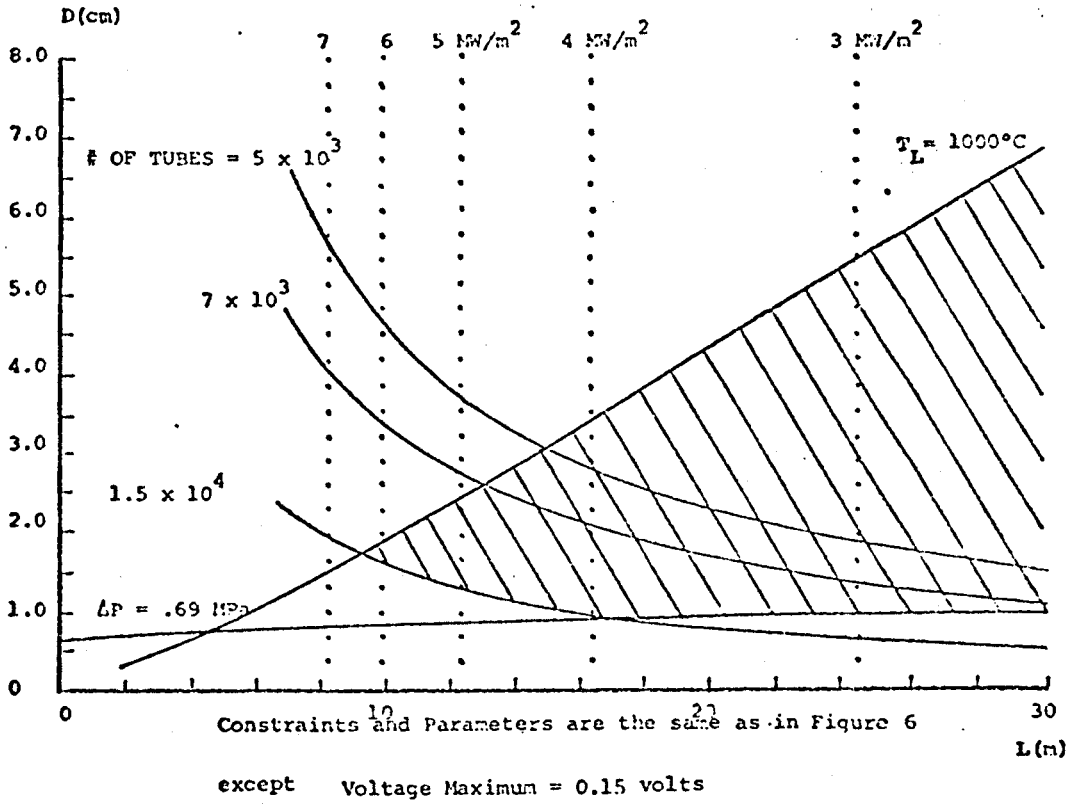

FIGURE 9. FLIBE - TZM DESIGN WINDOW

(Case 4)

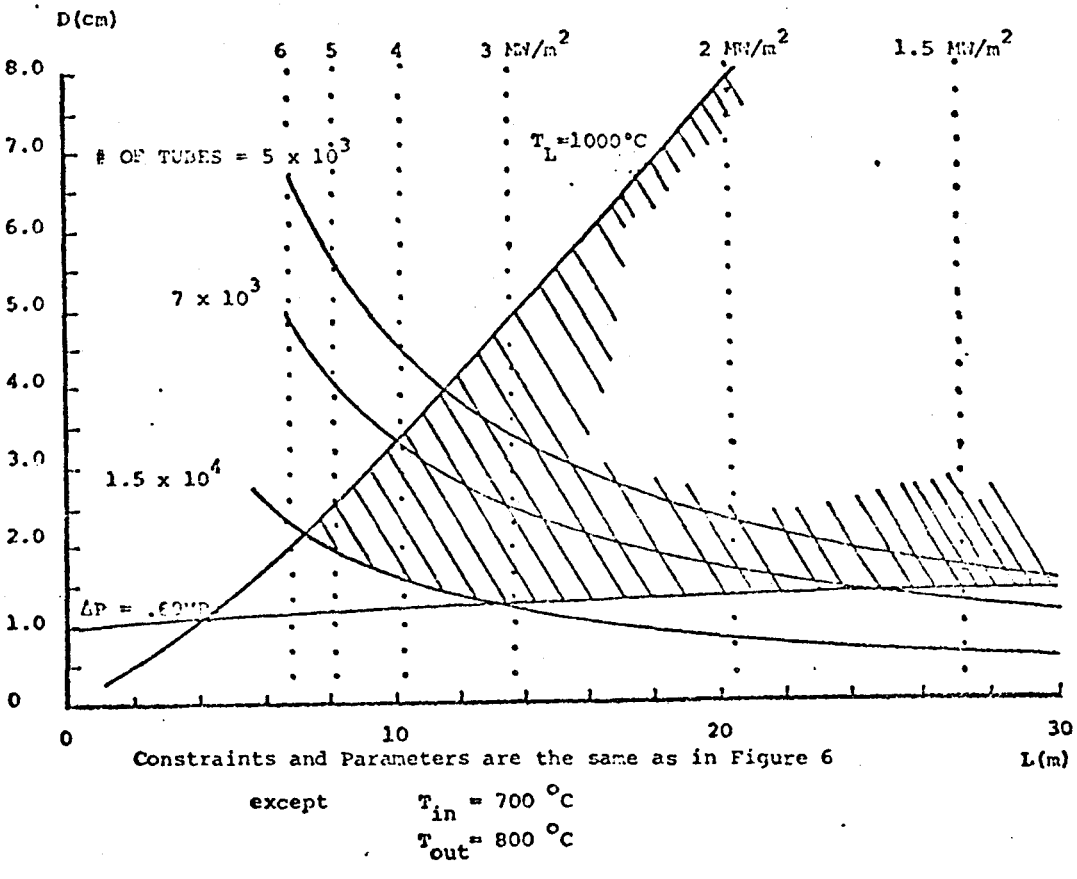

FIGURE 10. FLIBE - TZM DESIGN WINDOW

(Case 5)

III. SHELL COOLING

3.1 OBJECTIVES

The designs considered thus far have assumed that the coolant tubes are distributed throughout the blanket such that the surface heat flux anywhere on a tube is a constant. To come as close as possible to this condition requires the accurate placement of all the tubes as determined by the neutronic heating rates and numerical calculation of the heat conduction problem.

Another possible tube configuration was also examined. This distribution assumes that the coolant tubes are located only at several discrete radial locations, forming cylindrical shells and separating the lithium (as shown in figure 11). The advantages hoped for such a configuration are:

1.) Reduction of hot spot effects due to flow irregularities (an extreme case of irregularities would be a blockage in which case ability to operate under a local failure might exist.)

2.) Easier construction

3.) Possible neutronic improvement

If a single tube has a flow blockage the heat from the lithium pool can be easily conducted to neighboring tubes without excessive structur l temperatures. This would be especially important for flibe with a low Reynolds number where a relatively small flow reduction might cause the transition from turbulent to laminar flow.

It should be considerably easier to construct large assemblies

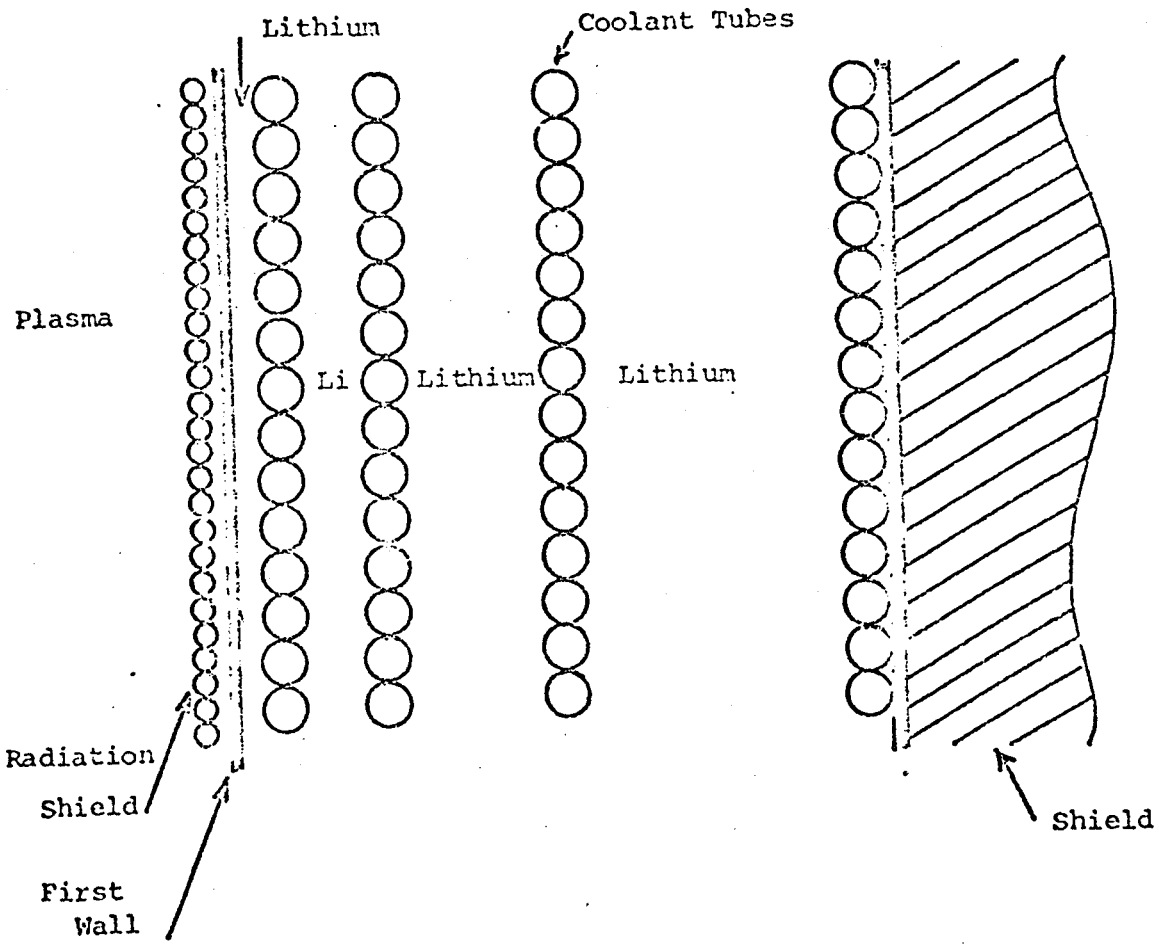

FIGURE 11. SHELL COOLING CONCEPT

of tubes in concentric shells as opposed to distributing them nearly homogeneously throught the blanket, each at a precise location.

Finally, it was hoped that the breeding ratio might be improved by a kind of spatial self shielding whereby the coolant and structural material which cause parasitic losses are located at only a few discrete radial locations. There was some evidence for this in the neutronic studies done for the High Field Compact Tokamak Reactor study accomplished at M.I.T.[29]

For volumetric energy generation rates that can be represented as an exponential function of radius, or a sum of exponential functions, the solution of the heat conduction equation in a 1-D cylindrical geometry is straight forward as shown in Appendix 3. Linear correlations for the thermal conductivity of lithium can be easily incorporated by using a change in variables.

3.2 SHELL DESIGN EXAMPLE - HFCTR

A shell cooling configuration was proposed to the High Field Compact Tokamak Reactor (HFCTR) design group who were considering a stagnant lithium blanket with heat removal by flibe using distributed tubes and TZM as the structural material. Initial neutronic studies appeared to show an improvement in the tritium breeding ratio using the shell approach[29] Primarily because of this, the shell configuration was incorporated in the conceptual reactor design study. The thermal analysis was based on the results of Appendix 3.1 and will be presented as a numerical example for the concept.

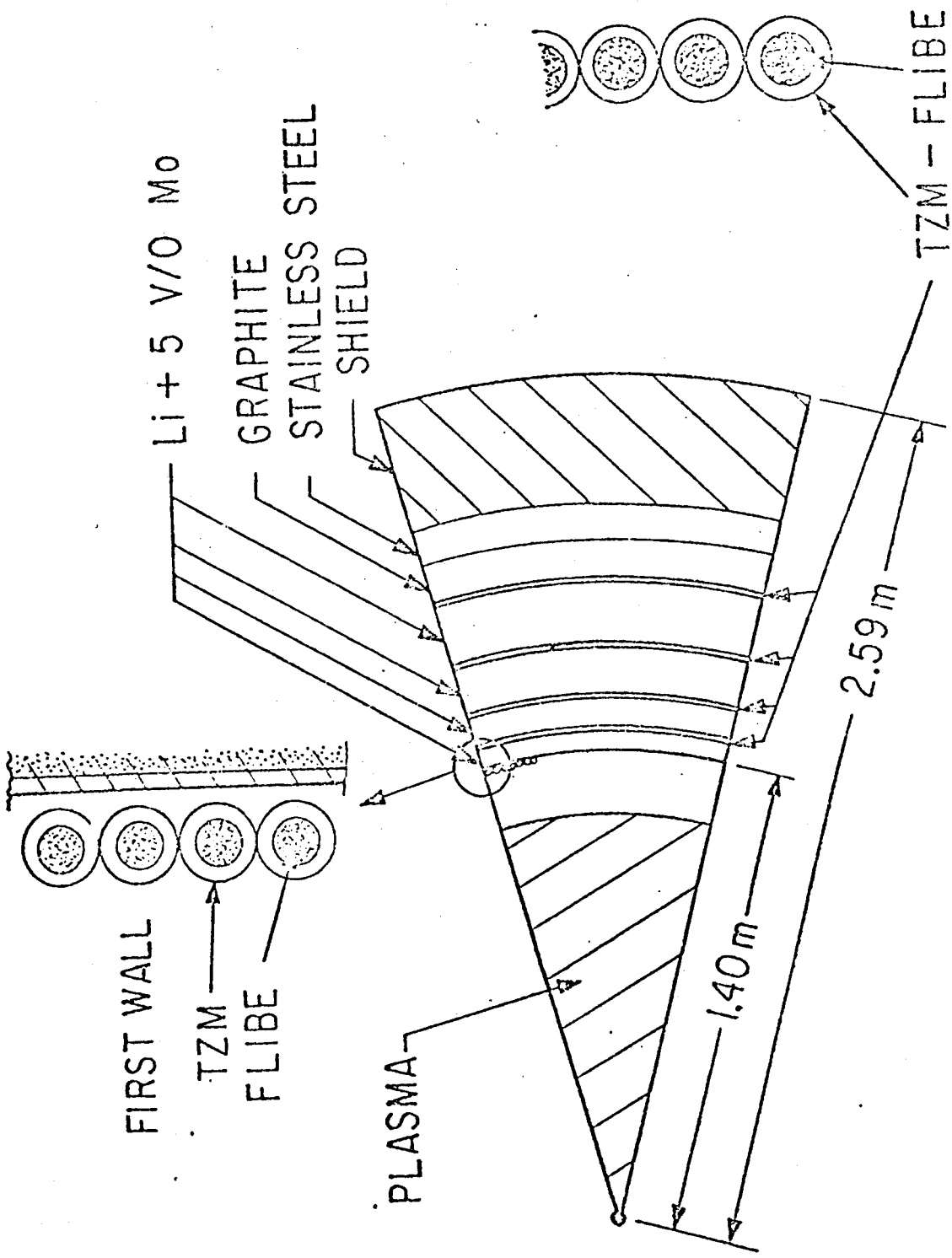

FIGURE 12. HYBRID SHIELD DESIGN

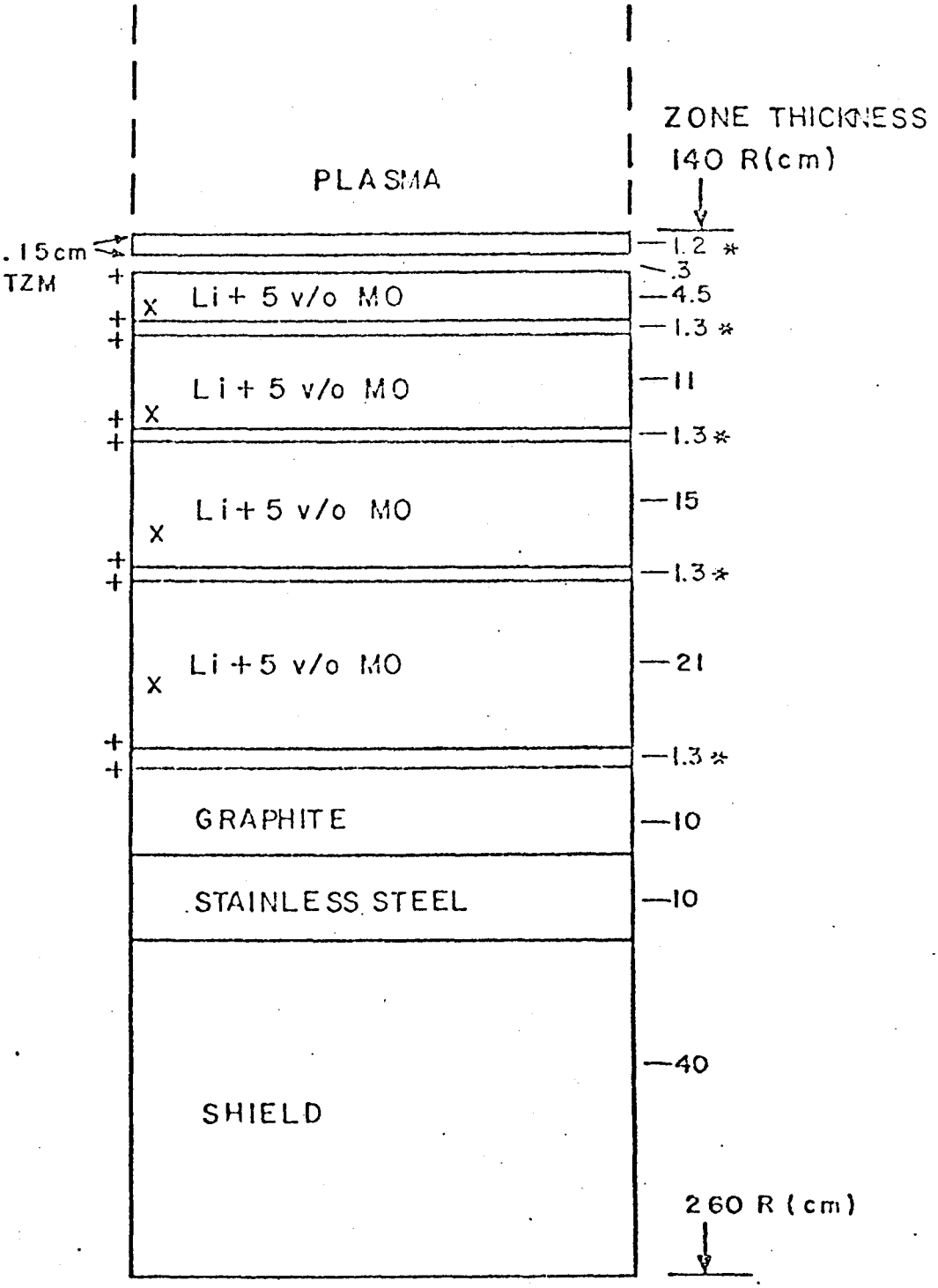

FIGURE 13. NEUTRONIC MODEL FOR HFCTR DESIGN

The average neutronic wall loading for the HFCTR design was $4MW/m^2$ with a peak wall loading for $5.6\ MW/m^2$. The maximum design temperature for the lithium pool was 1000°C to allow TZM structural members to be placed anywhere within the pool. The surface heat flux due to particles and radiation was removed by a separate first wall bank of cooling tubes. The proposed configuration is shown in figure 12.

Before the detailed heating rate calculation could be done, the tube distribution was required. The optimum distribution gives the same peak lithium temperature in all breeding regions. To determine this however, actually requires a knowledge of the spatial heat distribution. To start, a volumetric heating rate was assumed based on the wall loading and other published designs.[12,32] The assumed q''' was given by

$$q''' = 20\ e^{-4(r(m)-r_o)}\ MW/m^3.$$

In addition, the peak tube wall temperature was taken to be 650°C for all shells. The radial location of the first three tube shells was then varied so as to give the same peak lithium temperature in all regions of 1000°C.

The tube distribution determined in this manner was then used for the breeding ratio calculations[29] and also for the heating rate calculation employing the NEBULA Code.[29] The neutronic model is shown in figure 13. The 121 group calculation gave a breeding ratio of 1.23

for this configuration. The heating rates were calculated by the Nebula Code for a number of finite zones and a least squares fit was made to express the heating rates in terms of the following exponentials for a 10 MW/m^2 neutron wall loading

1st Lithium Zone	$q''' = 31.189\ e^{-3.68(r-1.4158)}$
2nd & 3rd Lithium Zones	$q''' = 27.1814\ e^{-3.21(r-1.4158)}$
4th Lithium Zone	$q''' = 27.1814\ e^{-3.21_r(-1.4158)} + 3.828\ e^{-18.19(1.9658-r)}$

where 1.4158m = Start of first lithium region

1.9658m = End of last lithium region

For a 5.6 MW/m^2 loading, the lithium temperatures were recalculated using the normalized form of the above relations and the results of section 4.2 as shown in figure 14. The peak temperatures were found to vary between 940°C and 1027°C, close enough to the design limit not to warrant further iterations.

From the analytic results, the heat flux on each bank of coolant tubes can be easily determined. Knowing this, the coolant velocity for each channel which will give the same desired bulk coolant temperature rise for all tubes can be found. The differing velocities can be obtained by either orificing or supplying differing pressure heads to each shell. The details for the remaining thermo-hydraulic parameters for the HFCTR design can be found in reference 29. Briefly the inlet temperature was 544°C with a bulk coolant temperature rise for

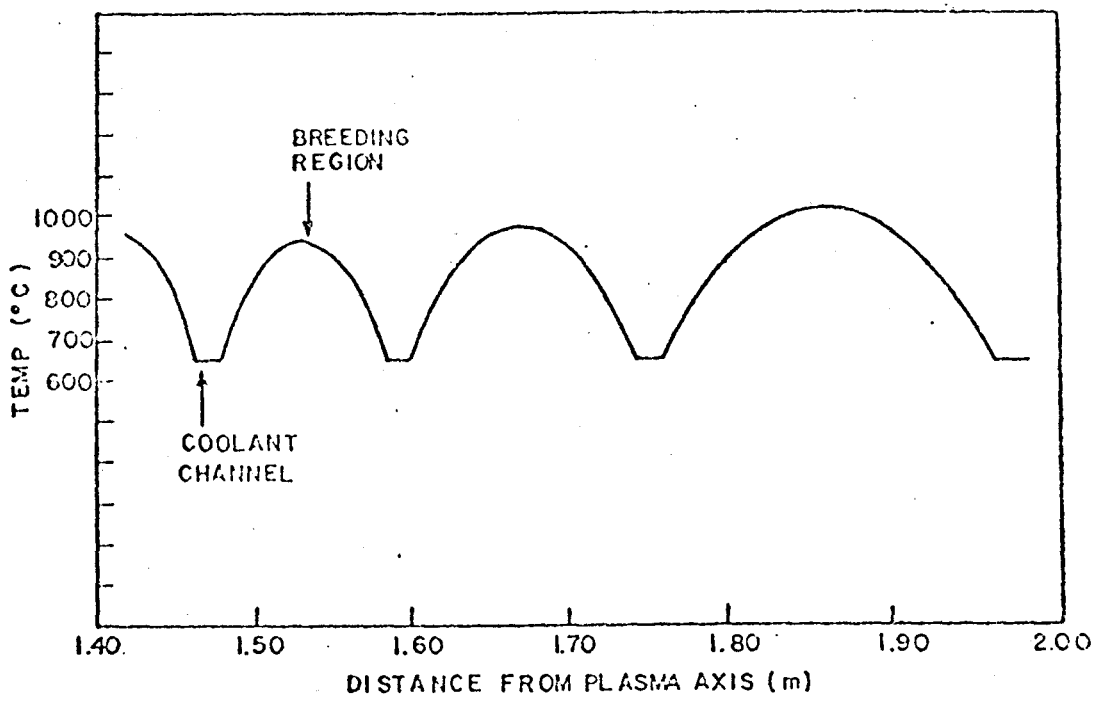

FIGURE 14. PEAK TEMPERATURE PROFILE FOR HFCTR DESIGN

all tubes of 36°C and an average tube length in the torroidal direction of 4.7m. The average film temperature drop was 60°C and a maximum wall exit temperature of approximately 650°C. The pumping power to heat removal ratio was quite small, on the order of 0.3%.

3.3 WALL LOADING LIMITS WITH MULTIPLE SHELLS

The assumption of equal wall temperatures is only an approximation. With the same bulk temperature for all channels and different surface heat fluxes and flow velocities, the wall and film temperature drops will differ slightly between channels. An iterative program was developed (Appendix 3.4) which accounts for these effects and determines the maximum allowed wall loading given the following:

1) Blanket inner and outer radii (r_i, r_o)
2) Number of shells
3) Tube diameter, thickness and length
4) Maximum pool temperature
5) Coolant physical properties
6) Inlet temperature
7) Exit temperature (or velocity in 1 channel)
8) Exponential constant for $q''' = A_o \exp(-b(r-r_i))$

The program solves for the shell radial locations, coolant flow velocities and heating rate which gives the specified maximum lithium pool temperature in all regions and the specified bulk coolant temperature rise for all tubes.

In general, the coolant velocities will be highest for the shell closest to the plasma and decrease with increasing radius. To achieve this orificing would be required.

For a given reactor design, the length of the shells, or tubes in the torroidal direction would depend on the major radius and the desired number of modules.

As a numerical example the allowed neutron wall loading was found for 3, 4 and 5 shells using TZM as the structural material with flibe and helium coolants. The assumed design conditions are given in table 3.1

TABLE 3.1 SHELL COOLING EXAMPLE

First Wall Radius r_i (m)		2.8
Outer Breeding Zone Radius r_o (m)		3.4
Maximum Lithium Temperature °C		1000
Average Tube Torroidal Length (m)		5.0
Tube Diameter (cm)	Flibe	2.0
	He	2.4
Tube Thickness (mm)	Flibe	1.0
	He	1.5
Coolant Inlet Temperature °C		600
Coolant Exit Temperature °C	Flibe	650 & 800
	He	800
Heating Rate		$q''' + A\ EXP(-4(r-r_i))$

As in the HFCTR design, a separate radiation shield removes the surface heat flux on the first wall and there is a small stagnant lithium region behind the first structural wall, in front of the first shell of cooling tubes.

The inner and outer blanket radii were arbitrarily assumed but the results should not be very sensitive to their absolute values but more so on the thickness of the zone. The maximum pool temperature of 1000°C allows structural TZM members anywhere in the breeding zone. The tube length is an arbitrary choice. A length of 5m would allow a machine with a major radius of 6.4m to be divided into octants. Tube diameters were chosen which gave small pumping power to heat removal ratios. The tube diameters will also have some effect on the breeding ratio, but that was not evaluated for this work. The tube thickness was chosen as 1mm for flibe as a minimum practical. For the helium case 1.5mm was chosen to reduce the hoop stress. At 1000 PSI the hoop stress is 8000 PSI which appears acceptable. The inlet and outlet temperatures for helium were chosen to be the same as for the distributed tube design presented previously. For flibe the same inlet temperature of 600°C was used but the exit temperature was reduced to 650°C. An 800°C exit temperature would have resulted in laminar flow for tubes at the rear of the blanket with only a 5m length.

The results are given in table 3.2.

Table 3.2 WALL LOADING WITH MULTIPLE SHELLS

n	Coolant	T_{Exit} (C°)	A_o (MW/m^3)	P_W (MW/m^2)
3	He	800	3.44	0.77
3	Flibe	800	4.10	0.92
3	Flibe	650	7.81	1.75
4	He	800	7.44	1.67
4	Flibe	800	8.82	1.98
4	Flibe	650	16.7	3.76
5	He	800	13.7	3.07
5	Flibe	800	16.1	3.61
5	Flibe	650	30.3	6.81

The shell radial locations, coolant velocities and average wall temperatures are given in Appendix 3.5.

The wall loading calculations here are only meant to be indicative of the general range possible, and to give a methodology to be used in design after preliminary neutronic heating rates are found. Because of the small amount of heat removed by the last shell it may be desirable to use fewer tubes and space them somewhat apart. In addition, some heat would be removed from the shield section. The principal variable that determines the allowable wall loading for a given n is the difference between the maximum pool temperature and the coolant exit temperature.

3.4 CONCLUSIONS ON SHELL CONCEPT

Compared to a distributed tube design, a shell design requires more coolant tubes, a range of coolant velocities, requiring orificing, high peak heat fluxes and low minimum coolant velocities. With 316SS tubes the heat fluxes to tubes near the first wall could limit the allowable wall loading due to thermal stresses. With a molten salt and TZM structure, the heating rates near the last channel must be known well and the coolant velocity high enough to insure turbulent flow. The induced voltage will place an upper limit on the velocity in the first shell and for a given ΔT this will also limit the maximum velocity for the last shell. For a given design there may, therefore, be only a small range of allowable ΔT or velocities.

It appears that the shell concept is most applicable for high wall loading with TZM and flibe.

Several variations are possible on the configuration given in this chapter. The first wall has a stagnant lithium section behind it, in the hope of improving breeding. For pulsed operation, this wall would experience a large temperature change. It may be desirable to have the first shell of tubes next to this wall, in close contact.

Another possibility is to design the blanket so that no structural members are needed in the region of maximum pool temperature. Higher allowed pool temperatures would then allow increased wall loadings.

It would be desirable to do a neutronic study to investigate more

accurately, the effects of spatially separating the coolant into a few radial locations on the breeding ratio. This may be even more important if other salts which do not contain lithium are investigated.

In general, the advantages in breeding, hot spot effects and construction offered by the shell concept appear viable, but they must be balanced against the disadvantages of an increased number of tubes, higher peak thermal stresses and a smaller latitude in design choices for ΔT.

IV. OVERALL COOLANT COMPARISON AND EVALUATION

4.1 Introduction

In this chapter, a comparison will be made between helium, flibe and lithium on as common a basis as possible, with the objective of determining which coolant has the best thermal-hydraulic characteristics. The physical model and calculations for lithium as a coolant are taken from J. Chao's thesis.[3]

Table 4.1 gives the coolant-material systems to be considered here.

Table 4.1 SYSTEMS FOR COMPARISON

System	Coolant	Structural Material
1	Lithium	316SS
2	Helium	316SS
3	Helium	TZM
4	Flibe	TZM

TZM was not used with lithium as a coolant because its high electrical conductivity would cause excessively high MHD induced pressure drops for the tubular design considered. 316SS was not used with Flibe because of the high melting point of the eutectic (459°) as discussed previously.

Two methods of comparison will be used for the four systems. In the first method, a common wall loading will be selected and design points determined for each of the systems. The pumping power,

number of tubes and other system parameters will then be compared. For the second method, the maximum wall loading will be found for each of the four systems when the number of tubes is limited to 20,000 and the peak pool temperature to 1000°C.

The reactor geometry is the same as used for the design window examples in Chapter 1 and 2. The major radius is 6 m and the first wall radius is 2.25 m with a 60 cm thick breeding zone. The results are insensitive to the first wall shape and an elongated "D" shape with the same first wall area would give nearly the same results. The size is roughly comparable to a HFCTR,[29] NUMAK[30] or DEMO[31] sized machine.

As before, the surface heat flux is to be removed by a radiation shield and possibly a divertor. Tritium breeding and heating calculations were not done separately for all systems but based on previous work, it was assumed that each fusion neutron would deposit a net energy of 15.2 MEV in the breeding region. This heat is to be removed by cooling tubes distributed such that for each system the heat removed per unit length is the same for all tubes.

4.2 CHOICES FOR COMPARISON

Table 4.2 summarizes the limits and fixed parameters chosen.

The limits and parameters for the helium and Flibe systems are the same as used previously and have been applied to the lithium-cooled system also. There are some differences, however, between quantities which are imposed and those which are allowed to vary up to a constraint value. These differences result from the different physical models used and MHD effects.

Table 4.2 LIMITS AND PARAMETERS

	L_i-316SS	He-316SS	He-TZM	FLIBE-TZM
$T_{W\ Max}$(°C)	≤ 500	≤ 500	≤1000	≤1000
σ(MPa)	48.3	48.3	48.3	48.3
T_{in}(°C)	200	200	600	600
T_{out}(°C)	400	400	800	800
$T_{Li\ Max}$(°C)	600/1000	≤600	≤1000	≤1000
K(%)	≤2	2	2	≤2
ΔT_W(°C)	≤17	≤17	≤27	≤27
B.R.	≥1.15	≥1.15	≥1.15	≥1.15

4.3 PHYSICAL MODEL FOR THE LITHIUM COOLED SYSTEM

A schematic diagram for the blanket arrangement analyzed in Reference 3 is shown in figure 15.[3] The cooling tubes lie in the torroidal direction and the lithium coolant is supplied and removed by headers which enter and exit radially. Each torroidal segment has 2N headers with n cooling tubes between a pair of headers. The tubes are spaced along a header so that the heat removed per unit length is the same for all tubes.

The principal MHD induced pressure drop for the blanket and shield regions occur in the radial headers. It is assumed that the outside of the headers which pass through the stagnant lithium can be electrically insulated. The method used to calculate the pressure drop is given in reference 3 and is based on the correlations suggested by Hoffman and

Carlson.[22]

The bulk coolant temperature rise is the same for all tubes and is achieved by orificing so that the flow velocity is the same for all tubes.

The headers are to be tapered with the maximum diameter at the rear of a shield region behind the lithium. For a given N the largest header diameter possible is given by

$$D_H = \frac{2\pi R_s}{N} \tag{4.1}$$

Where R_s is the radius from the plasma center to the outside of the shield region. The methodology for constructing a design window for the lithium system is discussed in Reference 3. The result for this system is shown in figure 16. The horizontal axis is the coolant tube length. The vertical axis is not a continuous variable, but rather the number of tubes between a pair of headers. The constraint on D_H is shown for a 60 cm breeding zone with a 65 cm shield region with 180 pairs of headers per torroidal segment. The coolant velocity into the headers is fixed at 0.1 m/sec so that for longer tube lengths with the same ΔT and wall loading, a higher mass flow rate and hence larger header diameter is required. Lines for 20,000, 40,000, 60,000 and 70,000 tubes are shown. With a given maximum lithium pool temperature and geometry, the allowable wall loading depends only on the number of tubes between headers. Interpolated integer values of neutron wall loadings are shown for 2 MW/m^2 through 6 MW/m^2.

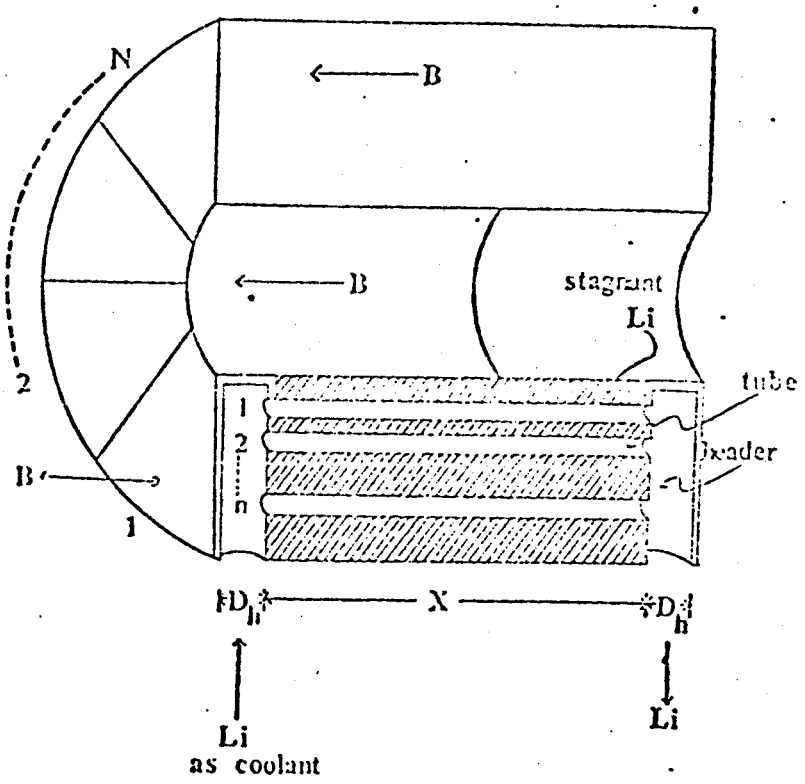

FIGURE 15. LITHIUM COOLANT GEOMETRY[3]

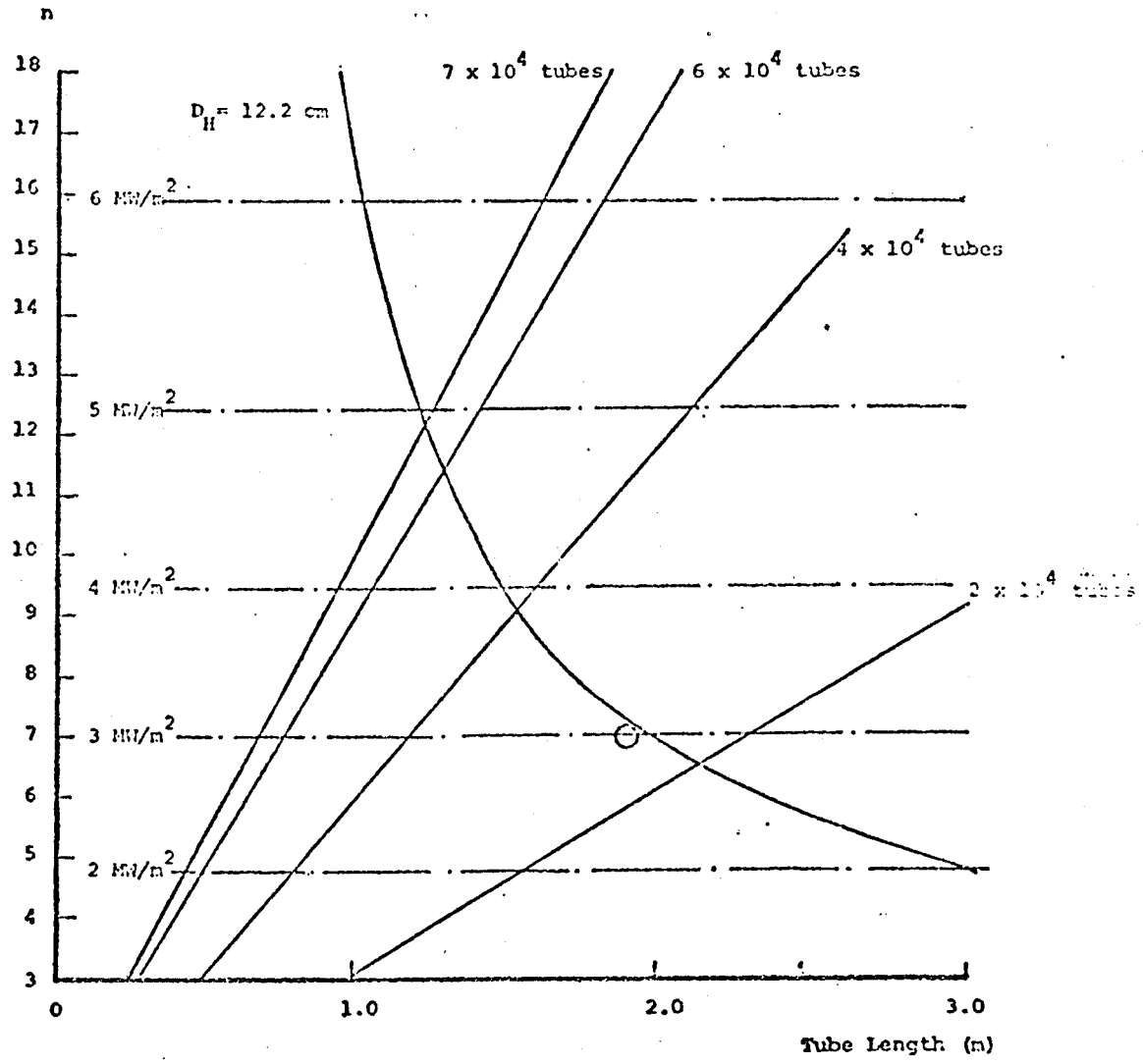

FIGURE 16. LITHIUM COOLANT - 316SS DESIGN WINDOW[3]

4.4 DESIGN POINT COMPARISON

4.4.1 3 MW/m^2 Wall Loading Comparison

For systems 1 through 4 a design point was chosen for a 3MW/m^2 neutron wall loading. These points are circled on the corresponding design windows graphs (figures 16, 1, 4 and 6). A summary of the system parameters is given in Table 4.3.

Table 4.3

3 MW/m^2 COOLANT COMPARISON

	L_i-316SS	He-316SS	He-TZM	Flibe-TZM
$N_t x10^3$	24.3	10	10	3.36
D (cm)	3.2	2.6	2.55	2.5
L (m)	1.96	7.6	7.0	27.2
t (mm)	1.28	1.02	1.82	1.0
η_s (%)	1.9	2.0	3.3	2.0
η_c (%)	N/A	11	10	12
K (%)	1	2.0	2.0	0.04
$T_{Li\ Max}$ (°C)	600	580	987	940
ΔT_W (°C)	18.2	13.7	5.2	3.0
W_S (MW/m^2)	.297	.28	.304	.24
ΔT_F (°C)	26.5	74.1	74	62
H (W/m^2-°C)	$1.12x10^4$	$3.74x10^3$	$4.15x10^3$	$4.06x10^3$
σ (MPa)	48.3	48.3	48.3	5.2
$T_{t\ Max}$ (°C)	446	488	880	862

With the given assumptions the performance of the lithium and helium stainless steel systems are surprisingly similar. The principal difference is that more tubes are required for the lithium system. If multiple passes were employed for the lithium system the number of tubes could be significantly reduced, making the two systems even more similar.

The He-TZM system parameters are quite close to the He-316SS design except for the higher coolant temperatures which should permit higher thermal efficiencies.

The Flibe-TZM system has by far the most favorable parameters. The pumping power is almost insignificant, fewer tubes are needed and low coolant pressures and hoop stresses are possible.

4.4.2 P_W Maximum Comparison

A second comparison of design points for the four systems was made to find the maximum wall loadings when 20,000 tubes and 1000°C in the lithium pool were allowed. The helium systems were limited to a 15% void fraction to insure adequate tritium breeding. The lithium-cooled system was allowed 1000°C in the pool assuming no 316SS in the high temperature regions. The system parameters for the selected design points are given in table 4.4.

Again, the Flibe system has the most favorable characteristics. Wall loading above 10 MW/m^2 are possible based on only the constraints considered here, although such wall loadings are no doubt unrealistically high due to high material damage rates. Using only 10,000 tubes gave the MW/m^2 wall loading listed in Table 4.4.

Table 4.4 P_W Max Comparison

	L_i-316SS	He-316SS	He-TZM	Flibe-TZM
$N_t x10^3$	20	20	20	10
D (cm)	3.2	2.4	2.45	2.0
L (m)	1.32	6.0	6.0	17.6
t (mm)	1.28	.944	1.75	1.0
η_s (%)	3.1	2.77	5.62	3.59
η_c (%)	N/A	15.0	15.6	15.2
K (%)	1.0	2.0	2.0	.05
T_{Li} Max (°C)	1000	596	994	961
ΔT_W (°C)	24.1	15.6	6.0	4.0
W_S (MW/m^2)	.416	.343	.373	.364
ΔT_F (°C)	34	85.1	83.6	72.9
h (W/m^2-°C)	$1.12x10^4$	$4.04x10^3$	$4.46x10^3$	$4.99x10^3$
σ (MPa)	48.3	48.3	48.3	48.3
T_t Max (°C)	458	500	890	877
P_W MW/m^2	4.7	5.5	6	7

4.5 CONCLUSIONS

4.5.1 316SS Systems

For the tubular stainless steel systems considered, helium and lithium are nearly equally effective as coolants in terms of their thermo-hydraulic characteristics. Both appear capable of acceptable

steady-state performance for the range of wall loadings currently considered. The helium systems required fewer tubes but a higher pumping power and have a slightly lower breeding ratio. These conclusions are based on the assumption that it will be possible to fabricate a sandwich insulation for the lithium coolant pipes exterior to the shield (but not for the tapered header) which will make MHD pressure drops in that region insignificant. If the header could be electrically insulated from the flowing lithium the lithium pressure and pumping power would be significantly lower than for helium. Conversely, if the sandwich construction proves to be impractical, a different configuration would have to be found for the lithium coolant.

4.5.2 TZM Systems

If TZM structures can be fabricated and material testing shows acceptable properties after irradiation, then the TZM-Flibe system has the best thermo-hydraulic characteristics of the systems studied. The pumping power required is extremely small and low system pressures are required. Long tubes can be used without excessive pressure drops so the number of tubes and welds are small.

The TZM-Helium system has similar parameters compared to the 316SS-He system. The principal difference is the increase in thermal efficiency possible at the higher temperatures. For this system, the limiting constraint was the maximum pool temperature instead of the tube wall temperature or wall temperature drop as in the 316SS design. (thermal stress considerations)

4.5.3 General Considerations

Table 4.5 is a summary of the principal advantages and disadvantages for the coolants considered. Some of these characteristics were not explicitely considered in this study but because of their impact some comments should be made here.

Helium has the advantages of being chemically inert (except for trace impurity effects on refractory metals); having a well-developed technology for its use as a heat transfer medium, and being insensitive to MHD effects. There are disadvantages however. The higher pressure and large amount of stored mechanical energy gives a potential for catastrophic failure. For a stagnant pool design, consideration must be given to the probability and consequences of a tube failure causing pressurization of a module. This consideration can have a serious effect on the structural design. Finally, the void fractions will require some additional shielding or an increased breeding zone thickness. The effect of neutron streaming through the helium ducts will also have to be considered.

Lithium gives good breeding ratios with low to moderate pumping power. Circulating the hot lithium coolant does however, increase the possibility of a spill. Since lithium burns with nitrogen or concrete this is a serious hazard. The header system proposed requires an invention of either a sandwich construction method or an insulator compatible with hot lithium. Finally, the liquid lithium would transport activated corrosion products out of the blanket, complicating handling problems.

Flibe, while having the excellent heat transfer properties, suffers from its own set of problems. It requires an advanced material, such as TZM. The development of construction techniques and a data base on irradiated and basic properties will take time. A scheme will have to be developed for filling the system and preventing the pipes from accidentally being plugged by frozen flibe. It too, will transport corrosion products outside the blanket.

Table 4.5 GENERAL CHARACTERISTICS

COOLANT	ADVANTAGES	DISADVANTAGES
He	1) Chemically inert	1) High pressure & stored mechanical energy
	2) Present technology	2) Possible module pressurization due to tube failure
	3) No MHD effects	3) Void Fraction requires thicker blanket and shield
		4) Neutron streaming
Lithium	1) Good Breeding Ratios	1) Increased chance of hot lithium spill
	2) Moderate pumping power	2) Material or design development required to minimize MHD effects (Insulator or "Sandwich")
		3) Mass transport of activated corrosion products
Flibe	1) Lowest pumping power	1) Advanced material required (TZM)
	2) Lowest # of tubes	2) Coolant freezing in pipes
	3) Lowest Hoop stress	3) Difficult to fill system & star
	4) Highest Heat Removal capacity	4) Mass transport of activated corrosion products

V. RADIATION SHIELD TUBE ANALYSIS

5.1 Introduction

A possible configuration for a fusion reactor first wall is a parallel array of coolant tubes. They could be welded or brazed together to form a vacuum boundary as proposed in some designs [33,34] or the coolant tubes could serve as a radiation shield for a thicker structural wall behind them as in the original Princeton Reference Design [35]. In this chapter, an analytic solution will be presented for the steady state thermal stresses developed when the tubes are constrained to remain straight but allowed to expand axially. In addition, copper cladding is proposed as a method of reducing the peak stresses in a 316SS stainless steel tube.

5.2 SIMPLE TUBES

The problem is linear so that the stresses due to volumetric heating can be calculated separately and added to the stresses resulting from a surface heat flux.

For a uniform volumetric energy generation rate (q''') the radial and circumferential stresses in a circular tube are given by [36]

$$\sigma_r = q''' \frac{Ka^2}{4k} \left[(1-\rho^{-2}) \left[\frac{\ln C}{1-1/C^2} - \frac{1}{4C^2} - \frac{3}{4} \right] - \ln \rho + \frac{1}{2} \right.$$

$$\left. - \frac{1}{2\rho^2} + \frac{1}{4C^2} \left[\rho^2 - \frac{1}{\rho^2} \right] \right] \qquad (5.1)$$

(5.2)

$$\sigma_{\theta_3} = q''' \frac{Ka^2}{4k} \left[(1+\rho^{-2}) \left[\frac{\ln C}{1-1/C^2} - \frac{1}{4C^2} - \frac{3}{4} \right] - \frac{1}{2} + \frac{1}{2\rho^2} + \frac{1}{4C^2} (3\rho^2 + \frac{1}{\rho^2}) \right]$$

where

a = Outside radius

b = Inside radius

C = a/b

ρ = r/b

K = $\alpha E/(1-\nu)$

5.2.1 Analytic Solution for the Temperature Field T(r,θ)

The surface heat flux seen by a tube can be approximated by a cosine distribution on the side facing the plasma and an adiabatic rear half for a radiation shield tube. If there is a heat flux from both sides the stresses can be calculated separately and added.

The solution to Laplace's equation in the annular region bounded by the inner and outer radii is symmetric about θ=0 as is given by[37]

$$T(r,\theta) = \sum_{n=0}^{\infty} F_n(r) \cos n\theta \qquad (5.3)$$

where

$$n \geq 1 \quad F_n(r) = \frac{C_n}{r^n} + D_n r^n \qquad (5.4)$$

The following boundary conditions were assumed

$$r=a \quad o \leq \theta \leq \pi/2 \qquad \frac{\partial T}{\partial r} = \frac{q''}{k} \cos\theta \tag{5.5}$$

$$\pi/2 < \theta \leq \pi \qquad \frac{\partial T}{\partial r} = 0 \tag{5.6}$$

$$r=b \quad k\frac{\partial T}{\partial r} = H\,(T-T_f) \tag{5.7}$$

Equation 5.7 assumes a heat transfer coefficient that is independent of θ and a given bulk fluid temperature. The non-uniform heat flux will actually cause some θ dependence in H[38] but this effect should be small and is not included in this analysis.

The boundary conditions at r=a can be expressed by a Fourier cosine series. This gives

$$\frac{\partial T}{\partial r} = a_o + \sum_{n=1}^{\infty} a_n \cos n\,\theta \tag{5.8}$$

where

$$n=o \quad a_o = \frac{q''}{\pi k} \tag{5.9}$$

$$n=1 \quad a_1 = \frac{q''}{2k} \tag{5.10}$$

$$n \geq 2 \quad a_n = \begin{cases} \dfrac{2q''}{\pi k}\left[(-1)^{\left(\frac{n}{2}+1\right)}\right] & n \text{ even} \\ 0 & n \text{ odd} \end{cases} \tag{5.11}$$

The coefficients C_n and D_n in 5.4 can be found by applying boundary conditions (5.7) and (5.8) and equating like orders of cos n θ

For n=1 equation (5.7) and (5.8) give

$$-\frac{kC_1}{b^2} + k D_1 = H \left(\frac{C_1}{b} + D_1 b\right) \tag{5.12}$$

$$-\frac{C_1}{a^2} + D_1 = \frac{q''}{2k} \tag{5.13}$$

Solving for C_1 and D_1 gives

$$C_1 = \frac{q''a^2b^2}{2k}\left[\frac{k - Hb}{k(a^2-b^2)+Hb(a^2+b^2)}\right] \tag{5.14}$$

$$D_1 = \frac{q''a^2}{2k}\left[\frac{k+Hb}{k(a^2-b^2)+Hb(a^2+b^2)}\right] \tag{5.15}$$

From (5.11) $C_n = D_n = 0$ for n odd.

Let $n = 2m$ $m = 1, 2, ...$

Applying the boundary conditions in a similar manner gives the following result.

$n = 2m$ $m = 1, 2, ...$

$$C_n = \frac{q''}{\pi km}\,\frac{(-1)^{m+1}}{(2m)^2-1}\left[\frac{a^{2m+1}(2mk-Hb)}{2mk\ (C^{4m}-1)+Hb(C^{4m}+1)}\right] \tag{5.16}$$

$$D_n = \frac{1}{b^{4m}}\left[\frac{2mk+Hb}{2mk-Hb}\right] C_n \tag{5.17}$$

$C_n = D_n = 0$ n odd

Where $C = a/b$

If the zeroth order terms due to the surface heat flux and also the volumetric energy generation rate are included the total solution for the temperature is then given by

$$T(r,\theta)= \frac{a}{k}\left(\frac{q''}{\pi}+\frac{q'''a}{2}\right)\ln\left(\frac{r}{b}\right)-\frac{q'''}{4k}(r^2-b^2)+\frac{\pi(a^2-b^2)q'''+2aq''}{2\pi bH} \tag{5.18}$$

$$+\sum_{n=1}^{\infty}\left(\frac{C_n}{r^n}+D_n r^n\right)\cos(n\theta)+T_F$$

5.2.2 Analytic Solution for the Thermal Stresses

The assumption will be made that the tubes are allowed to expand in the axial direction but that no bending is possible. If tubes close to the plasma were allowed to bow out then the outermost sections could act as limiters and incur large surface heat fluxes. The assumption of no bending could also be applied to tubes with a large radius of curvature, say running in the poloidal direction, which are allowed to expand to a larger radius, but not to change shape.

The solution for the stresses will be given by the plain strain solution for no axial expansion[37] with the addition of a uniform axial stress σ_z equal to $\alpha E\bar{T}$[39]. The result is

$$\sigma_r=\sigma_{r_3}+\frac{\alpha E T_o}{2(1-\nu)}\left[\left(\frac{a}{r}\right)^2\left(\frac{r^2-b^2}{a^2-b^2}\right)\ln\frac{a}{b}-\ln\frac{r}{b}\right] \tag{5.19}$$

$$+\frac{\alpha E r}{2(a^2+b^2)(1-\nu)}\left(1-\frac{b^2}{r^2}\right)\left(1-\frac{a^2}{r^2}\right)C_1\cos\theta$$

(5.20)

$$\sigma_\theta = \sigma_{\theta_3} + \frac{\alpha E T_o}{2(1-\nu)}\left[\left(\frac{a}{r}\right)^2 \left(\frac{r^2+b^2}{a^2-b^2}\right) \ln\frac{a}{b} - \ln\frac{r}{b} - 1\right]$$

$$+ \frac{\alpha E r}{2(a^2+b^2)(1-\nu)}\left(3 - \frac{a^2+b^2}{r^2} - \frac{a^2b^2}{r^4}\right) C_1 \cos\theta$$

$$\sigma_{r\theta} = \frac{\alpha E r}{2(a^2+b^2)}\left(1 - \frac{a^2}{r^2}\right)\left(1 - \frac{b^2}{r^2}\right) C_1 \sin\theta$$

$$\sigma_Z = \nu(\sigma_r+\sigma_\theta) - \alpha E (T-\overline{T})$$

Where $T_o = \frac{a\, q''}{\pi k}$

$$\overline{T} = \frac{a}{k}\left(\frac{a^2}{a^2-b^2} \ln\frac{a}{b} - \frac{1}{2}\right)\left(q'' + \frac{q'''a}{2}\right) - \frac{(a^2+b^2)}{8k} q'''$$

$$+ \frac{\pi(a^2-b^2)q'''+2aq''}{2\pi bH} + T_F$$

Imposing the constraint against all bending produces a compressive axial stress on the side facing the plasma which can be much larger than the σ_θ stress.

5.2.3 Numerical Examples

As a numerical example, a 316SS tube was examined for the conditions listed in Table 5.1. (The program given in Appendix 4.1 was used for the calculations.) The value chosen for the heat transfer coefficient was arbitrary. It could be attained by helium at 60 atm and 700°K flowing at 140 m/sec or by a salt such as HITEC[35] flowing at 3.5 m/sec.

TABLE 5.1 316SS Tube Example

(Physical Properties Evaluated at 800°K)

$\alpha = 20.3 \times 10^{-6}\ K^{-1}$

$E = 156.2 \times 10^{9}\ Pa$

$\nu = .3$

$b = 6$ mm (Inside Radius)

$a = 7$ mm (Outside Radius)

$q'' = .25\ MW/m^2$

$q''' = 10\ MW/m^3$

$H = 8.2 \times 10^{3}\ W/m^2\text{-}°K$

Figure 17 shows the temperature versus theta for the inner and outer surfaces of the tube. Figure 18 shows σ_z and σ_θ for the inner and outer surfaces of the tube. For this case, corresponding to a 1 MW/m^2 neutron wall loading, the peak stress is -104 MPa (-15 ksi)

The peak stress is a strong function of the heat transfer coefficient. Figure 19 shows the effect of changing H on the peak stress with all other parameters kept constant.

The values for H above $8.2 \times 10^{3}\ W/m^2\text{-}°C$ would be very difficult to achieve with either helium or a molten salt coolant. For helium, the pumping power would become extremely high or for the molten salt a high velocity would be required which would cause a high induced voltage in the portion of the tube perpendicular to the torroidal field.

The peak stress is sensitive to the thickness of the tube as

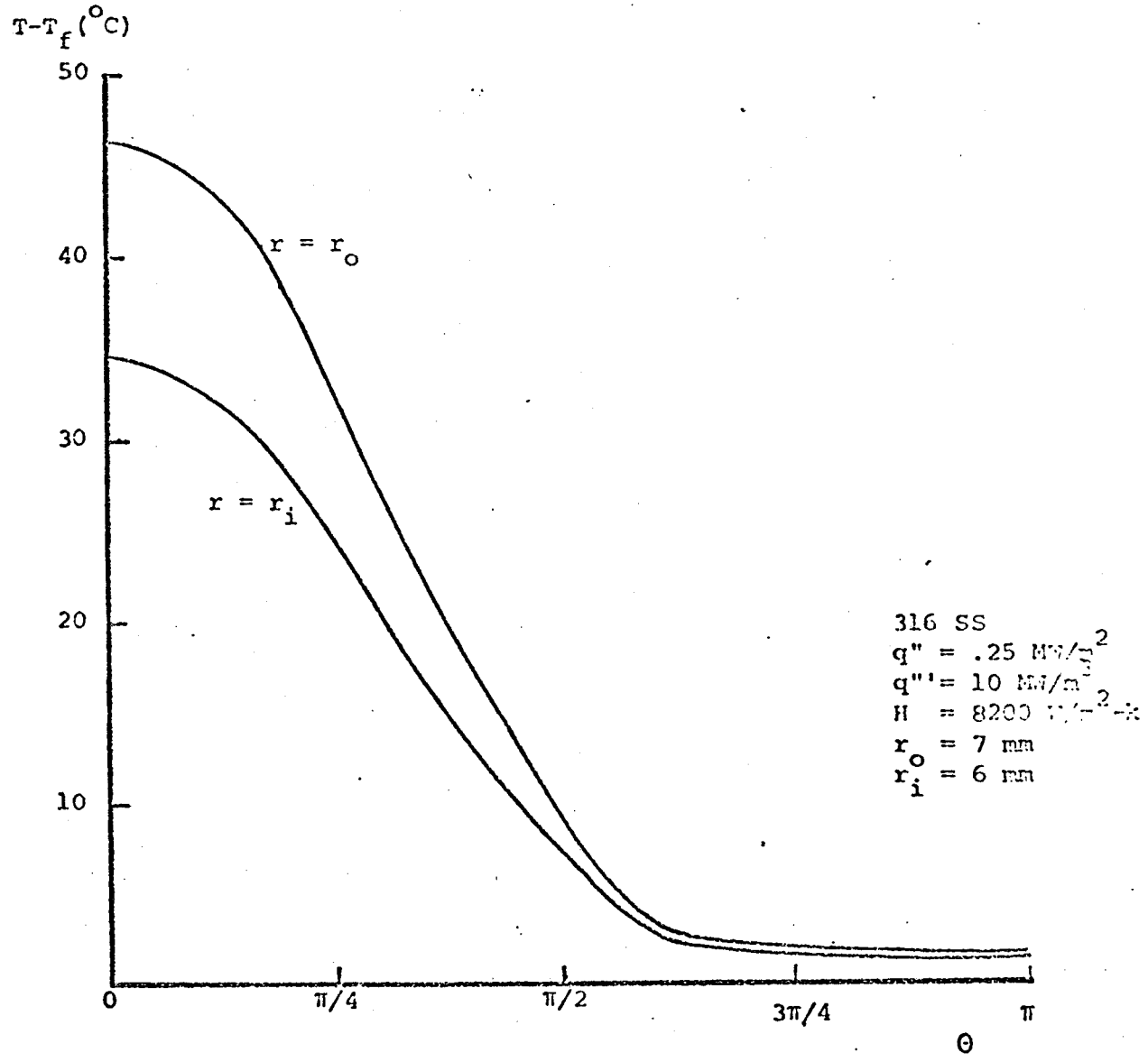

FIGURE 17. RADIATION SHIELD TUBE WALL TEMPERATURE

VS.

ANGLE

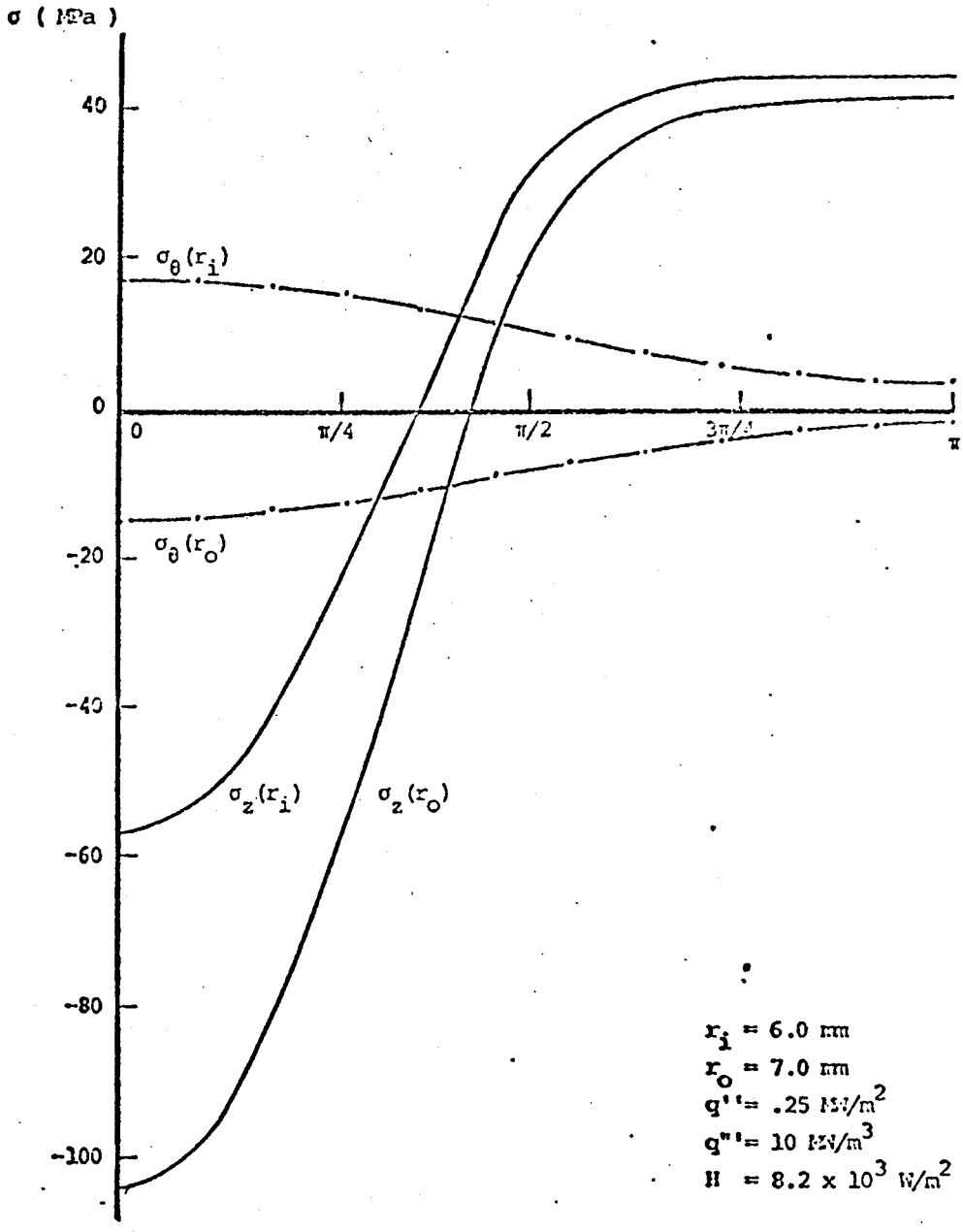

FIGURE 18. RADIATION SHIELD TUBE THERMAL STRESS

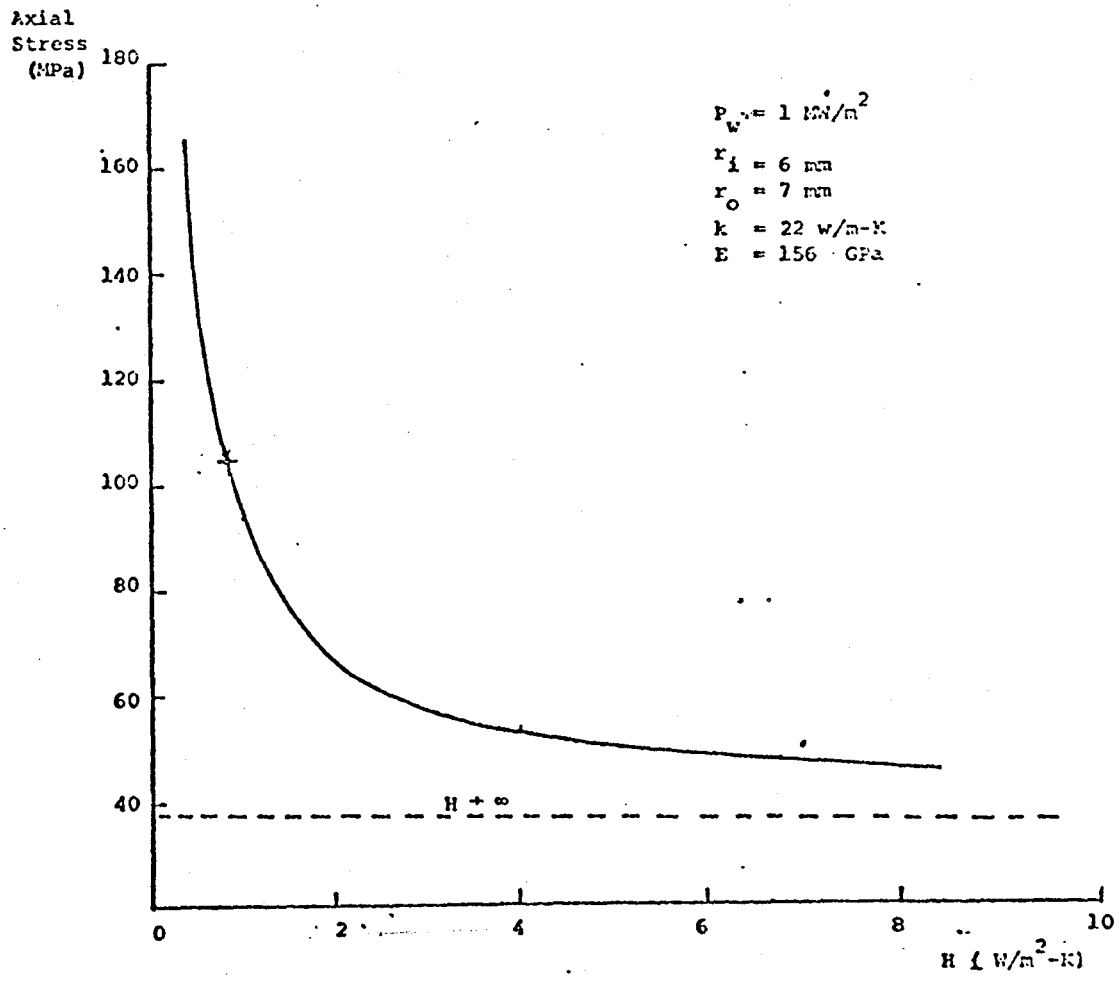

MAXIMUM AXIAL STRESS vs. HEAT TRANSFER COEFFICIENT

FIGURE 19. RADIATION SHIELD TUBE PEAK THERMAL STRESS

VS.

HEAT TRANSFER COEFFICIENT

would be expected from a thin plate approximation, but changing the radius has little effect. This is shown in Table 5.2 where only a and b are changed from Table 5.1 for a 316SS tube with a 1 MW/m^2 neutron wall loading.

TABLE 5.2

Effect of Radius and Thickness on Peak Stress

b (mm)	a (mm)	$\lvert\sigma_z\rvert$ Maximum (MPa)
6	7	104
9.5	10.5	106
10	11	106
14	15	106
6	6.6	88.9
9	10.5	126

The results of this section were also applied to several different materials using the same wall loading, geometry and heat transfer coefficient as in the first example. Table 5.3 gives the physical properties used, and the peak circumferential and axial stress.

For near term applications 316SS will most likely be used. More is known about its irradiated properties and the technology for its use is well established. The next section will discuss a possible technique for reducing the large axial bending stress.

TABLE 5.3

Material Comparison

Material	α $\times 10^{-6}$	E GPa	ν	k W/m-k	$\lvert\sigma_\theta\rvert_{Max}$ MPa	$\lvert\sigma_z\rvert_{Max}$ MPa
316SS	20.3	156.2	.3	22	17.1	104
TZM	6.0	250	.3	101	2.2	27.5
Copper	20.3	95.1	.35	359	2.0	19.1
Titanium	9.3	92	.3	12	9.9	37.5

5.3 COMPOSITE TUBES

5.3.1 Objectives

The large axial stress in the tubes considered in the previous section result from the temperature difference between the hot side facing the plasma and the cooler adiabatic rear half. One possible was to reduce this stress would be to remove heat from the region behind the radiation shield in order to balance the heat flux on the tube. Such a scheme was used in the Cassette Blanket Concept.[32] There are several difficulties with this however. First, for pulsed operation when the plasma extinguishes, the heat flux will be nearly zero on the plasma side, but still close to the steady state value on the side bounding the blanket. The stresses then are nearly the same as for the first case, only the signs would be reversed. Also, the mechanical design to provide good heat transfer would be difficult. If the tubes were simply welded together with lithium behind them, the probability of a leak would be high.

The concept proposed and investigated in this chapter is to coat the tubes with a high thermal conductivity material in order to conduct more of the surface heat flux to the rear half.

The first coating material considered was anisotropic carbon deposited so that the thermal conductivity in the circumferential direction was high but in the radial direction low. To find the temperature field a finite difference code was developed and will be discussed in the next section.

5.3.2 Thermal Analysis Finite Difference Code for Cylindrical Geometry and Anisotropic Materials

The finite differnce code TUBETEMP was written and is given in Appendix 4.2. In this section, the basic finite difference equations will be given and some numerical results.

For an interior point the following form of the heat conduction equation was assumed.

$$k_r \frac{\partial^2 T}{\partial r^2} + \frac{k_r}{r} \frac{\partial T}{\partial r} + \frac{k\theta}{r^2} \frac{\partial^2 T}{\partial \theta^2} + q''' = 0 \qquad (5.21)$$

where k_r = thermal conductivity in the radial direction

$k\theta$ = thermal conductivity in the theta direction.

The finite difference approximation used for interior nodes is the following (See figure 20).

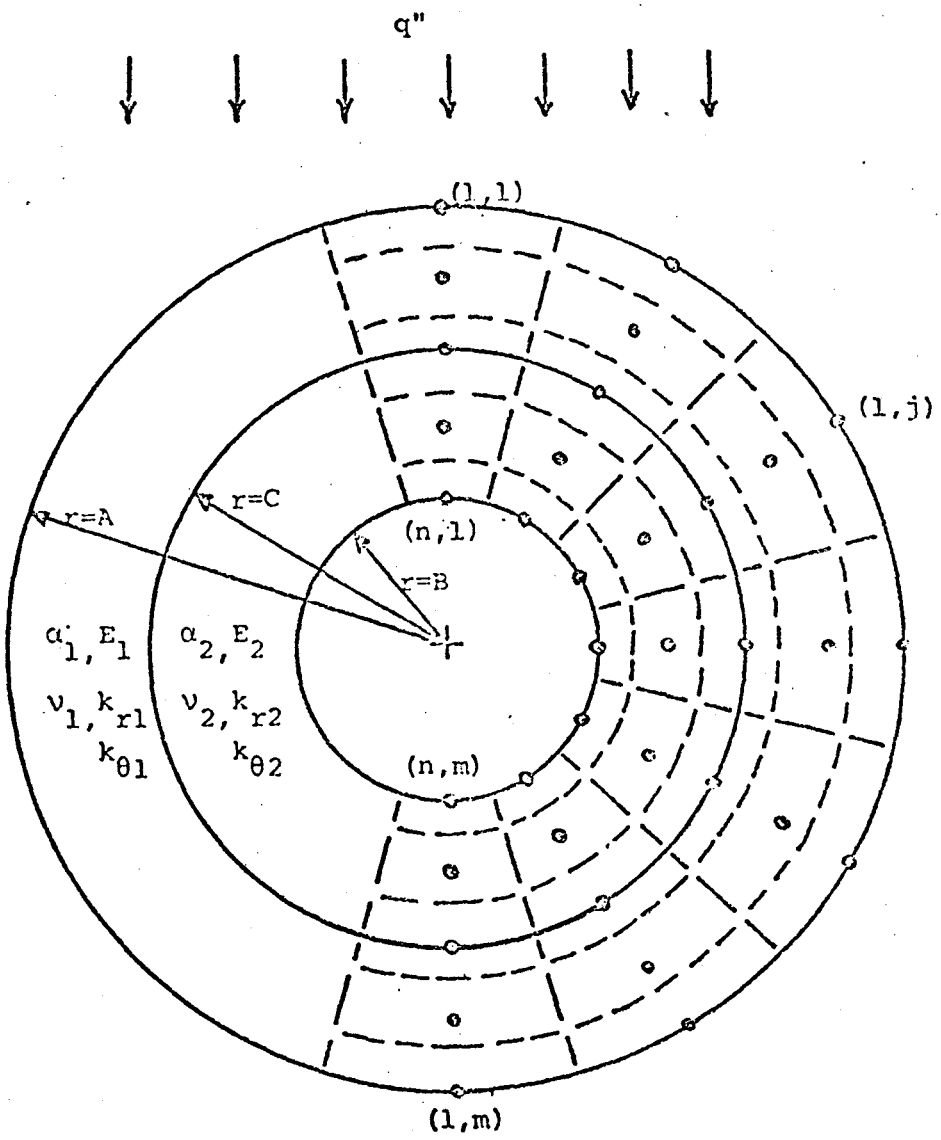

FIGURE 20. FINITE DIFFERENCE MODEL FOR COMPOSITE TUBE

$$k_r \frac{T(i1,j)-2T(i,j)+T(i2,j)}{\Delta r^2} + \frac{k_r}{r_{ij}} \frac{T(i1;j)-T(i2,j)}{2\Delta r} \tag{5.22}$$

$$+ \frac{k_\theta}{r_{ij}^2 \Delta\theta^2} (T(i,j1)-2T(i,j)+T(i,j2)) + q''' = 0$$

Where: $i1 = i-1$ $\quad j1 = j-1$

$i2 = i+1$ $\quad j2 = j+1$

$\Delta r = (A-B)/(n-1)$ $\quad 1 \leq i \leq n$

$\Delta\theta = \pi/(m-1)$ $\quad 1 \leq j \leq m$

$r_{ij} = A-(i-1)\Delta r$

$\theta_{ij} = (j-1)\Delta\theta$

For elements on the outside surface, the additional surface heat flux must be included. Taking an energy balance on a surface element (i=1) and solving for T(1,J) gives

$$T(1,J) = C_1\, T(2,J) + C_2 \left[T(1,J1) + T(1,J2) \right] + C_3 \tag{5.23}$$

where

$$C_1 = \left[1 + \frac{k_{\theta 1}}{k_{r1}} \frac{\Delta r^2}{(a\Delta\theta)^2 (1-\Delta r/2\,a)} \right]^{-1}$$

$$C_2 = \left[2 + 2\frac{k_{r1}}{k_{\theta 1}} \frac{(a\Delta\theta)^2 (1-\Delta r/2a)}{\Delta r^2} \right]^{-1}$$

$$C_3 = \frac{q''(j)+q''' \Delta r/2(1-\Delta r/4a)}{\frac{k_{r1}}{\Delta r}(1 - \frac{\Delta r}{2a}) + \frac{k\theta 1 \Delta r}{(a\Delta\theta)^2}}$$

$$q''(j) \simeq q'' \cos\theta_{ij}$$

It will be assumed that the two tube materials are in perfect thermal contact, and therefore, at the boundary the temperature will be the same for both materials. Using a common node at the boundary and performing an energy balance, the following expression for T(i,j) was obtained.

$$T(i,j) = C_4\, T(i,j) + C_5\, T(i2,j) + C_6\left[T(i,j1)+T(i,j2)\right] + C_7 \tag{5.24}$$

Where

$$C_4 = \left[1+\frac{k_{r2}}{k_{r1}}\,\frac{(1-\Delta r/2C)}{(1+\Delta r/2C)} + \frac{k_{\theta 1}+k_{\theta 2}}{k_{ri}(1+\Delta r/2C)}\,\frac{\Delta r^2}{(C\Delta\theta)^2}\right]^{-1}$$

$$C_5 = \left[1+\frac{k_{r1}}{k_{r2}}\,\frac{(1+\Delta r/2C)}{(1-\Delta r/2C)} + \frac{k_{\theta 1}+k_{\theta 2}}{k_{r2}(1-\Delta r/2C)}\,\frac{\Delta r^2}{(C\Delta\theta)^2}\right]^{-1}$$

$$C_6 = \left[2+2\left(\frac{C\Delta\theta}{\Delta r}\right)^2 \frac{k_{ri}(1+\Delta r/2C)+k_{r2}(1-\Delta r/2C)}{k_{\theta 1}+k_{\theta 2}}\right]^{-1}$$

$$C_7 = q''' \left[\frac{k_{r1}(1+\Delta r/2C)+k_{r2}(1-\Delta r/2C)}{\Delta r^2} + \frac{k_{\theta 1}+k_{\theta 2}}{(C\Delta\theta)^2}\right]^{-1}$$

For elements on the inside surface at r=B a constant heat transfer coefficient (h) and bulk coolant temperature (T_f) were assumed. Performing an energy balance on these elements gives the following:

$$T(n,J) = C_8\, T(n-1,J) + C_9\, T(n,J2) + T(n,j1) + C_{10} \tag{5.25}$$

Where

$$C_8 = \left[1+\frac{k_{\theta 2}}{k_{r2}}\left(\frac{\Delta r}{B\Delta\theta}\right)^2 \frac{1}{(1+\Delta r/2B)} + \frac{h\Delta r}{k_r(1+\Delta r/2B)}\right]^{-1}$$

$$C_9 = \frac{1}{2}\left[1 + \frac{kr2}{k_{\theta 2}}\left(\frac{B\Delta\theta}{\Delta r}\right)^2 (1+\Delta r/2B) + \frac{h(B\Delta\theta)^2}{k_{\theta 2}\Delta r}\right]^{-1}$$

$$C_{10} = \frac{\frac{\Delta r}{2}\left(1+\frac{\Delta r}{4B}\right) q''' + h\,T_F}{\frac{k_{r2}}{\Delta r}\left(1+\frac{\Delta r}{2B}\right) \div \frac{k_{\theta 2}\Delta r}{(b\Delta\theta)^2} + h}$$

Several finite difference codes were tried. The first included the time dependent term. The solutions using this method were time-consuming and contained more information than needed. An efficient solution scheme for the steady state temperature field used the above equations, and inverted the resulting 5 stripe matrix directly.

A graph of film temperature drop versus angle is shown in Figure 21 for the 316SS tube considered previously with a 2 mm coating of anisotropic pyro carbon having the following conductivity:

k_θ = 100 w/m-K

k_r = 2 w/m-K

As can be seen there is a considerable smoothing of the temperature profile.

Unfortunately, the mechanical properties of pyro carbon are not good and there is a large difference in the coefficients of thermal expansion between the carbon and 316SS. Keeping such a coating intact

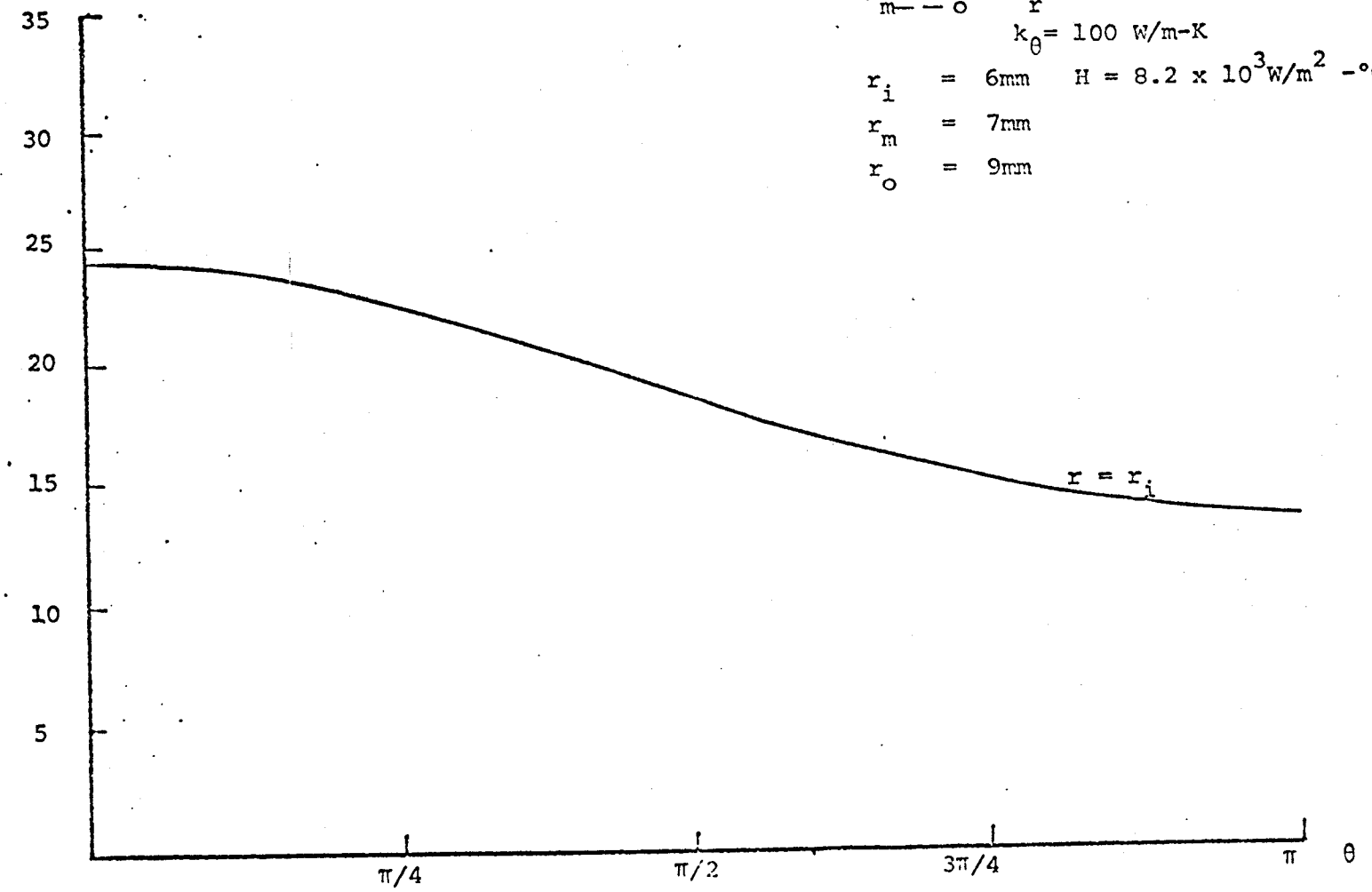

FIG. 21. FILM TEMPERATURE DROP VS θ WITH ANISOTROPIC CARBON COATING ON 316SS

could prove very difficult.

Copper was tried as an alternative coating (or cladding) and found to have nearly the same beneficial effect on the temperatures. In addition, its coefficient of thermal expansion is nearly the same as 316SS. Since the copper appeared much more attractive, the carbon concept was not pursued further. With copper it was also possible to develop analytic solutions for the temperature fields and thermal stresses.

5.3.3 Analytic Solutions for the Temperature Field

The boundary conditions on the temperature for the composite tube are assumed to be the following:

$r = r_o$ (outside radius)

$$\frac{\partial T_1}{\partial r} = \frac{q''}{k_1} \cos\theta \qquad 0 \leq \theta < \pi/2$$

$$0 \qquad \pi/2 \leq \theta \leq \pi$$

$r = r_m$ (boundary between two regions)

$$k_1 \frac{\partial T_1}{\partial r} = k_2 \frac{\partial T_2}{\partial r}$$

$$T_1 = T_2$$

$r = r_i$

$$k_2 \frac{\partial T_2}{\partial r} = H\,(T - T_F)$$

A solution in terms of a Fourier Series expansion can be found in a manner similar to section 5.1.1.

Assume

$$T_i = T_{oi} + \sum_{n=1}^{\infty} F_{ni}(r) \cos n\theta = T_{oi} + T_{1i}$$

Where the symmetry around $\theta=0$ justifies the use of a cosine expansion and the subscript i refers to either region 1 or 2.

The solution for the cylindrically symmetric component of temperature is found to be: (5.26)

$$r_i \leq r \leq r_m: \quad T_{02} = \frac{q'''}{4k_2}\left[(r_i^2 - r^2) + 2r_o^2 \ln \frac{r}{r_i}\right] + \left(\frac{r_o^2 - r_i^2}{2Hr_i}\right) q'''$$

$$+ \frac{q''r_o}{\pi k_2}\left[\ln\left(\frac{r}{ri}\right) + \frac{k2}{r_i H}\right] + \frac{q''r_o}{\pi r_i H} + T_F$$

$r_m \leq r \leq r_o$:

$$T_{01} = \frac{q'''}{4k_1}\left[\frac{k_1}{k_2} r_i^2 + \left(1 - \frac{k_1}{k_2}\right) r_m^2 - r^2 + 2r_o^2\left(\ln \frac{r}{r_m} + \frac{k_1}{k_2} \ln \frac{r_m}{r_i}\right)\right]$$

$$+ \frac{(r_o^2 - r_i^2)q'''}{2Hr_i} + \frac{q''r_o}{\pi k_1}\left[\ln\left(\frac{r}{r_m}\right) + \frac{k_1}{k_2} \ln\left(\frac{r_m}{r_i}\right)\right] + \frac{q''r_o}{\pi r_i H} + T_F$$

The solution for the higher harmonics is given by

$$r_m \leq r \leq r_o: \quad T_{12} = \sum_{m=1}^{\infty}\left[X_{1m}\left(\frac{r}{r_o}\right)^{-m} + X_{2m}\left(\frac{r}{r_o}\right)^{m}\right] \cos m\theta$$

$$r_i \leq r \leq r_m \quad T_{11} = \sum_{m=1}^{\infty}\left[X_{3m}\left(\frac{r}{r_i}\right)^{-m} + X_{4m}\left(\frac{r}{r_i}\right)^{m}\right] \cos m\theta$$

Where m = 1, 2, 4, 6, 8, ... (m even for $m \neq 1$)

$$X_{4m} = \frac{2\,Q_m\,C_{2m}}{C_{3m}\,(C_{2m}+1)+C_{4m}\,(C_{2m}-1)}$$

$$X_{3m} = C_{1m}\,X_{4m}$$

$$X_{2m} = \frac{C_{4m}}{C_{2m}+1}\,X_{4m} - \frac{Q_m}{C_{2m}}$$

$$X_{1m} = C_{2m}X_{2m} - C_{3m}X_{4m}$$

$$C_{1m} = \frac{mk_2 - Hr_i}{Hr_i + mk_2}$$

$$C_{2m} = \left(\frac{r_m}{r_o}\right)^{2m}$$

$$C_{3m} = \frac{k_2}{k_1}\left[-C_{1m}\left(\frac{r_i}{r_o}\right)^{m} + \left(\frac{r_m^2}{r_o r_i}\right)^{m}\right]$$

$$C_{4m} = -C_{1m}\left(\frac{r_i}{r_o}\right)^{m} - \left(\frac{r_m^2}{r_o r_i}\right)^{m}$$

$$Q_m = -\frac{r_o}{m}\,a_m$$

$$a_1 = \frac{q''}{2k_1}$$

$m \geq 2$ $\quad a_m = \frac{2q''}{\pi k}(-1)^{\left(\frac{m}{2}+1\right)}$ $\quad$ m even

$$a_m = 0 \qquad \text{m odd}$$

The solution for the temperature field using the Fourier series was compared to the solution using the previously derived finite difference method for a sample problem. The 316SS tube with the properties given in Table 5.1 was used with a 2 mm thick copper cladding. With approximately 300 points in the finite difference mesh the temperatures at all points, using both methods agreed with $\pm$0.05°C with a peak temperature rise of approximately 40°C. The temperature profile as a function of angle is shown in figure 22. For comparison, the tube temperatures without the coating are also shown. The front to back temperature difference, the peak temperature, the peak ΔT_w and the peak heat flux to the coolant are all reduced.

5.3.4 Analytic Solution for Composite Tube Thermal Stresses

An analytic elastic plain strain analysis for composite tubes has been published by U. Takeuti and Y. Tanigawa in reference 45. In their solution, a temperature profile was specified on the outside surface with an inside surface temperature of zero. A steady state analysis of the copper clad tube was performed using their solution method with several modifications:

1) The temperature field caused by the surface heat flux as found in the previous section was used to calculate the plane strain stresses using the methods of reference 45. (This required some modification of their expressions due to the boundary conditions assumed for this problem. The program used to make the calculations is given in Appendix 4.3.)

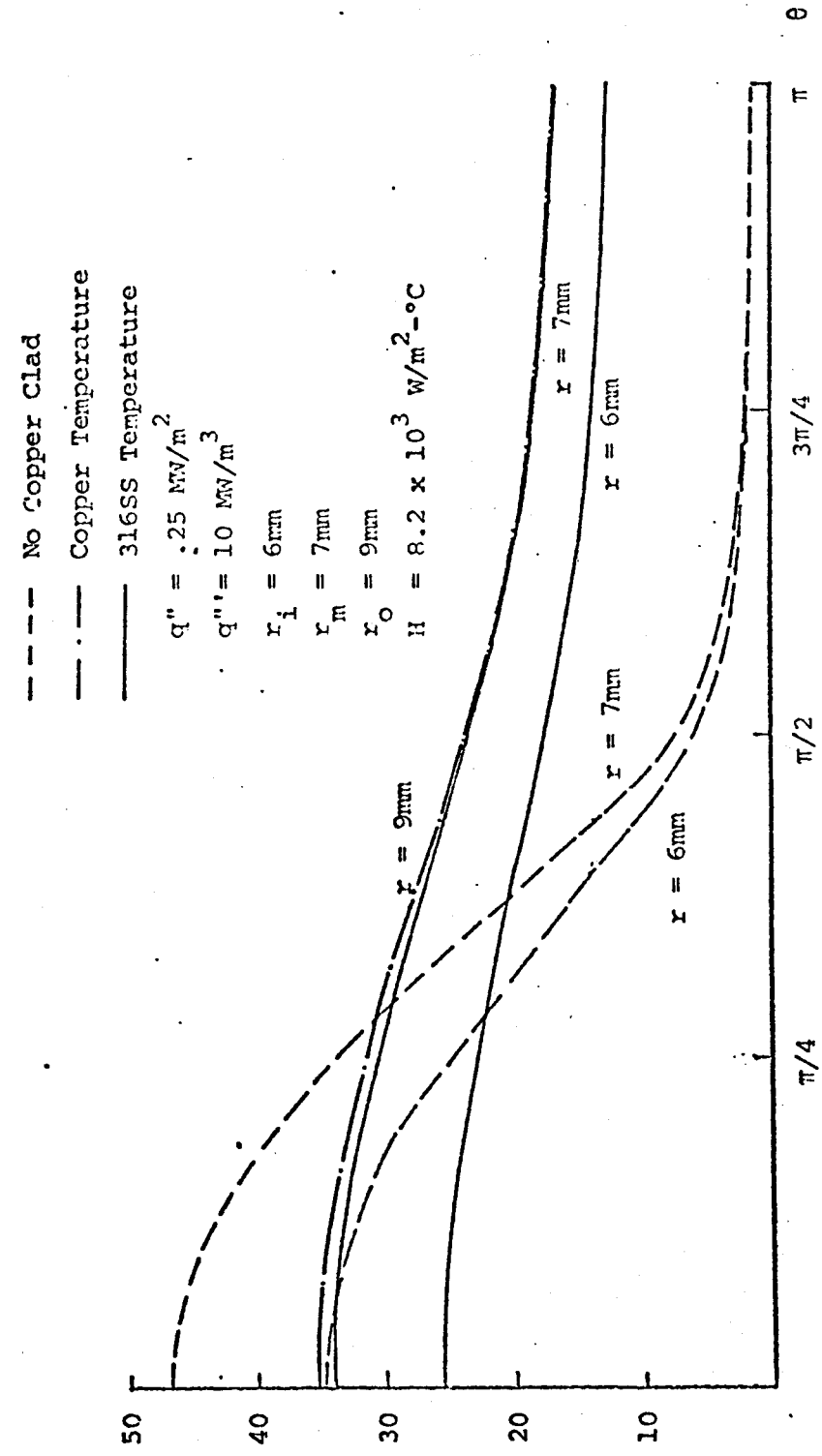

FIGURE 22. TEMPERATURE PROFILE FOR COPPER-CLAD 316SS TUBE

2) The stresses due to a uniform q'" in both tubes was added to the stresses resulting from the surface heat flux.

3) A uniform axial strain ε_z was imposed on the plane strain solution so as to give a net axial force of zero when the axial stresses are integrated over the cross section.

In reference 45, Fourier series solutions for the stresses in the two regions are found by applying the boundary conditions on stresses and displacements with a known temperature solution. For the problem considered here, the temperature on the inner surface is a function of θ. This requires an additional term to be carried through the analysis to obtain the plane strain stresses due to the surface heat flux.

The plane strain stresses due to a uniform q"' were found in a straight forward manner using a displacement approach.

To allow for axial expansion without any bending, a uniform strain was applied such that the net tensile axial force would just cancel the compressive axial force from the plain strane solution. The governing equations from Timoshenko[46] are

$$U_i = C_{1i} r + \frac{C_{2i}}{r}$$

$$\frac{\sigma_{ri}}{E_i} = \frac{C_{1i}}{(1+\nu_i)(1-2\nu_i)} - \frac{C_{2i}}{(1+\nu_i) r^2} + \frac{\nu_i}{(1+\nu_i)(1-2\nu_i)} \varepsilon_{Zi}$$

$$\frac{\sigma_{Zi}}{E_i} = \varepsilon_{Zi} \frac{(1-\nu_i)}{(1+\nu_i)(1-2\nu_i)} + \frac{2\nu_i C_{1i}}{(1+\nu_i)(1-2\nu_i)}$$

Where U_i is the radial displacement function for the inner or outer regions. The six unknowns C_{1i}, C_{2i}, and ε_{Zi} can be found from the boundary conditions

$\sigma_{r1}(r_m) = 0$

$\sigma_{r2}(r_i) = 0$

$\sigma_{r1}(r_m) = \sigma_{r2}(r_m)$

$U_1(r_m) = U_2(r_m)$

$\varepsilon_{Z1} = \varepsilon_{Z2}$

$\pi(r_o^2-r_m^2)\,\sigma_{Z1}+\pi(r_m^2-r_i^2)\sigma_{Z2} = -F_Z$

r_i = inside radius

r_o = outside radius

r_m = boundary radius between two regions

Where F_Z is the net axial force obtained from the plane strain solution by integrating σ_Z over the entire cross section. Only the uniform and cylindrically symmetric components of temperature will give a net contribution to F_Z. A uniform temperature other than the reference temperature will give stresses in the r, θ and Z directions unless $\alpha_1=\alpha$; $\nu_1=\nu_2$ and $E_1=E_2$.

5.4 Copper Clad - 316SS Design Example

For the same 316SS tube parameters and heat transfer coefficient as given in Table 5.1, the effect of varying thicknesses of copper was examined. The program used is given in Appendix 4.3.

At 800°K $\alpha=20.3\times10^{-6}K^{-1}$ for both copper[40] and 316SS[41]. The peak stress in the 316SS versus the thickness of the copper clad is shown in figure 23 for a 1 MW/m^2 wall loading. (The volumetric heating rate was

estimated to be 10 MW/m^3.) The optimum thickness is 1.6 mm of copper which gives a σ_z stress of -40 MPa at $\theta=0$ and +40 MPa at $\theta=\pi$. Thinner coatings give higher compressive stresses on the plasma side and thicker coatings give higher tensile stresses on the adiabatic side. The stresses in the copper are lower than in the steel. Figure 24 shows the distribution of σ_z on the inside and outside of the 316SS for the 1.6 mm coating. The numerical results are given in Appendix 4.3.

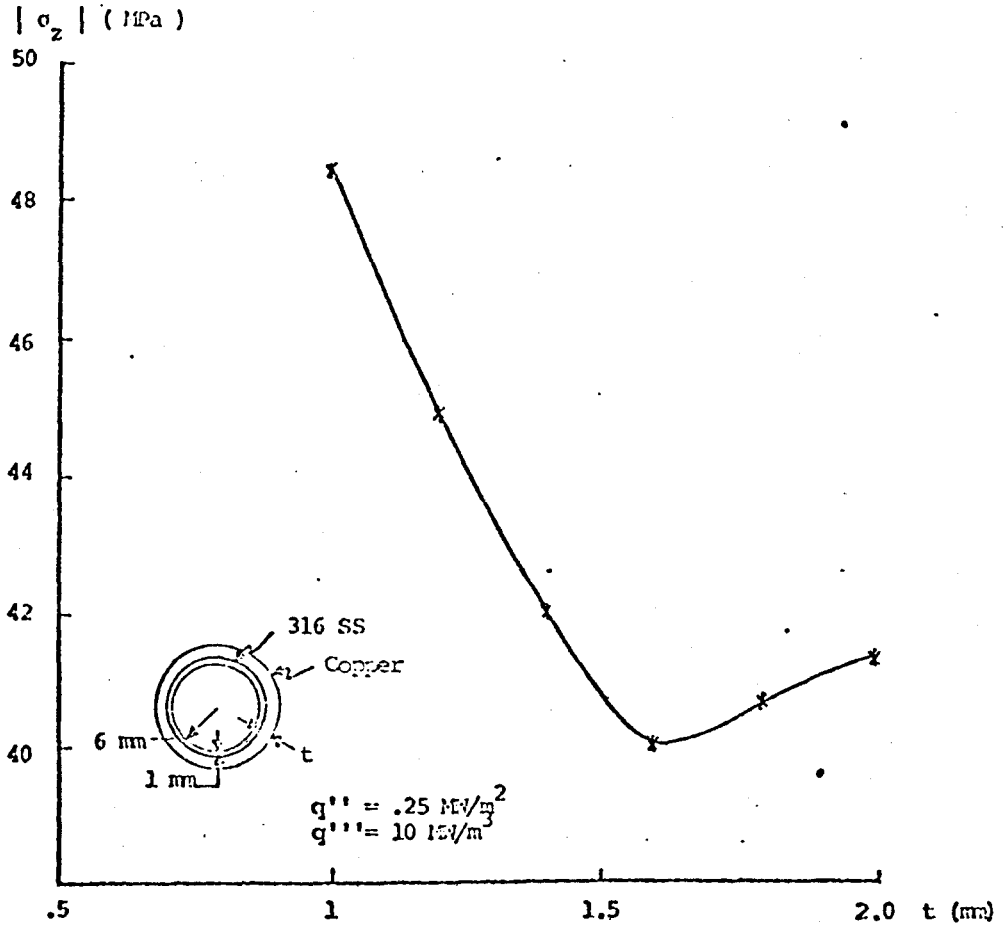

Absolute Value of Peak Stress vs. Copper Coating Thickness

FIGURE 23. ABSOLUTE VALUE OF PEAK STRESS

VS.

COPPER COATING THICKNESS

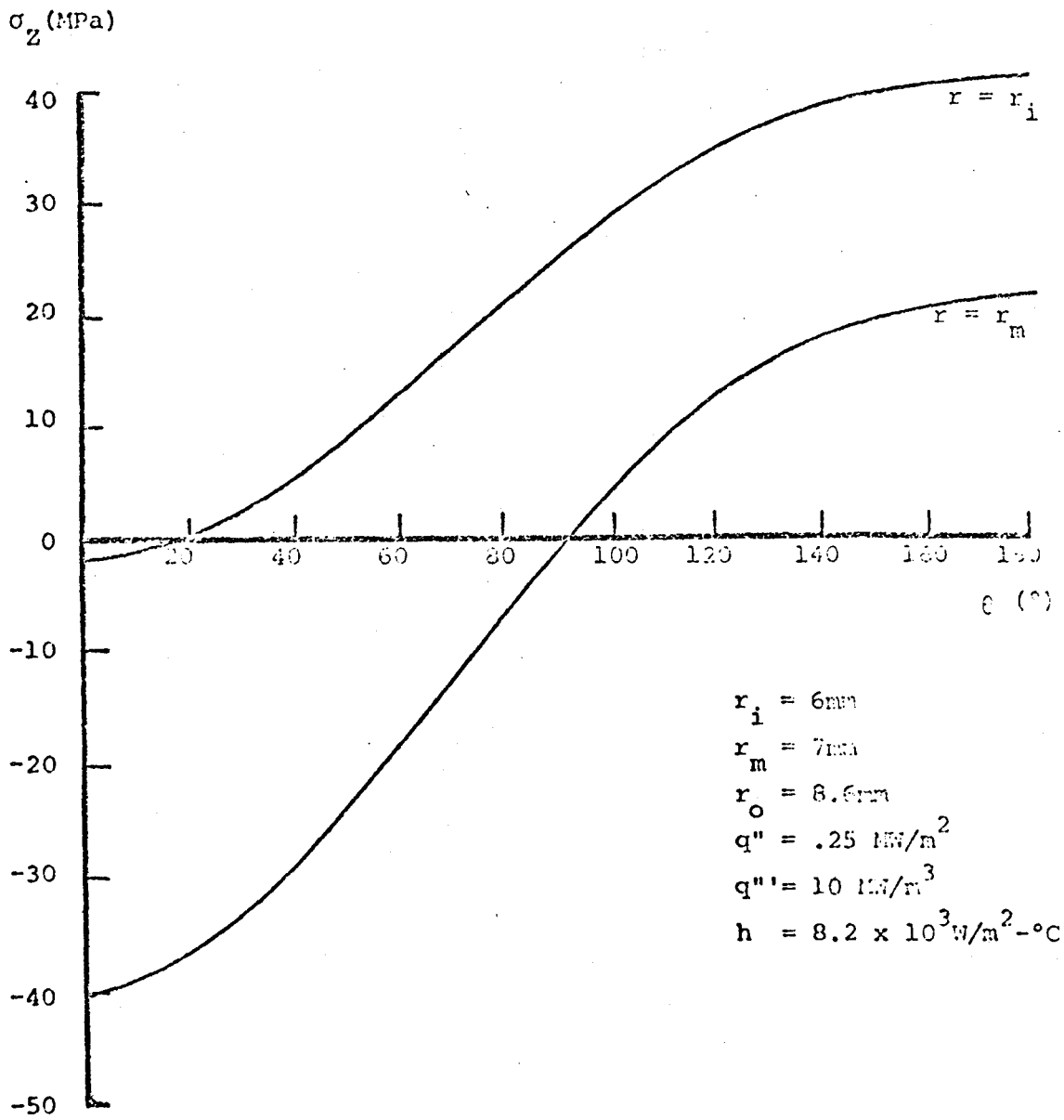

FIGURE 24. AXIAL STRESS VS. ANGLE

VI. FIRST WALL ARMOR

6.1 Introduction

The first wall concept considered in this chapter has a thick (1 cm - 4 cm) structure facing the plasma. This structure is essentially a thermal mass with cooling tubes welded or brazed to the rear surface (away from the plasma). There are two objectives for having the thick wall:

1) To protect the cooling tubes from off-normal energy dumps due to plasma disruptions or thermal transients.

2) For short pulse lengths the thermal mass can significantly reduce the thermal fluctuations seen by the cooling tubes, reducing the alternating component of thermal stress, thereby giving a longer fatigue lifetime.

If such a thick wall was restrained against bending large thermal stresses would be generated, both in the wall and the tubes. To reduce these stresses, it is proposed to cut or forge a checkerboard pattern of grooves most of the way through the block as shown in Figure 25. The portion of the wall undergoing large temperature excursions would then be free to strain as required to relieve the stresses. The wall is not meant to be a structural member but only as a protective sacrificial piece.

6.2 Thermal Analysis

A simplified thermal analysis to estimate the transient temperatures was performed using a 1-D slab geometry with the following boundary conditions

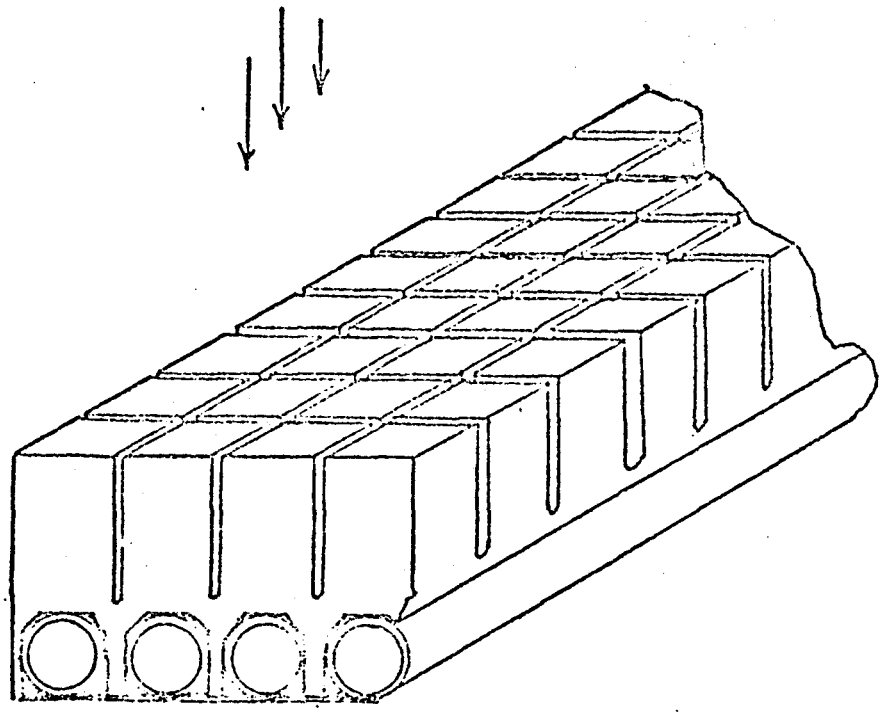

25.A FIRST WALL ARMOR

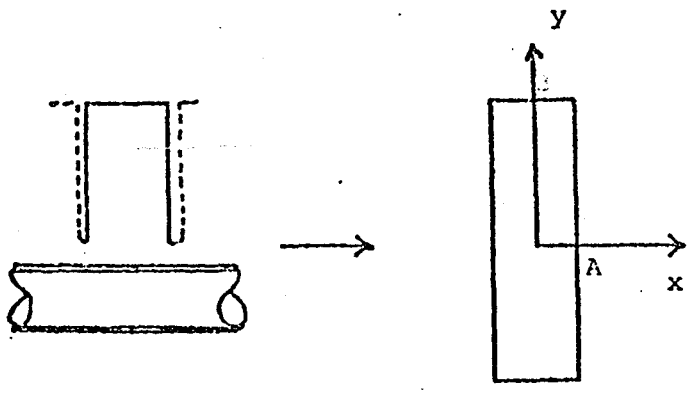

25.B 2D MODEL

FIGURE 25. FIRST WALL ARMOR CONCEPT

$t = 0$ $\qquad T = T_F$

$x = 0$ $\qquad -k \frac{\partial T}{\partial X} = q''_o$

$x = L$ $\qquad -k \frac{\partial T}{\partial X} = h\ (T-T_F)$

with

$q''' = Ae^{-bx}\phi(t)$

T_F = Fluid temperature (assumed constant)

$q''_o = q''\phi(t)$

a = thermal diffusivity

$$\phi(t) = \begin{cases} 1 & 0 \leq t < t_B \\ 0 & t_B \leq t < t_C \end{cases}$$

L = thickness

The function $\phi(t)$ is periodic with a period t_C.

An analytic and finite difference solution were both obtained for this problem and programs to calculate the temperature are given in Appendix 5. The analytic solution method parallels a development given by Boley and Weiner.[47] The solution for a steady energy generation rate is found and then the method of superposition is used to find the pulsed response. For a steady q" and q''' the solution is given by

$$T = T_S(x) + T_C(X,t) \tag{6.1}$$

where

$$T_S = \frac{-A}{b^2k}\left(e^{-bx} - e^{-bL}\right) - \frac{A}{bk}(X-L) + \frac{A}{bk}(1-e^{-bL}) - \frac{q''}{k}X$$

$$T_C = \sum_{n=1}^{\infty} A_n e^{-a\lambda_n^2 t} \cos \lambda_n X$$

and where λ_n are the roots of the equation

$$\cot \lambda_n L = \frac{\lambda_n k}{L}$$

and $A_n = (C_1 \cdot C_2 + C_3 + C_4)/C_5$

$$C_1 = D_o/(b^2 + \lambda_n^2)$$

$$C_2 = e^{-bL}(\lambda_n \sin \lambda_n L - b \cos \lambda_n L) + b$$

$$C_3 = D_1 \frac{L}{\lambda_n} \sin \lambda_n L - \frac{1}{\lambda_n^2}(1 - \cos \lambda_n L)$$

$$C_4 = \frac{D_2}{\lambda_n} \sin \lambda_n L$$

$$D_o = \frac{A}{b^2 k}$$

$$D_1 = \frac{A}{bk} + \frac{q''}{k}$$

$$D_2 = \frac{k}{H}\left(\frac{A}{bk} \cdot e^{-bL} - \frac{q''}{k} - \frac{A}{bk}\right) - \frac{A}{b^2 k} e^{-bL} - \frac{q''L}{k} - \frac{AL}{bk}$$

These results were used with several materials (Carbon, Silicon Carbide 316SS and TZM). The solution using a finite difference method agreed closely with the analytic solution. Also, after this solution method was developed, a slightly different method of solution was published by Fillo.[48] The program in Appendix 5 was found to give the same results as a published solution for a thin 316SS wall.

For the application considered here, TZM appears to be the most

favorable material because it has the highest ρC_p product and it is capable of very high temperature operation.

To illustrate the capacity of a TZM block to protect the coolant tubes an arbitrary case was selected. Figure 26 shows the temperature on the inside and outside of a 2 cm thick TZM block which is exposed to a 20 MW/m^2 surface heat flux for 1/2 sec. (Such a heat flux could be obtained if the plasma dumped all its thermal energy in a small fraction of the first wall area over the assumed time.) While the front surface temperature increases 560°C the rear surface only increases about 30°C, corresponding to a heat flux to the coolant of 0.3 MW/m^2, for the assumed heat transfer coefficient.

A second example is shown in Figure 27 where a 3.5 cm block is used to provide thermal inertia for short pulse operation. A steady state temperature profile is never reached for the 40 second burn and 20 second dwell cycle. Even with the low duty factor of this cycle, the heat flux to the coolant only varies approximately $\pm$ 10% around a mean value, instead of going to zero as it would without the block. This gives the possibility of a reduced alternating component of thermal stress in the coolant tubes which should reduce fatigue damage.

6.3 Thermal Stress Analysis

Without grooves, the large temperature difference across a thick wall due to the surface heat flux would cause high thermal stresses in both the wall and the tubes brazed to the rear surface. It is assumed that the coolant tubes and wall are restrained against bending but are free to expand in the plane of the cooling tubes. Grooves cut most of the way through the block reduce the stresses. A simplified model was

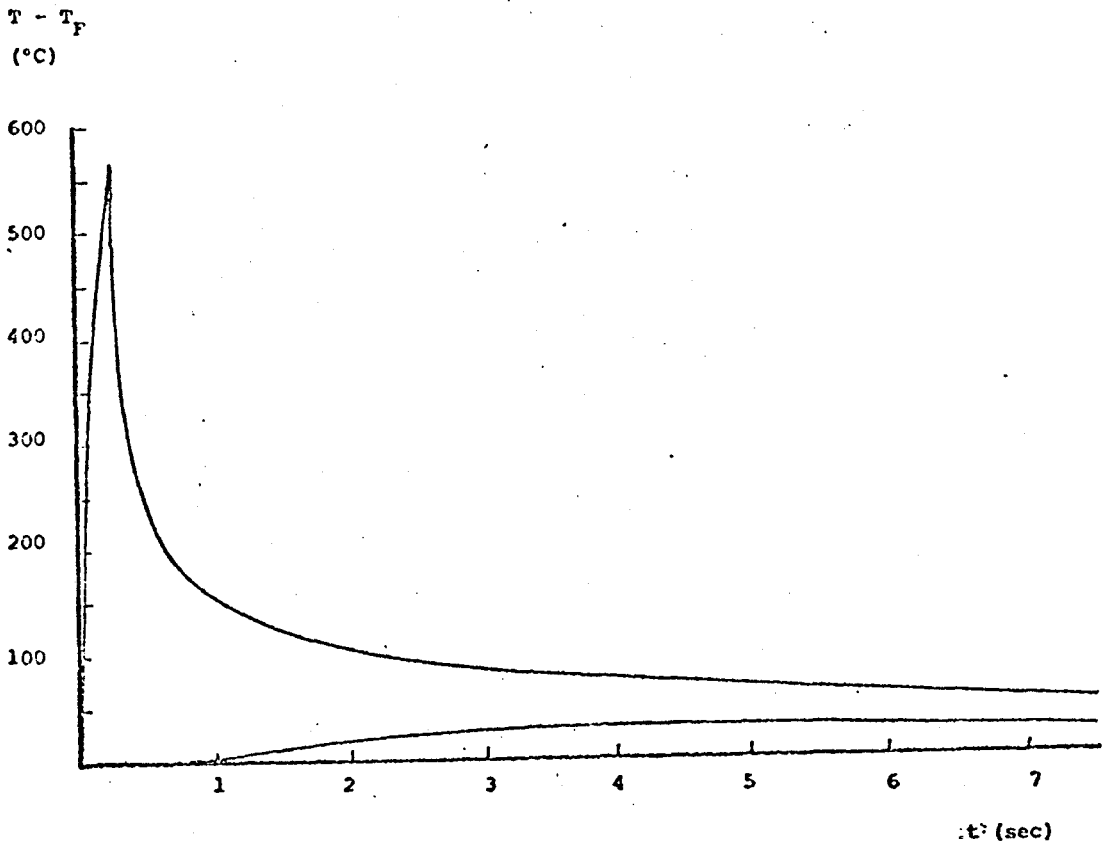

TZM

Density = 10200 kg/m^3

C_p = 795 J/kg -K

k = 98 W/m -K

H = 10^4 W/m^2 -K

q" = 20 MW/m^2 for 1/2 sec

FIGURE 26. SINGLE SHORT THERMAL PULSE RESPONSE OF TZM BLOCK

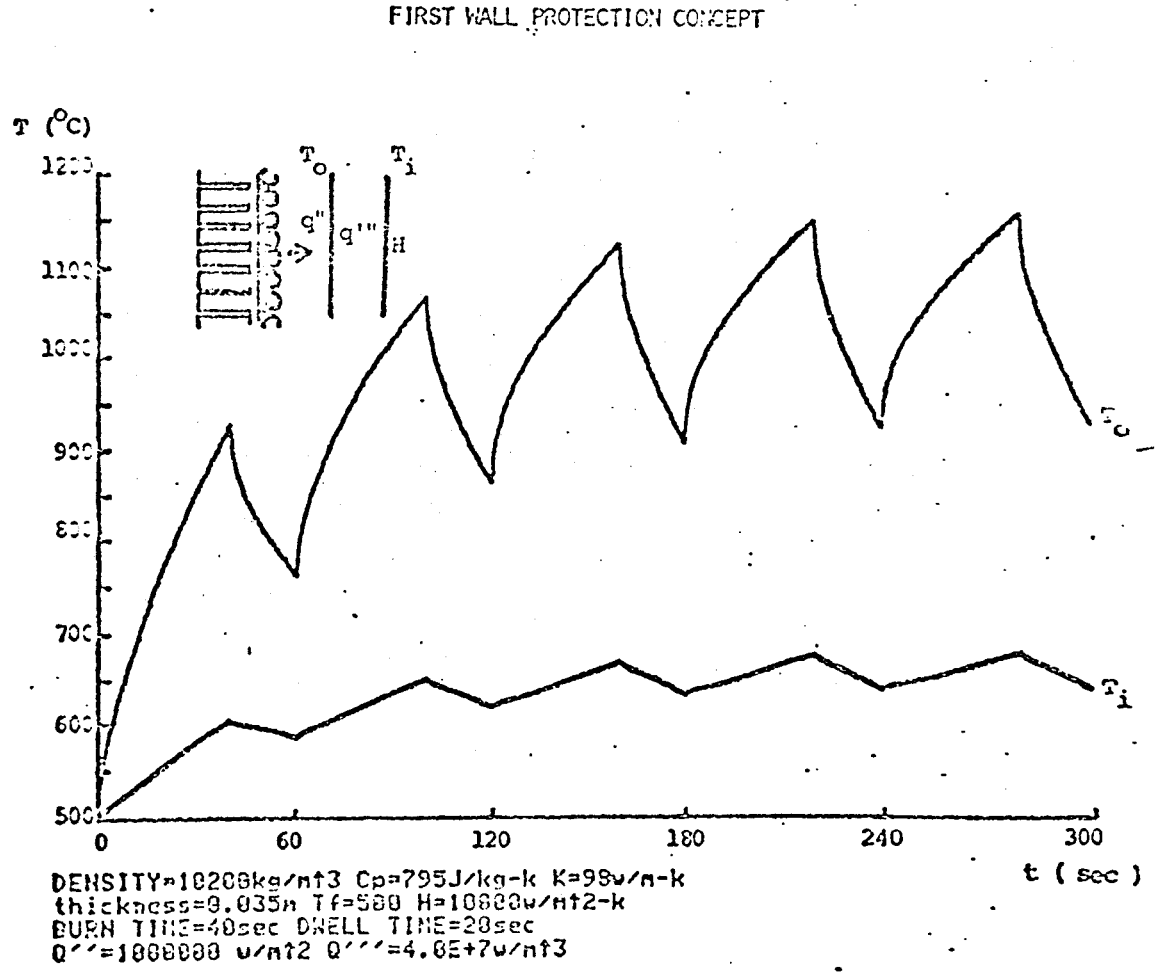

TEMPERATURE vs. TIME FOR A 1-D SLAB OF TZM

FIGURE 27. CYCLIC THERMAL RESPONSE TZM BLOCK

adopted to estimate the relation between stress reduction and groove spacing.

A detailed stress analysis would have required an extensive numerical procedure for a specific tube size, spacing and restraint system. It was felt that at the initial stage a simplified approach was more appropriate.

To estimate the effects of the grooves, the small blocks were modeled as finite sized plane stress rectangles as shown in Figure 25B. The temperature distributing was taken to be a function of y only and to be symmetric about x=0. This is equivalent to allowing expansion along the x axis but no bending. (See Figure 25B) Several approximate solution methods for this problem are available in the literature. The approximate variational method developed by Heldenfels and Roberts, and discussed in reference 49 was used. A program using that method is given in Appendix 5.

Figure 28 shows the stresses for a linear temperature distribution when the grooves are far apart. Near the middle, the peak stress in the X direction equals $\frac{1}{2}\alpha E\Delta T$ as expected. Near the edge, the X component of stress falls to zero and there develops a y component of stress which is needed to keep the x=0 boundary straight, and which has peak value of nearly $\frac{1}{2}\alpha E\Delta T$.

As the ratio of A/B is made smaller the magnitude of these peak stresses, when normalized to $\alpha E\Delta T$ decrease. Figures 29 and 30 show this effect for σ_x and σ_y respectively. When A/B is <1 a considerable

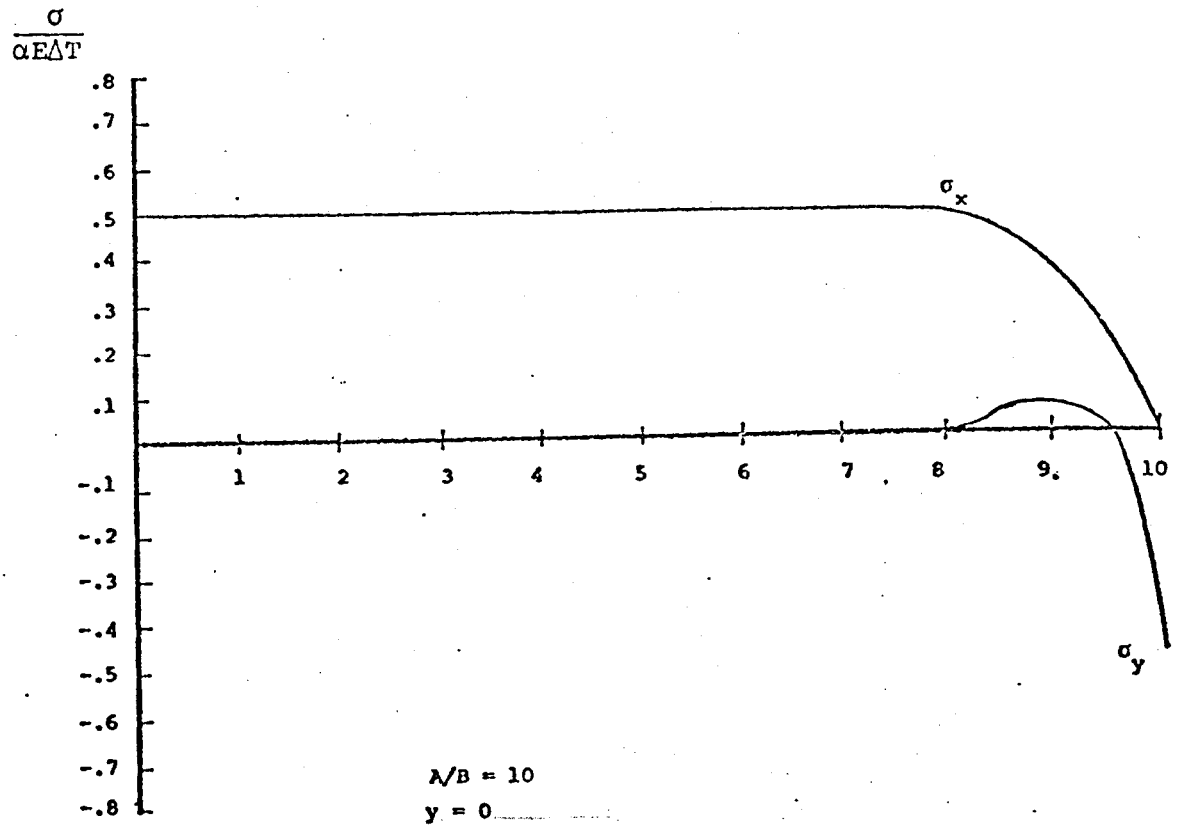

FIGURE 28. THERMAL STRESS VS. POSITION FOR PLANE STRESS FINITE RECTANGLE WITH LINEAR TEMPERATURE DISTRIBUTION

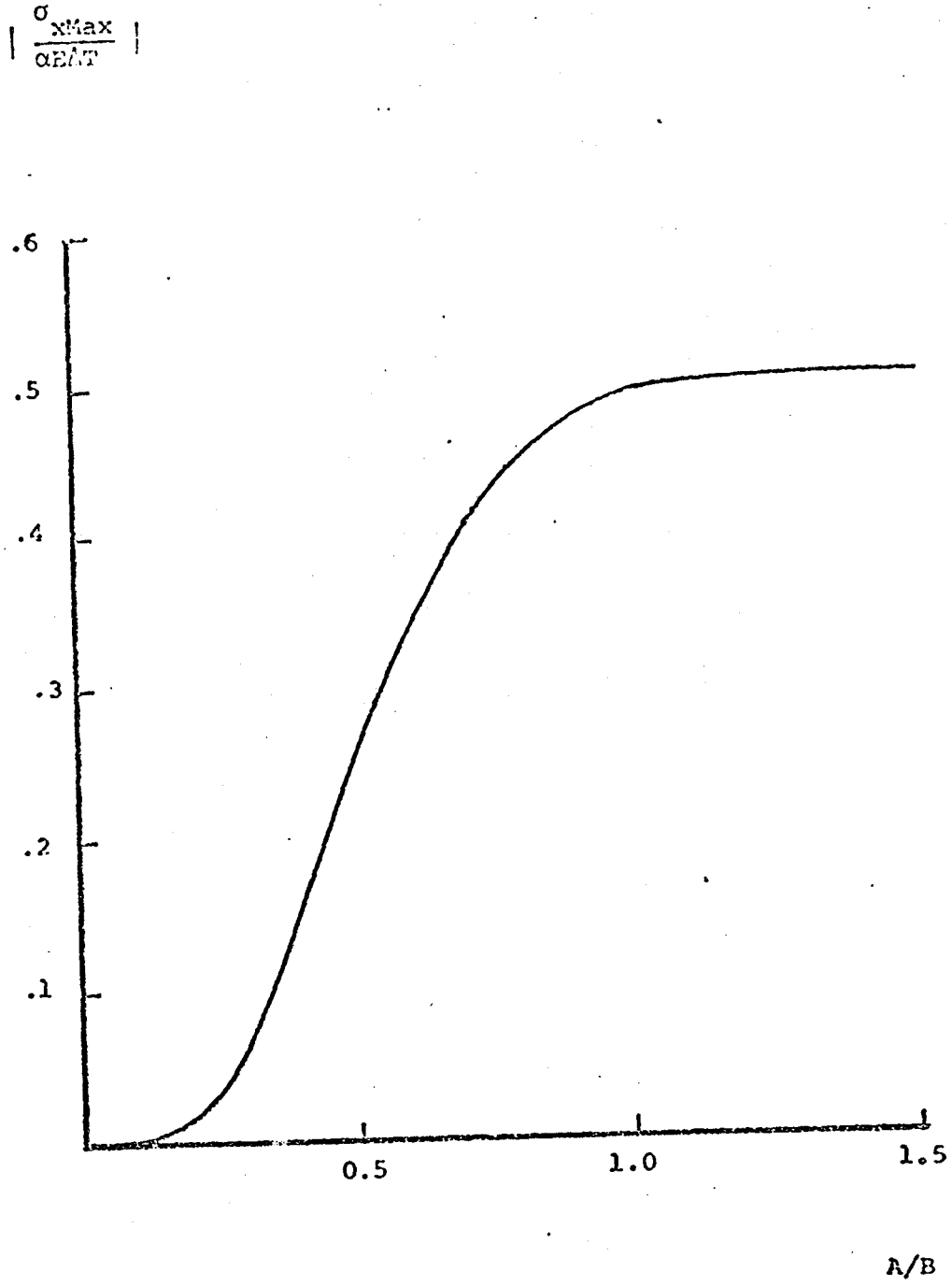

FIGURE 29. $\left|\frac{\sigma_{xMax}}{\alpha E \Delta T}\right|$ VS. A/B

$\left| \frac{\sigma_{yMax}}{\alpha E \Delta T} \right|$

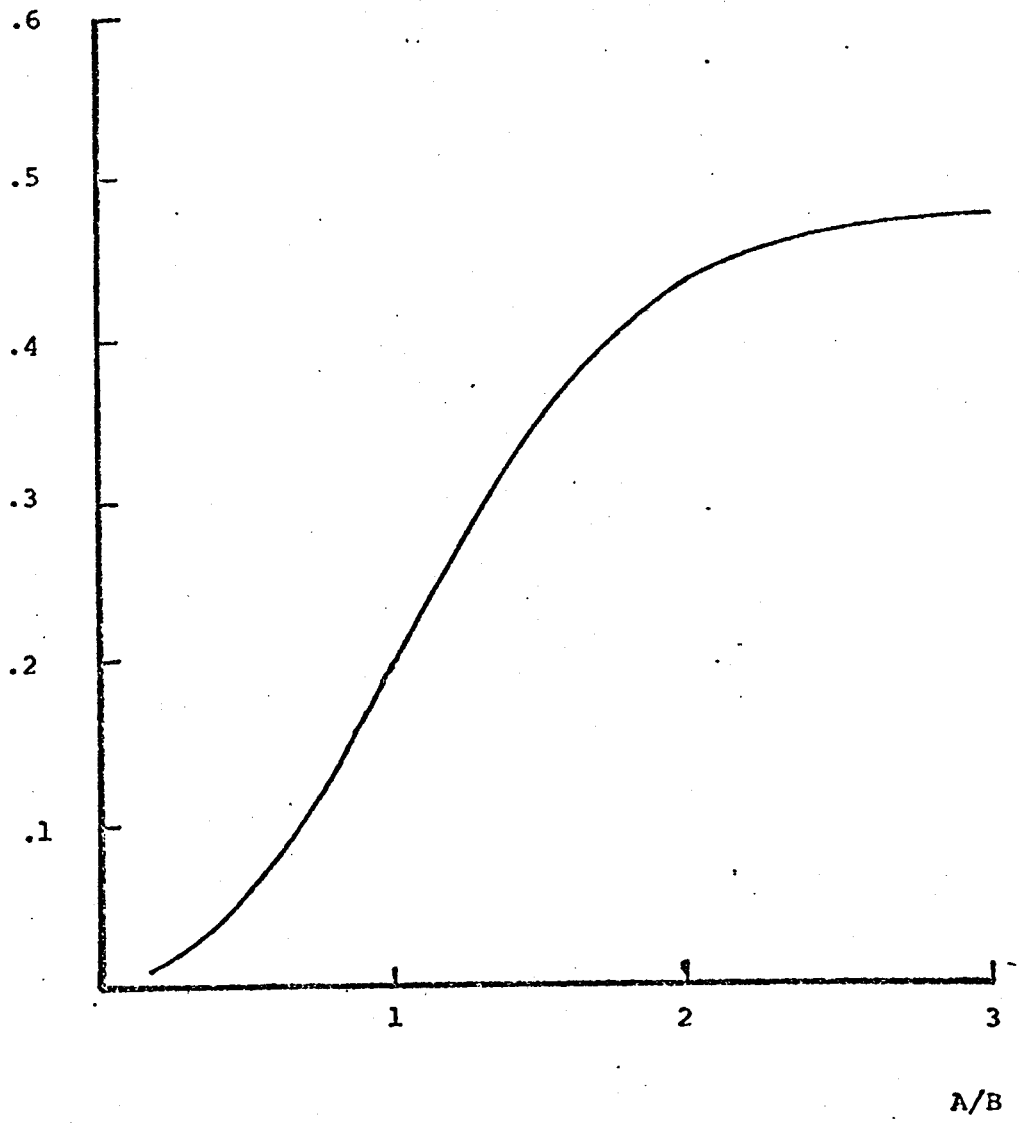

FIGURE 30. $\left| \frac{\sigma_{yMax}}{\alpha E \Delta T} \right|$ VS. AB.

reduction is evident.

A numerical example is given in Figure 31 for a TZM block with a 0.25 MW/m^2 surface heat flux. The stress at y = 0 versus thickness of the block is plotted for a block with no grooves, grooves 1 cm apart (A=.5cm) and grooves 2 cm apart.

6.4 Conclusions

The results indicate that the thermal stresses resulting from the temperature difference across a thick block, restrained against bending, can be significantly reduced by grooves cut nearly through the block and spaced apart by a distance less than or equal to the thickness. The thermal mass of the block can be used to reduce the alternating component of thermal stress for the tubes which reduces fatigue damage. In addition, the block protects the tubes from thermal transients, which makes the restrictions on plasma control much less demanding and the consequences of sub-system failures less severe.

Further detailed analysis is required to determine the effects of stress concentrations at the base of the notches. These stresses will depend on the actual manner in which the tubes and wall are restrained and the way the tubes are attached to the wall. A crack at the base of a notch, however, would not be a fatal flaw since it most likely would not propagate into the tube wall which is a separate structural piece.

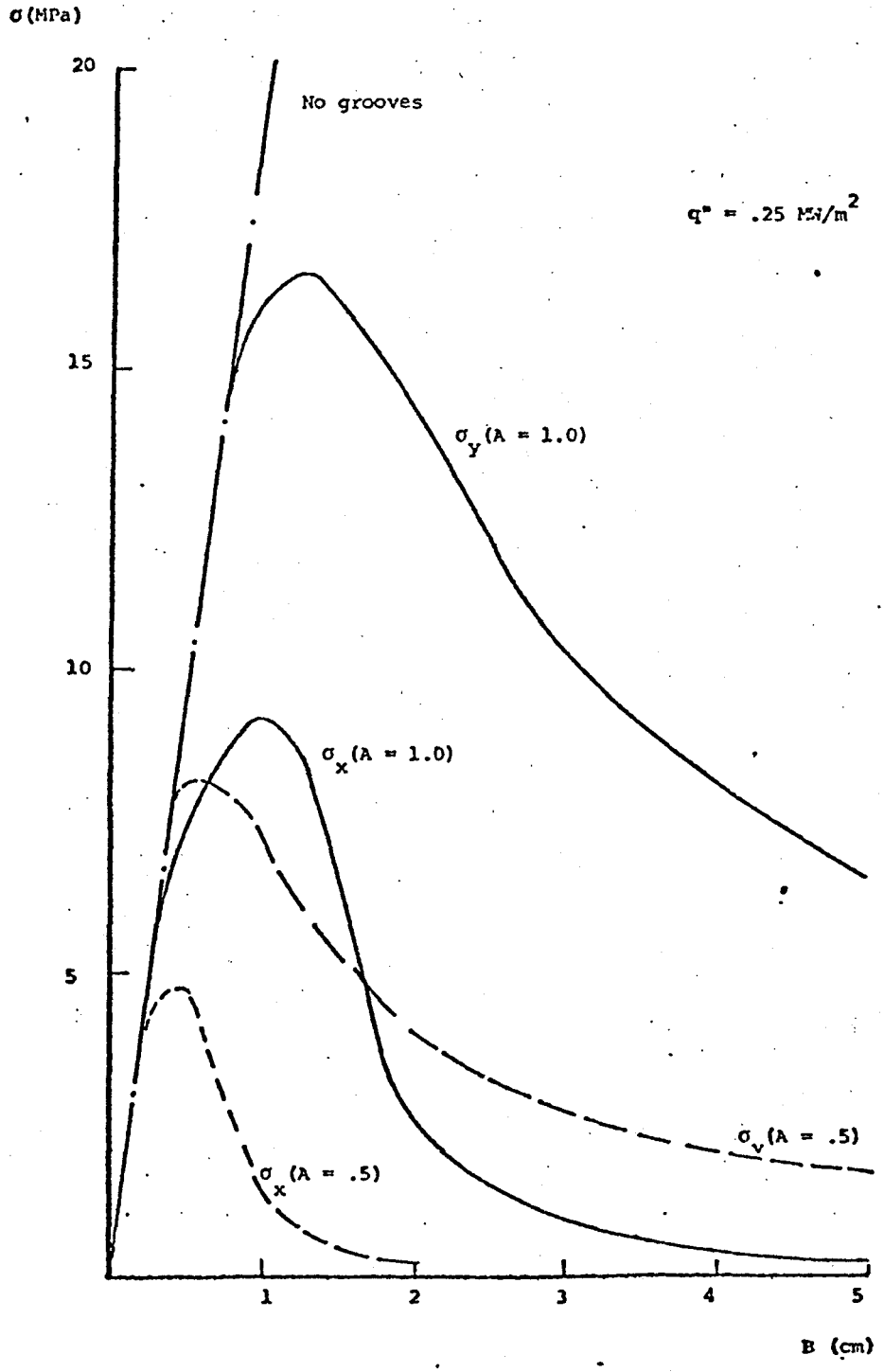

FIGURE 31. THERMAL STRESS VS. TZM BLOCK THICKNESS

VII. CONCLUSIONS & RECOMMENDATIONS FOR FUTURE WORK

7.1 Summary & Conclusions

This thesis has examined the use of helium and the molten salt flibe as coolants for a fusion reactor blanket. Two structural materials, 316 Stainless Steel and TZM (a molybdenum alloy) were considered. The first wall and interior blanket regions were analyzed separately because of their different constraints and operating conditions.

A stagnant lithium pool was employed for tritium breeding in the interior blanket. Heat removal was accomplished by coolant tubes distributed either in a shell configuration or throughout the blanket such that the heat removal per unit length was the same for all tubes. The latter configuration gave a smaller number of tubes and lower peak thermal stresses. For this configuration with helium coolant analytic expressions relating the neutron wall loading to the major design parameters of interest were found. The expressions should be quite useful in parametric studies since detailed design configurations and analysis are not required. Comparisons with several designs in the literature were made and the agreement between the analytic expressions and detailed designs was good. In addition, for both helium and molten salts a design window methodology was developed which gives the allowed range of coolant tube geometry (D,L,t, # of tubes) for a required set of design parameters and constraints. Both helium and flibe were found to be capable of the required heat removal for wall loadings of interest

(1 - 4 MW/m^2) with known constraints. Flibe with 316SS was not considered since 600°C structural material temperatures were required. Flibe with TZM gave the lowest number of tubes, lowest thermal stress, lowest hoop stress and by far, the lowest pumping power.

A shell cooling design was adopted for the HFCTR conceptual reactor. The advantages over the distributed tubes appears to be an increased breeding ratio and improved reliability. The penalty is a larger number of tubes and higher thermal stresses.

A tubular radiation shield was considered and a linear elastic thermal stress analysis accomplished under the assumption of no bending. Relatively high axial compressive stresses were found. Copper cladding was proposed and analyzed. It was found to be capable of significantly reducing the peak thermal stress. A second first wall configuration employing a thick sacrificial TZM block was also considered. A checkerboard pattern of grooves appears capable of significantly reducing the steady state thermal stresses. The large thermal mass of the block will protect the coolant tubes from plasma energy dumps and for short pulse operation it can reduce fatigue damage by reducing the alternating component of thermal stress. Further work is needed to estimate the effects of stress concentrations at the base of the notches.

7.2 Recommendations for Future Work

There remains a tremendous amount of work to be done in the area

of blanket engineering before a design could be considered as a safe reliable device to be operated by a utility. Some areas for further analysis will be given below but the list is far from complete.

7.2.1 Interior Blanket (Stagnant Lithium Pool)

Several general areas in need of further study relating to a stagnant lithium pool are:

(1) Natural convection and consequences.

(2) Rate of helium bubble nucleation and growth, and possibility of trapped pockets of helium.

(3) Effects of Pulsed Magnetic Fields in terms of mechanical forces, fluid circulation and effects of lithium pool on magnetic field seen by the plasma during the start-up.

(4) Effect of magnetic field on slow lithium flow. Does it cause channeling so that the entire lithium volume is not sampled for tritium removal?

(5) Cold Start Procedures. How is the frozen lithium to be heated up to operating temperature? Can fusion neutrons be used or must the lithium be melted first?

(6) Phase change effects during pulsed operation. How does the volume change affect the structure?

(7) Alternate Molten Salt Coolant Investigation. If a salt with a lower melting point could be found for use with 316SS it could yield an attractive design.

Structural Considerations for Module Design

1. Module Structural Design

Can a closely packed module design be developed for use with helium coolant which would allow for rupture of a coolant tube?

2 Development of a numerical code to predict structural lifetime based on changes in material properties due to irradiation, structural loads and thermal stresses.

7.2.2 First Wall Design

(1) Accident tolerant design. Any accident which causes a plant shut-down for replacement of the first wall would be extremely expensive. For a realistic design something like the first wall armor is a necessity. A desirable goal would be to develop a design using 316SS and copper or another high conductivity material which would protect the coolant tubes from the plasma, prevent small coolant leaks from quenching the plasma, and allow for operation with local failures.

(2) More realistic treatment of the spatial distribution of the charged particle flux from the plasma. There will most likely be some variation of the charged particle flux with poloidal angle, causing hot spots.

(3) Integration of first wall design with the use of a divertor or cold gas blanket.

REFERENCES

1. D. J. Rose and M. Clark, Jr., "Plasmas and Controlled Fusion, Massachusetts Institute of Technology, 1961.

2. IAEA International Conference on Fusion, Innsbruck, Austria. Summary - "Fusion Forefront", DOE/Office of Fusion Energy, November 1978.

3. J. Chao, "Thermal - Hydraulic and Neutronic Considerations for Designing a Lithium - Cooled Tokamak Blanket", Ph.D. Thesis, Massachusetts Institute of Technology, December 1973.

4. A. P. Fraas, "Comparative Study of the More Promising Combinations of Blanket Materials, Power Conversion Systems, and Tritium Recovery and Containment Systems for Fusion Reactors", ORNL/TM-4999, November, 1975.

5. J. T. D. Mitchell, J. A. Booth, "Wall Loading Limitations in a Helium - Cooled Fusion Reactor Blanket, Culhorn Laboratory, CLM-M126, November 1973.

6. E. E. Bloom, F. W. Wiffen, et al., "Temperature and Fluence Limits for a Type 316 Stainless Steel CTR First Wall", Nuclear Technology, Vol. 31., October 1976.

7. ASME Boiler and Pressure Vessel Code, Section III, Code Case 1592, Class I Components in Elevated Temperature Service, 1974 Edition.

8. Hancox, R and Booth, J. A., "The Use of Liquid Lithium as a Coolant in a Toroidal Fusion Reactor Part II, Stress Limitations," CLM-R116, 1971.

9. Charlot, L. A., and Westerman, R. E., "Helium Coolant Compatibility with Candidate Fusion Reactor Structural Materials", BNWL-1842, Battelle Pacific Northwest Laboratories, July 1974.

10. Devan, J. H. "Compatibility: Fusion Reactor First Wall Materials" WASH-1206, USAEC (1972)

12. "UWMAK-III, A Noncircular Tokamak Power Reactor Design", EPRI-ER-368.

13. Lyon, R. M., ed., "Liquid Metal Handbook", Sponsored by the Committee on the Basic Properties of Liquid Metals, Office of Naval Research, Department of the Navy, in Collaboration with USAEC and Bureau of Ships, Department of the Navy, June, 1952.

14. Fraas, A. P., "Problems in Coupling a Gas Turbine to a Thermonuclear Reactor", ASME Gas Turbine and Fluids Engineering Conference and Products Show, San Francisco, CA, March 1972.

15. Melese -D'Hospital, G. and Hopkins, G. R., "Gas Cooling for Fusion Reactor Blankets", 5th Intersociety Energy Conversion Engineering Conference, Los Vegas, September 1970.

16. Uckan, N. A., et al., "The ELMO Bumpy Torus Reactor", ORNL-KM-6084.

17. Homeyer, W. G., "Thermal and Chemical Aspects of the Thermonuclear Blanket Problem", Massachusetts Institute of Technology, Research Laboratory of Electronics, Technical Report No. 435, June 1965.

18. Grimes, W. R., and Cantor, S., "Molten Salts as Blanket Fluids in Controlled Fusion Reactors", Oak Ridge National Labs., ORNL-TM-4047, December 1972.

19. Moszynski, J. R. et al., "Cooling of Controlled Thermonuclear Fusion Reactors of Toroidal Configurations", Technology of Controlled Thermonuclear Fusion Experiments and the Engineering Aspects of Fusion Reactors, USAEC, April 1974.

20. Rosenthal, M. W., et al., "Molten-Salt Reactor Experiments - History, Status and Potential", Nucl. Appl. Tech. 8, 107 (1970).

21. Cantor, S., ed. "Physical Properties of Molten Salt Reactor Fuel, Coolant and Flush Salts", ORNL-TM-2316, August 1968.

22. Hoffman, M. A. and Carlson, G. A., "Calculation Techniques for Estimating the Pressure Losses for Conducting Fluid Flow in Magnetic Fields' USAEC Rept. UCRL-51010, Lawrence Radiation Laboratory, 1971.

23. El-Wakil, M. M., "Nuclear Heat Transport", International Textbook Co., 1971.

24. Selle, J. E., "Corrosion Studies of Two Austenitic Stainless Steels in Liquid Lithium", ORNL-TM-5817, May, 1976.

25. Bloom, E. E., Wiffen, F. W., et al., "Temperature and Fluence Limits for a Type 316 Stainless Steel CTR First Wall", Nuclear Technology, Vol., 31 October 1976.

26. Keiser, J. R., and Lawrence, E. J., "Salt Corrosion Studies", p. 75 in Molten-Salt Reactor Program Semiannual Progress Report for period ending February 29, 1976, ORNL-5131, August 1976.

27. Class notes, Course 22.314, Massachusetts Institute of Technology, September 1978, unpublished.

28. Bettis, E. S., and Robertson, R. C., "The Design and Performance Features of a Single-Fluid Molten-Salt Breeder Reactor", Nucl. Appl. Tech. 8, 190 (1970).

29. Cohn, D. R., et al., "High Field Compact Tokamak Reactor (HFCTR) Conceptual Design", Massachusetts Institute of Technology, Plasma Fusion Center Research Report RR-78-2, March 1978.

30. Conn, R. W., et al., "NUMAK: An Attractive Reactor for the Main Line of Tokamaks", The Technology of Controlled Nuclear Fusion, p. 351, Transaction of the Third Topical Meeting, Santa Fe, May, 1977.

31. Steiner, D., et al., "ORNL Fusion Power Demonstration Study: Interim Report", ORNL-TM-5813, Oak Ridge National Labs, March 1977.

32. Werner, R. W., "ORNL Fusion Power Demonstration Study: The Concept of the Cassette Blanket", ORNL/TM-5964, October 1977.

33. Wells, W. M., "ORNL Fusion Power Demonstration Study: Lithium as a Blanket Coolant", ORNL/TM-6214, April 1978.

34. UWMAK II, "A Conceptual Tokamak Power Reactor Design" UWFDM-112, October 1975.

35. Mills, R. G., ed., "A Fusion Power Plant", MATT-1050, Plasma Physicals Laboratory, Princeton University, August 1974.

36. Y.B. Fridman (Ed.) "Strength and Deformation in Nonuniform Temperature Fields", Consultants Bureau Enterprises, Inc., New York, N.Y., 1962.

37. Boley, B. A., and Weiner, J., "Theory of Thermal Stresses", New York, Wiley 1960.

38. Kays, W., "Convective Heat and Mass Transfer", New York, McGraw-Hill, 1966.

39. Timoshenko, S. P. and Goodier, J. N., "Theory of Elasticity", Third Edition, New York, McGraw-Hill, 1970.

40. Touloukian, Y. S., et al., "Thermal Expansion Metallic Elements and Alloys", Thermophysical Properties of Matter, Vol., 12, Perdue Research Foundation, 1975.

41. ASME Bouler and Pressure Vessel Code Table T-1420-1A,1B.

42. Samsonou, G, Akademna Nauk URSR, Kiev. Instytut Problem Materialoznavstva, Handbook of the Physico-Chemical Properties of the Elements, Plevum, 1968.

43. Davis, J. W., and Kulcinski, G. L., "Assessment of Titanium for Use in the First Wall/Blanket Structure of Fusion Power Reactors", EPRI ER-386, April 1977.

44. Hopkins, G.,"Fusion Reactor Studies: Potential of Low Z Materials for the First Wall, GA-A13430 General Atomic Co., San Diego, CA, September 1975.

45. Takeuti, Y. and Tanigawa, Y, "Asymetrical Transient Thermoelastic Problems in a Composite Hollow Circular Cylinder", Nuclear Engineering and Design, 45 (1978) 159-172.

46. Timoshenko, S. P., and Goodier, J. N., ibid, p. 443.

47. Boley, B. and Weiner, J., ibid, p. 200

48. Fillo, J. A., "First Wall Fusion Blanket Temperature Variation - Slab Geometry", Nuclear Engineering and Design 48 (1978), 330-339

49. Johns, D. J., "Thermal Stress Analysis", (1st ed.), Oxford, New York, Pergamom Press, 1965.

APPENDIX 1.1 - HELIUM BLANKET WINDOW GRAPH

This appendix contains a listing and description of a program to graph a design window in the D versus L plane using the analytic expressions developed in Chapter 1. It has been removed for conciseness. The full report may be obtained from the M.I.T. library system as:

T.McManamy, 'Fusion Reactor Blanket Heat Removal Using Helium and Flibe', Ph.D. thesis, M.I.T., Nuclear Engineering, February 1979.

APPENDIX 1.2 $\Delta T_{LITHIUM}$ ESTIMATE

It will be assumed that the cross section of the region of lithium being cooled by a tube can be approximated as circular with a diameter D_C and a uniform energy generation rate q"'. For a tube diameter D from energy conservation

$$\pi D W_S = \frac{\pi}{4} (D_C^2 - D^2)\, q''' \qquad \text{A1.1.1}$$

or

$$D_C = D^2 + \frac{4DW_s}{q'''}$$

For a tube outside wall temperature T_W let

$$t(r) \equiv T(r) - T_W$$

The equation to be solved is then

$$\nabla^2 t(r) + \frac{q'''}{k} = 0$$

with the boundary condition

$$r = \frac{D}{2} \qquad t \neq 0$$

$$\frac{dt}{dr} = 0$$

$$r = \frac{D_C}{2} \qquad \frac{dt}{dr} = 0$$

after integrating the equation for t(r) and applying the boundary conditions the solution for $t\left(\frac{D_C}{2}\right)$ is found to be given by

$$t\left(\frac{D_C}{2}\right) \equiv \Delta T_{Li} = \frac{q'''}{16k}\left[D_C^2 \left(2 \ln \frac{D_C}{D} - 1\right) + D^2\right] \qquad \text{A1.1.2}$$

substituting for D_c from A.1.1.1 gives

$$\Delta T_{Li} = \left(\frac{q'''D^2}{16k} + \frac{DW_s}{4k}\right) \ln\left(1 + \frac{4W_s}{Dq'''}\right) - \frac{DW_s}{4k}$$

APPENDIX 2 - FLIBE BLANKET WINDOW GRAPH

This appendix contains a description and listing of a program to graph a design window in the D versus L plane using the analytic expressions developed in Chapter 2 for a stagnant lithium blanket with flibe coolant. It has been removed from this report for conciseness. The full report may be obtained from the M.I.T. library system as:

T. McManamy, Ph.D. thesis, 'Fusion Reactor Blanket Heat Removal Using Helium and Flibe', Nuclear Engineering, February, 1979.

APPENDIX 3.1 ANALYTIC SOLUTIONS FOR TEMPERATURE PROFILES

SHELL COOLING

3.1.1 Single Region

It is assumed that the blanket will be divided into a small number of modules. Each module will be several meters long. The temperature gradients in the axial direction along the tubes will be much smaller then in the radial direction, assuming cylindrical geometry. The neutronic heating rates are assumed to be known and capable of being represented by exponential functions.

The basic equation for the steady state temperature distribution to be solved is

$$\nabla(k\nabla T) + q'''(r) = 0 \qquad \text{(A3.1)}$$

It will be assumed that the thermal conductivity is constant and that the radial conduction is dominant. Given the boundary conditions

$$r = r_i \qquad T = T_i$$
$$r = r_o \qquad T = T_o \qquad \text{(A3.2)}$$

and the energy generation rate q'''

$$q''' = A\, e^{-b(r-r_i)}$$

equation A3.1 becomes

$$\frac{1}{r}\frac{d}{dr}\left(r\frac{dt}{dr}\right) + b^2 Be^{-br} = 0 \qquad \text{(A3.3)}$$

where $B \equiv \frac{Ae^{br_i}}{k\,b^2}$

The solution of (3.3) is

$$T = C_1 \ln r + C_2 + B\,\{S_1(br_i) - S_1(br) - e^{-br}\} \qquad (A3.4)$$

where

$$S_1(X) = \int_x^\infty \frac{e^{-x}}{x}\,dx$$

$$C_1 = \frac{T_i - T_o + \frac{A}{b^2 k}\,\{1 + e^{br_i}(S_1(br_i) - S_1(br_o) - e^{-b(r_o - r_i)}\}}{\ln(r_i/r_o)}$$

$$C_2 = \frac{T_i + A}{b^2 k} - C_1 \ln r_i$$

For large temperatures rises in the lithium it may be desirable to use a linear correlation for the thermal conductivity of lithium. The same solution as for constant k can be used with a simple change of variables.

for

$$k = k_o\,(1 + \beta_o T)$$

$$T = \frac{k - k_o}{\beta_o k_o} \equiv \frac{k - k_o}{\beta}$$

so that

$$\nabla T = \frac{\nabla k}{\beta}$$

$$\nabla\,(k \nabla T) = \frac{\nabla^2 k^2}{2\beta^2}$$

the equation $\nabla(k\nabla T)+q''' = 0$

becomes $\nabla^2 k^2+2k_o\beta_o q''' = 0$

which is formally similar to $\nabla^2 T+q'''/k = 0$

with the substitutions $k^2 \Rightarrow T$ (A3.5)

$$2k_o\beta_o \Rightarrow \frac{1}{k} \quad \text{(A3.6)}$$

The solution given by equation (3.4) with a linear correlation for lithium thermal conductivity was used to generate figure A1. This gives the temperature difference between the walls (assumed to be at the same temperature) and the peak pool temperature as a function of the thickness of the region and A where

$$q''' = A\, e^{-4(r-r_i)} \quad MW/m^3$$

A 1 MW/m^2 neutron wall loading corresponds to $A_o \approx 4.6$ MW/m^2. Since approximately 50 cm of lithium are required to breed tritium it becomes obvious that the peak pool temperature would become extremely high (or boiling would start) if the entire blanket were cooled only on the inside and outside. Thus, more then one lithium region is required.

3.1.2 COMBINATION LITHIUM AND GRAPHITE REGIONS

Typical neutronic heating rate calculations show an increase in the heating rate near the rear of the breeding zone if there is a reflector such as graphite behind it. To model this effect, the following geometry was assumed.

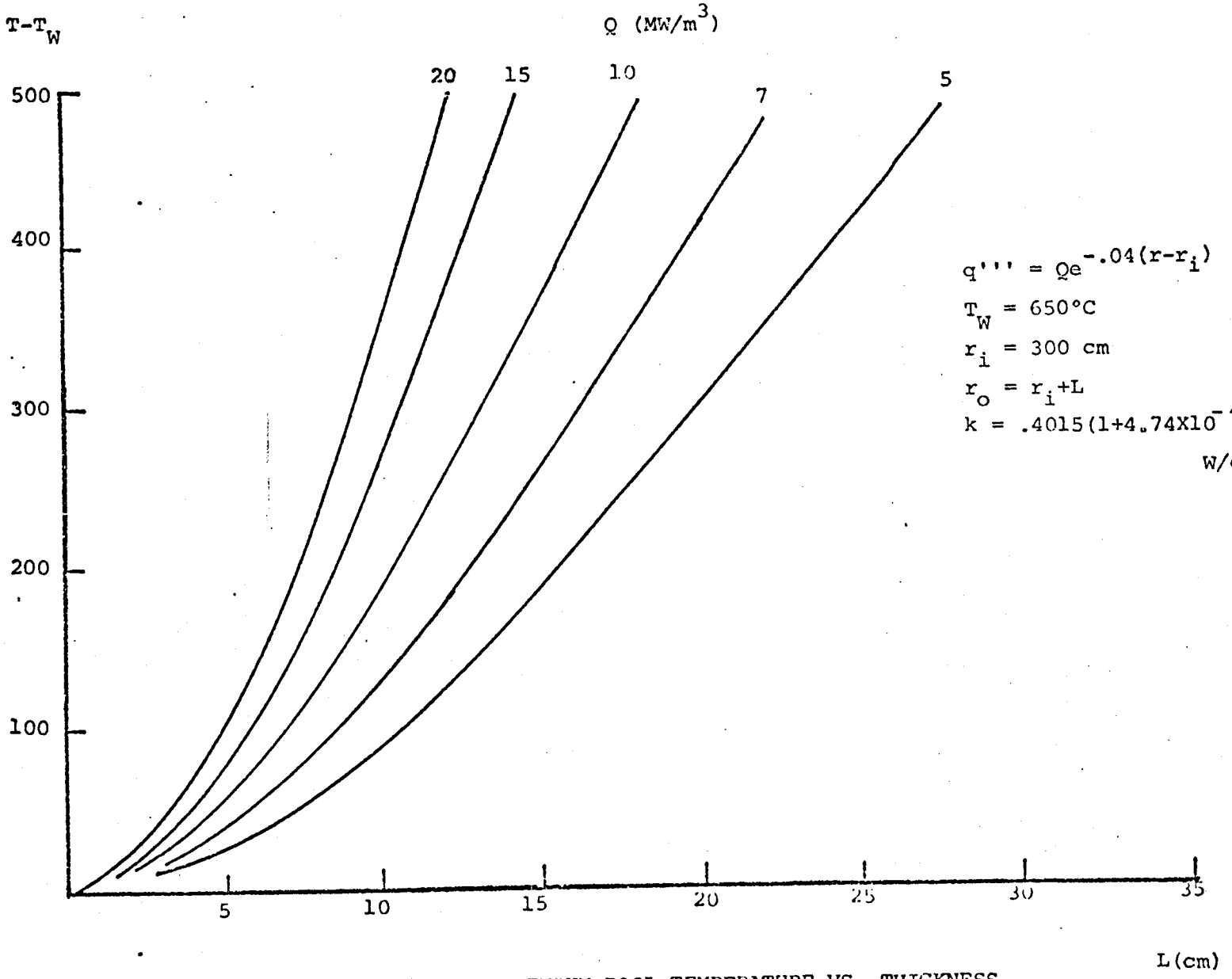

FIG. A1 PEAK LITHIUM POOL TEMPERATURE VS. THICKNESS

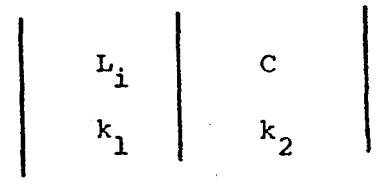

where: $r_1 \leq r < r_2$ = Lithium Zone (A3.7)

$$q''' = A_1 e^{-b_1(r-r_1)} + A_2 e^{-b_2(r_2-r)}$$

$r_2 \leq r \leq r_3$ => Carbon Zone (A3.8)

$$q''' = A_3 e^{-b_3(r-r_1)}$$

The following boundary conditions were assumed

$$r = r_1 \qquad T_1 = T(r_1) \tag{A3.9}$$

$$r = r_2 \qquad T_1 = T_2 \tag{A3.10}$$

$$r_1 k_1 \frac{dT_1}{dr}\Big|_{r_1} - r_3 k_2 \frac{dT_2}{dr}\Big|_{r_3} = \int_{r_1}^{r_3} q''' \, r\,dr \tag{A3.11}$$

$$r = r_3 \qquad T_2 = T(r_2) \tag{A3.12}$$

In the lithium zone, two exponential functions are assumed to include a component due to reflection from the carbon zone.

An analytic solution for the temperature can be found and is given by the following:

(A3.13)

$$r_1 \leq r \leq r_2 \quad T_1(r) = T(r_1) + B_1(e^{-b_1 r_1} - e^{-b_1 r}) + B_2(e^{b_2 r_1} - e^{b_2 r}) + C_1 \ln \frac{r}{r_1}$$
$$+ B_1 (S_1(b_1 r_1) - S_1(b_1 r)) + B_2 \int_{r_2}^{r} \frac{e^{b_2 r}}{r} dr$$

$$r_2 \leq r \leq r_3 \quad T_2(r) = T(r_2) + B_3(e^{-b_3 r_2} - e^{-b_3 r}) + C_2 \ln (r/r_2) \tag{A3.14}$$
$$+ B_3(S_1(b_3 r_2) - S_1(b_3 r))$$

Where

$$B_1 = \frac{A_1}{k_1 b_1^2} e^{b_1 r_1}$$

$$B_2 = \frac{A_2}{k_1 b_2^2} e^{-b_2 r_2}$$

$$B_3 = \frac{A_3}{k_3 b_3} e^{b_3 r_1}$$

$$K_1 = T(r_1) + B_1 (e^{-b_1 r_1} - e^{-b_1 r_2}) + B_2 (e^{b_2 r_1} - e^{b_2 r_2})$$

$$+ \int_{r_1}^{r_2} \left(B_1 \frac{e}{r}^{-b_1 r_1} + B_2 \frac{e}{r}^{b_2 r} \right) dr$$

$$K_2 = T(r_3) + B_3 (e^{-b_3 r_3} - e^{-b_3 r_2}) - B_3 \left(S_1(b_3 r_2) - S_1(b_3 r_3) \right)$$

$$K_3 = k_1 \quad B_1 e^{b_1 r_1} (1 + b_1 r_1) + B_2 e^{b_2 r_1} (1 - b_2 r_1)$$

$$K_4 = k_2 \quad B_3 e^{-b_3 r_3} (1 + b_3 r_3)$$

$$K_5 = \int_{r_1}^{r_2} \left[A_1 e^{-b_1 (r - r_1)} + A_2 e^{-b_2 (r_2 - r_1)} \right] r dr + \int_{r_2}^{r_3} A_3 e^{-b_3 (r - r_1)} r dr$$

$$K_6 = \left[1 - \frac{\ln (r_2 / r_1)}{\ln (r_2 / r_3)} \cdot \frac{k_2}{k_1} \right]^{-1}$$

$$C_1 = K_6 \left\{ \frac{1}{k_1} (K_5 - K_4 - K_3) + \frac{k_2}{k_1} \cdot \frac{K_1 - K_2}{\ln (r_2 / r_3)} \right\}$$

$$C_2 = \frac{\ln (r_2 / r_3) \cdot C_1 + K_1 - K_2}{\ln (r_2 / r_3)}$$

3.1.3 FIRST WALL REGION

A possible configuration for the shell cooling is to have in the first wall region, a stagnant lithium section with a surface heat flux on one side and cooling on the other side. Since such a section will have a very small depth compared to its radius, a 1-D slab geometry should give a good approximation.

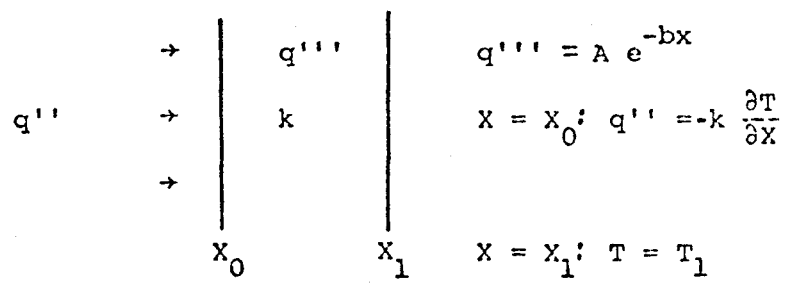

The temperature is given by

(A3.15)

$$T = T_1 + \frac{A}{bk} + \frac{q''}{k}\left[(X_1 - X)\right] - \frac{A}{b^2 K}\left[e^{-bx} - e^{-bx_1}\right]$$

The remaining appendices contain a description and listing of the programs used for this report. They have been removed here for conciseness, but may be obtained from the M.I.T. library system in:

T.McManamy, 'Fusion Reactor Blanket Heat Removal Using Helium and Flibe', Ph.D. thesis, M.I.T., Nuclear Engineering, February 1979.

Appendix 3.2 Shell Cooling, Single Region: Equation A3.4 with a linear correlation for the thermal conductivity of lithium is used to graph the lithium temperature for a single region, given the temperature on the two walls and the energy generation rate in the form $q'''=Qe^{-B(r-ri)}$.

Appendix 3.3 Shell Cooling for First Wall and Two Stagnant Regions: Equation A3.15 and equation A3.4 are used to graph the temperature versus radius for a first wall region and two stagnant regions given the wall locations, temperatures and energy generation rate.

Appendix 3.4 Shell Cooling - Combination Lithium and Graphite Region: The results of Appendix section 3.1.2 are used to graph the temperature versus radius for a region composed of two different materials and cooled only on the outside.

Appendix 3.5 Shell Cooling - Iterative Solution For N Regions: Portions of the previous shell cooling programs were combined in an iterative procedure in order to account for the different film and wall temperature drops for different channels which have different heat removal rates.

Appendix 4.1 Simple Tube Temperature and Stress: This program evaluates the temperature field and thermal stress for a radiation shield tube based on the analytic expressions given in Chapter 5.

Appendix 4.2 TUBETEMP Code: This program evaluates the temperature field for a composite tube allowing for different thermal conductivity in the radial and theta directions. The geometry and finite difference relations which are used are given in Chapter 5.

Appendix 4.3 TUBESTRESS Code: This program solves for the temperature field in a composite radiation shield tube using the analytic solution given in Chapter 5. It also solves for the thermal stresses using the analytic methods discussed in Chapter 5.

Appendix 5.1 Slab Transient Temperature: This program graphs the transient thermal response of a 1-D slab for a pulsed surface and volumetric heating source. An analytic solution method as discussed in Chapter 6 is used.

Appendix 5.2 Rectangle Stress: The approximate variational method of Heldenfels and Roberts as given in Reference 49 is used to calculate the stresses in a finite plane stress rectangle with a temperature distribution of the form $T(y) = T_0 - \Delta T\ (y/b)^n$.